

**SLOPE STABILITY STUDIES OF SOME WEAK ZONES
BETWEEN HOSPITAL COLONY AND JOTSOMA
BYPASS, KOHIMA, NAGALAND**

THESIS
SUBMITTED TO
NAGALAND UNIVERSITY

IN PARTIAL FULFILMENT OF THE REQUIREMENT FOR THE
DEGREE OF DOCTOR OF PHILOSOPHY IN GEOLOGY

BY

C. NOKENDANGBA CHANG



DEPARTMENT OF GEOLOGY
NAGALAND UNIVERSITY

2021

NAGALAND UNIVERSITY

August 2021

DECLARATION

I, Mr. C. Nokendangba Chang, hereby declare that the subject matter of this thesis is the record of work done by me, that the contents of this thesis did not form basis of the award of any previous degree to me or to the best of my knowledge to anybody else, and that the thesis has not been submitted by me for any research degree in any other University/Institute.

This thesis is submitted to the Nagaland University, in partial fulfilment for the degree of Doctor of Philosophy in Geology.

Candidate

Head

Supervisor



NAGALAND UNIVERSITY

(A Central University Estd by the Act of Parliament No.35 of 1989)

Headquarters: Lumami: Kohima Campus: Meriema-797004

DEPARTMENT OF GEOLOGY

Dr. Temsulemba Walling
Assistant Professor
Department of Geology

Mobile : 09436831189
E-mail : tem_wall@yahoo.com

CERTIFICATE

The thesis presented by Mr. C. Nokendangba Chang, MSc., bearing Registration No. 753/2017 (10th September 2015) embodies the results of investigations carried out by him under my supervision and guidance.

I certify that this work has not been presented for any degree elsewhere and that the candidate has fulfilled all conditions laid down by the University.

(Dr. Temsulemba Walling)
Supervisor

ACKNOWLEDGEMENT

First and foremost, I extend my heartfelt gratitude to my supervisor, Dr. Temsulemba Walling, Department of Geology, Nagaland University for his constant guidance, genuine dedication with invaluable advice, and encouragement during my entire research period, without which I would not have completed my work.

The success and final outcome of this work required a lot of guidance and assistance from many people and organisations. This work would not have been possible without the financial support of The Natural Resource Data Management System (NRDMS), Department of Science & Technology, Government of India, New Delhi.

I would like to extend my special thanks to Prof. Glenn T. Thong for his valuable suggestions, ever encouraging and motivating guidance throughout my work.

I wish to acknowledge the Department of Geology, Nagaland University for providing me with all the necessary facilities to carry out the analyses. The faculties and staffs, who were always there to help and assist me with my queries, are also sincerely acknowledged. Their immense knowledge and plentiful experience have encouraged me in all the time of my academic research.

I would also like to offer my special thanks to Dr. Supongtemjen, GIS Assistant, Nagaland GIS & Remote Sensing Centre, Planning & Coordination Department, Government of Nagaland for his assistance and help rendered to all my queries related to Remote Sensing and GIS.

I am grateful and indebted to Mr. Mehilo Apon, Dr. Ranjit Nayak, Mr. Sohi Tep, Mr. Benathung Patton and Mr. Khruvo Vadeo for their valuable contribution in the field as well as in the laboratory.

My sincere appreciation goes to all my fellow scholars and friends for their love, support and help rendered.

Last but not the least I thank my family members for their continuous prayer, motivation, love, moral and financial support without which I could not have completed my research work.

(C. NOKENDANGBA CHANG)

LIST OF TABLES

		Page No.
Table 2.1	Landslide classification according to Cruden and Varnes (1996)	9
Table 3.1	Soil classification according to Plasticity Index (Anon, 1979)	26
Table 3.2	Values of I_L and I_c according to consistency of soil (Atterberg, 1911)	27
Table 3.3	The relative weight of observational and laboratory-determined parameters used to calculate RMR (after Beniaowski, 1989)	32
Table 3.4	Values of adjustment factors (after Romana, 1985)	33
Table 3.5	Stability classes as per SMR values (after Romana, 1985)	34
Table 3.6	Field estimates of uniaxial compressive strength of intact rock (after Hoek and Brown, 1997)	35
Table 3.7	Values of the constant M_i for intact sedimentary rock group (after Hoek and Brown, 1997)	36
Table 3.8	Details of satellite imageries used in the study	36
Table 4.1.1	Moisture content and Consistency limits	43
Table 4.1.2	Shear strength parameters of the soils obtained from direct shear test	44-45
Table 4.1.3	Results obtained from point load test	46
Table 4.1.4	Slope mass rating	46
Table 4.1.5	Input data and mode of failure in kinematic analysis	47
Table 4.1.6	Location of VES stations	53
Table 4.1.7	Layer parameters for the VES points	54
Table 4.2.1	Moisture content and Consistency limits	59
Table 4.2.2	Shear strength parameters of the soils obtained from direct shear test	60-61

Table 4.2.3	Results obtained from point load test	63
Table 4.2.4	Slope mass rating	64
Table 4.2.5	Input data and mode of failure in kinematic analysis	65
Table 4.3.1	Moisture content and Consistency limits	75
Table 4.3.2	Shear strength parameters of the soils obtained from direct shear test	76
Table 4.3.3	Results obtained from point load test	78
Table 4.3.4	Determination of UCS from point load strength index using conversion factor	79
Table 4.3.5	Slope mass rating	79
Table 4.3.6	Input data and mode of failure in kinematic analysis	82
Table 4.3.7	GPM precipitation data for the study area	86
Table 4.3.8	Layer parameters for the VES points	87

LIST OF FIGURES

		Page No.
Fig. 1.1	Location map	4
Fig. 1.2	Lineament map of Nagaland showing study area	6
Fig. 2.1	Concept of shear strength in direct shear test	17
Fig. 2.2	Geometric representation and stereo-plots of structural discontinuities for (a) planar failure (b) wedge failure and (c) toppling failure; ϕ is the angle of internal friction	20
Fig. 2.3	Resistivity and conductivity values of common rocks and minerals (Moombarriga Geosciences, 2009)	21
Fig. 3.1	Plasticity chart as per IS: 1498-1970	27
Fig. 3.2	Specimen shape requirement for irregular lump test	30
Fig. 3.3	Correction chart for point load strength test (Instrumentation & Technologies, Aimil Ltd., India, AIM-206-1)	31
Fig. 3.4	General chart for GSI estimates from the geological observations	35
Fig. 3.5	Schematic diagram for the Schlumberger array field method	37
Fig. 4.1.1	Location map of Officer's Hill colony study area	40
Fig. 4.1.2	Study area (yellow dotted line); arrow points to fault trace (Inset: Damaged highway)	41
Fig. 4.1.3a	Slope map	42
Fig. 4.1.3b	Officers Hill colony landslide map	42
Fig. 4.1.4	Plasticity chart	44
Fig. 4.1.5	Failure curves of samples	45
Fig. 4.1.6	a - Pole diagram; b - Contour diagram; c - Stereographic projection	47

Fig. 4.1.7	Rose diagram	47
Fig. 4.1.8	Google Earth image showing lineament and photo locations	48
Fig. 4.1.9	Bedded sandstones overriding silty shales	48
Fig. 4.1.10	Flexure folds on left of fault plane	49
Fig. 4.1.11	A - Sheared rocks; B - Weathered shale with sulphur leaching (bleached)	49
Fig. 4.1.12	Normal fault in the study area	50
Fig. 4.1.13	A - Near-vertical beds in the study area; B - Slickenside in the bedrock	51
Fig. 4.1.14	Fractured and shattered rocks on the western bank of the Sitsie Rü	51
Fig. 4.1.15	Field photograph showing condition of slope due to strike-slip fault (Inset: Slickenside on western bank of river)	52
Fig. 4.1.16	Field photograph showing subsidence on the eastern bank of the stream (Inset: A - Subsidence of highway; B - Retaining walls for road support)	52
Fig. 4.1.17	A - Loose debris constituting slope material; B - Debris flows on unstable slope	53
Fig. 4.1.18	House damaged due to differential settlement (Slip zone 1)	53
Fig. 4.1.19	2D image showing pseudo-section of VES stations with elevations	54
Fig. 4.1.20	2D image showing a pseudo-section of the area with VES stations	55
Fig. 4.1.21	Tension fractures in the lower elevations of the study area	55
Fig. 4.2.1	Location map	57
Fig. 4.2.2	Affected area along AH 1; (Inset - Water logged area)	58

Fig. 4.2.3	Plasticity chart	60
Fig. 4.2.4	Failure curves of samples	61
Fig. 4.2.5	Rock exposures of the studied slopes	62
Fig. 4.2.6a	Pole diagrams	65
Fig. 4.2.6b	Contour diagrams	65
Fig. 4.2.6c	Stereographic projections	65
Fig. 4.2.7	Rose diagrams	66
Fig. 4.2.8	Google Earth image showing lineaments and photo locations	67
Fig. 4.2.9	Toe erosion along Dzulikha Rü	68
Fig. 4.2.10	Jointed and fractured rocks on the western bank of Dzulikha Rü	68
Fig. 4.2.11	A - Tension crack developed on the slope; B - Road damaged due to subsidence	69
Fig. 4.2.12	Exposures of shale and clay along stream section	69
Fig. 4.2.13	A - Subsidence along the road section; B - Damaged house	69
Fig. 4.2.14	A - Slope material constituting clay deposits; B - Water seepages observed during dry season	70
Fig. 4.3.1	Geological map of the Kevüza study area; Profile along X-Y (on map) depicting surface before and after the landslide event and subsurface geology	71
Fig. 4.3.2	a Google Earth (GE) image of 2010 before landslide; b GE image of 2011 landslide (yellow broken line - boundary of affected area); c Unmanned aerial vehicle (UAV) image showing landslides of 2018; d UAV image showing landslide of 2019; e, f Photos of damaged portions of highway at locations S1 & S2 due to landslides in 2018; g Photo of repaired highway after 2019 landslide event	72

Fig. 4.3.3	Effects of the landslides - a Large fissure on the highway at the eastern edge of the slide zone; b Collapsed pylon (major support for power cables to Kohima)	73
Fig. 4.3.4	K1, K2, K3, K4 Rock exposures in the study area; 1, 2, 3, 4 Soil sampling sites for geotechnical analyses; V1, V2, V3, V4, V5 Vertical electrical sounding sites (Pink lines) for resistivity survey profiles	74
Fig. 4.3.5	Plasticity chart	76
Fig. 4.3.6	Failure curves of samples	77
Fig. 4.3.7a	Pole diagrams	81
Fig. 4.3.7b	Contour diagrams	81
Fig. 4.3.7c	Stereographic projections	82
Fig. 4.3.8	Rose diagrams	83
Fig. 4.3.9	Lineament map of the study area; Red line within green circle represents resistivity survey lines VES 3 and VES 4 (see fig. 4.3.4)	84
Fig. 4.3.10[i]	Slickensides along fault planes	84
Fig. 4.3.10[ii]	g Blocks displaced due to thrusting; h Slickensides along fault plane; i Steeply inclined beds thrust (red arrow) over younger rocks; j Waterfall along exposed scarp of normal fault	85
Fig. 4.3.11	Outcrop of intensely folded and sheared rocks (See fig. 4.3.9)	85
Fig. 4.3.12	Precipitation curves showing peak values and landslide occurrences	87
Fig. 4.3.13	Apparent resistivity curves showing an inferred fault	88
Fig. 4.3.14	Interpreted resistivity and pseudo cross-sections	89
Fig. 5.1.1	Previous mitigation measures in the weak zone (Inset: A - Landslide during 2005; B - Needle pine plantation; C - Open fissures)	92

Fig. 5.1.2	Mitigation measures taken up during 2005-06 (Inset: A - Soils dumped along the highway; B - Chute damaged)	93
Fig. 5.1.3	Perforated pipes for subsurface use (Representational)	94
Fig. 5.1.4	Used tyres forming a protective wall against toe erosion (Representational; Source: Mr. Sukho Movi)	95
Fig. 5.1.5	Wire-mesh slope protection / Cable-net slope protection (Representational)	96
Fig. 5.2.1	Storm drain baffle	98
Fig. 5.2.2	Check dam	98
Fig. 5.3.1	Typical French drain (Source: https://northwestdrainage.com/wp-content/uploads/2020/09/northwest-french-drain-seattle-redmond-everett-drains.jpg)	100
Fig. 5.3.2	Dewatering by Sump pumping method	101
Fig. 5.3.3	Road made functional in Slide zone 1 - (A) Structures built with scrap tyres; (B) Upper and lower slopes temporarily stabilised using bamboo piles (Photo date: 10.04.2019)	101
Fig. 5.3.4	Crib wall retaining structure made of bamboo (Source: Rauch et al., 2002)	102

PARTICULARS OF THE CANDIDATE

NAME OF THE CANDIDATE	: Mr. C. Nokendangba Chang
DEGREE	: Ph.D
DEPARTMENT	: Geology
TITLE OF THE THESIS	: Slope stability studies of some weak zones between Hospital colony and Jotsoma bypass, Kohima, Nagaland
DATE OF ADMISSION	: 10 th September 2015
APPROVAL OF RESEARCH PROPOSAL	: 10 th September 2015
REGISTRATION NUMBER & DATE	: 753/2017 (10.09.2015)
EXTENSION OF Ph.D REGISTRATION PERIOD	: 10.09.2020 to 09.09.2021 (Enclosed)

Head of the Department

CONTENTS

	Page No.
Declaration	i
Certificate	ii
Acknowledgement	iii-iv
List of tables	v-vi
List of figures	vii-xi
Particulars of the candidate	xii
 CHAPTER 1 INTRODUCTION	 1-8
1.1 Location of the area	4-5
1.2 Geomorphology	5
1.3 Climate and rainfall	5
1.4 Drainage	5-6
1.5 Geological setting	6-7
Disang Group	7
Barail Group	7-8
1.6 Objectives	8
 CHAPTER 2 LITERATURE REVIEW	 9-22
2.1 Introduction	9
2.2 Classification of landslides	9-11
Falls	10
Topples	10
Slides	10
Flows	10
Creep	11
2.3 Previous studies	11
2.4 Geological parameters	11-14
Slope Morphometry	11-12
Hydrogeology	12

	Structure and lineaments	12-13
	Lithology	13
	Rainfall	13-14
2.5	Geotechnical parameters	14-17
	Moisture content	14
	Atterberg limits	14-16
	Liquid limit	15
	Plastic limit	15
	Shrinkage limit	15-16
	Shear strength parameters	16-17
	Types of shear tests based on drainage conditions	16
	<i>Unconsolidated undrained test</i>	16
	<i>Consolidated undrained test</i>	16
	<i>Drained test</i>	17
	<i>Direct shear test</i>	17
2.6	Rock mass rating and Slope mass rating	17-19
2.7	Kinematic analyses	19-21
	Plane failure	19
	Wedge failure	19-20
	Toppling failure	20-21
	Identification of mode of failure	21
2.8	Electrical resistivity tomography (ERT)	21-22
	Goelectric analysis for prediction of inferred faults	22
2.9	Factor of safety	22
CHAPTER 3	METHODOLOGY	23-39
3.1	Geotechnical parameters of soil	23-29
	Sample preparation	24
3.1.1	Atterberg limits	24-28
	Liquid limit	24-25
	<i>Casagrande method</i>	24-25
	<i>Cone penetrometer method</i>	25
	Plastic limit	25
	Index properties	25-27
	<i>Plasticity index</i>	25-26

	<i>Liquidity index</i>	26
	<i>Consistency index</i>	26-27
	Plasticity chart	27-28
	Shrinkage limit	28
3.1.2	Shear strength of soils	29
3.2	Rock mass rating and Slope mass rating	29-34
3.3	Kinematic analyses	34-36
3.4	Structural analyses	36
3.5	Electrical resistivity tomography	37-39
3.6	Analysis of Factor of safety	39
CHAPTER 4	RESULTS AND DISCUSSIONS	40-90
CHAPTER 5	CONCLUSIONS AND RECOMMENDATIONS	91-102
	REFERENCES	103-121
	BIO-DATA OF THE CANDIDATE	122

CHAPTER 1

INTRODUCTION

Landslides are down-slope movements of rocks, debris, or earth along a slide plane due to the influence of gravity. They are characterised by almost permanent contact between the moving masses and slide plane (Butler, 1976; Varnes, 1978; Crozier, 1984; Cruden, 1991; Smith, 1996). Landslides are worldwide problems that cause substantial economic, human, and environmental losses (Zêzere et al., 2008; García-Ruiz et al., 2010; Jenelius and Mattsson, 2012; Petley, 2012; Winter et al., 2016). They are primarily associated with mountainous terrain where activities such as surface excavations for highways, buildings, etc. take place (Uribe-Etxebarria et al., 2005; Turner and Schuster, 2006; Siddique et al., 2017). They are classified according to their mechanism (movement type), nature of displaced material (material type) or on their activity (state, distribution, style), which is the rate of development over a period of time (Cruden and Varnes, 1996). Different phenomena cause landslides, including intense or prolonged rainfall (Ding et al., 2010; Sengupta et al., 2010; Aier et al., 2012; Duc, 2012; Chandrasekaran et al., 2013; Lee et al., 2014; Aristizábal, 2015; Iverson and Ouyang, 2015; Iadanza et al., 2016; Umrao et al., 2016; Roccati et al., 2018; Senthilkumar et al., 2018; Dou et al., 2019), earthquakes (Gorum et al., 2011; Hadi et al., 2018; Roback et al., 2018; Strupler et al., 2018), rapidly melting snow (Cardinali et al., 2000; Nishii et al., 2013; Trandafir et al., 2015), and a variety of human activities (Vanacker et al., 2003; Knapen et al., 2006; Meusburger and Alewell, 2008; Laimer, 2017; Rahman et al., 2017; Cui et al., 2019). Landslides involve flowing, sliding, toppling, or falling movements; many exhibit a combination of two or more types of movement (Varnes, 1978; Crozier, 1986; Cruden and Varnes, 1996). Landslides are one of the most common events in mountainous terrain because of the physiographic setup and triggering factors as well as influence by geomorphic features such as slope (Crosta et al., 2013; Havenith et al., 2015), drainage (Korup, 2004; Korup et al., 2007) and structure (Agliardi et al., 2001; Kellogg 2001; Badger, 2002; Ambrosi and Crosta, 2006; Aksoy and Ercanoglu, 2007; Kojima et al., 2015; Park et al., 2016). Increased construction activities in such terrain have resulted in more frequent occurrence of landslides in recent times.

Rocks and soils undergo deformation due to the presence of water (Lim et al., 1996; Matsushi et al., 2006; Trandafir et al., 2008; Pellet et al., 2013; Senthilkumar et al., 2018; Cai et al., 2019; Li and Wang, 2019). It is because water exerts a lateral pressure on the mass that changes are brought about in the form of size, shape, and volume of the material. Various types of movements are also indicated due to swelling, shrinkage, or differential settlement. Slide affected areas and slopes usually have unconsolidated overburden and disturbed bedrock which allow easy access of percolating waters to saturate the slope-forming material and cause instability (Li et al., 2016; Sun et al., 2016; Gofar and Rahardjo, 2017; Yang et al., 2017; Watakabe and Matsushi, 2019). In the regolith and deeply jointed bedrocks, water from rainfall or surface runoff has a very high infiltration rate.

Land use practice and land cover also influence hill slope stability as these factors control the rate of weathering and erosion of the underlying rocks (Karsli et al., 2009; Reichenbach et al., 2014; Galve et al., 2015; Chen et al., 2019; Meneses et al., 2019). The response of the slope material relies primarily on ground permeability, therefore, granular soils tend to react to short duration intense rainfall events whereas clayey material are normally more sensitive to precipitation of long duration and moderate intensity. The decisive quantity of precipitation necessary to determine slope failure depends on the morphology of the slope, the mechanical and hydrological properties of the soil and the vegetation cover (van Asch et al., 1999).

Unplanned excavations of rock slopes for construction, rapid expansion of hydropower projects, poor road construction practices without proper understanding of the geological or geotechnical details of the rocks and soils decreases slope stability (Gorsevski et al., 2006; Kainthola et al., 2012; Singh et al., 2013). In this regard, geotechnical investigations and kinematic analyses can be of great assistance for better understanding of such issues. They are performed to evaluate soil and rock conditions that normally affect safety, cost effectiveness and design of structures, and for execution of proposed developmental works. Such studies use principles of soil and rock mechanics and joint analyses to investigate subsurface conditions and materials, determine relevant mechanical properties of these materials, evaluate stability of natural and man-made slopes, assess risks posed by site conditions, and design earthworks and structural foundations.

Geohazards such as landslides, earthquakes, etc. are common problems in north east India, which can be attributed to the complex geomorphic and tectonic

setting of the region. Nagaland is located in the extreme northeast of the Indian subcontinent bordering Myanmar. It lies between 25°11'12.09" and 27°02'8.74"N latitudes and 93°19'22.40" and 95°15'22.95"E longitudes. It occupies an area of 16,579 sq. km. The state is made up of high hill ranges with low-lying alluvial tracts along the western margin bordering Assam.

Nagaland represents a tectonically complicated and relatively young, immature, mountainous terrain. It forms part of a highly dissected major mobile belt of the westernmost morphotectonic unit of the Burmese Orogen. This belt, which is believed to be still rising, continues to the north into the eastern Syntaxial Bend of the Himalaya. To the east, lie the central lowlands of Myanmar and on the west, are the Karbi Anglong Precambrian massifs and Brahmaputra trough. The eastern margin represents part of the subducting Indian Plate beneath the Burma microplate. The subduction process that began during the Cretaceous is believed to be continuing (Nandy, 1976; Bhattacharjee, 1991). Aier (2005) discussed slope failure in parts of Kohima town and its environs and maintains that active tectonism in the region is responsible for the recurrence of slides over ~8-year intervals. Verma (1985) is of the view that intermittent release of tectonic stresses is responsible for the frequent earthquakes in the region. Sahu et al. (2006) have shown surface movements of ~36 mm/year along certain fault planes in the region. Kumar and Sanoujam (2007) have proposed movements of 3.9 mm/year along the Churachandpur-Mao Thrust based on GPS studies. Aier et al. (2011a), Longkumer (2019) and Moiya et al. (2019) have shown the effects of neotectonism in the region from their studies of the Quaternary sediments of parts of Nagaland. Aier et al. (2012) inferred the effects of tectonism in the region based on their studies of a major landslide near the study area. Intense and continuing tectonism is therefore attributed for the occurrence of large scale folding, jointing, fracturing, shearing, and faulting of the rocks in this geodynamically sensitive region. High intensity of rainfall and various geomorphic processes have further weakened the rocks through weathering and erosion, thereby causing large scale surface instability.

Kohima town is situated in the southern part of the state and is the capital city of Nagaland. The township occupies an area of about 17.5 sq. km with a population of 2,70,063 (Source: Census of India, 2011). The nearest rail head and airport are located at Dimapur, about 70 km west of Kohima. As per Khatsu and Van Westen (2004),

Kohima town is considered tectonically unstable as it lies in the seismic zone V which is liable to seismic intensity IX.

1.1 Location of the study area

The study area is located in the west of Kohima town and is incorporated in the Survey of India (SoI) topographic sheet no. 83K/2/NW and lies between $25^{\circ}39'30''$ - $25^{\circ}41'30''$ north latitudes and $94^{\circ}03'30''$ - $94^{\circ}06'00''$ east longitudes. Three major slope instabilities that has consistently plaque the study area for several decades that are located in the Officer's Hill colony, Merhülietsa colony and Kevüza area along Asian highway 1 (AH 1), has been identified for thorough investigation (Fig. 1.1).

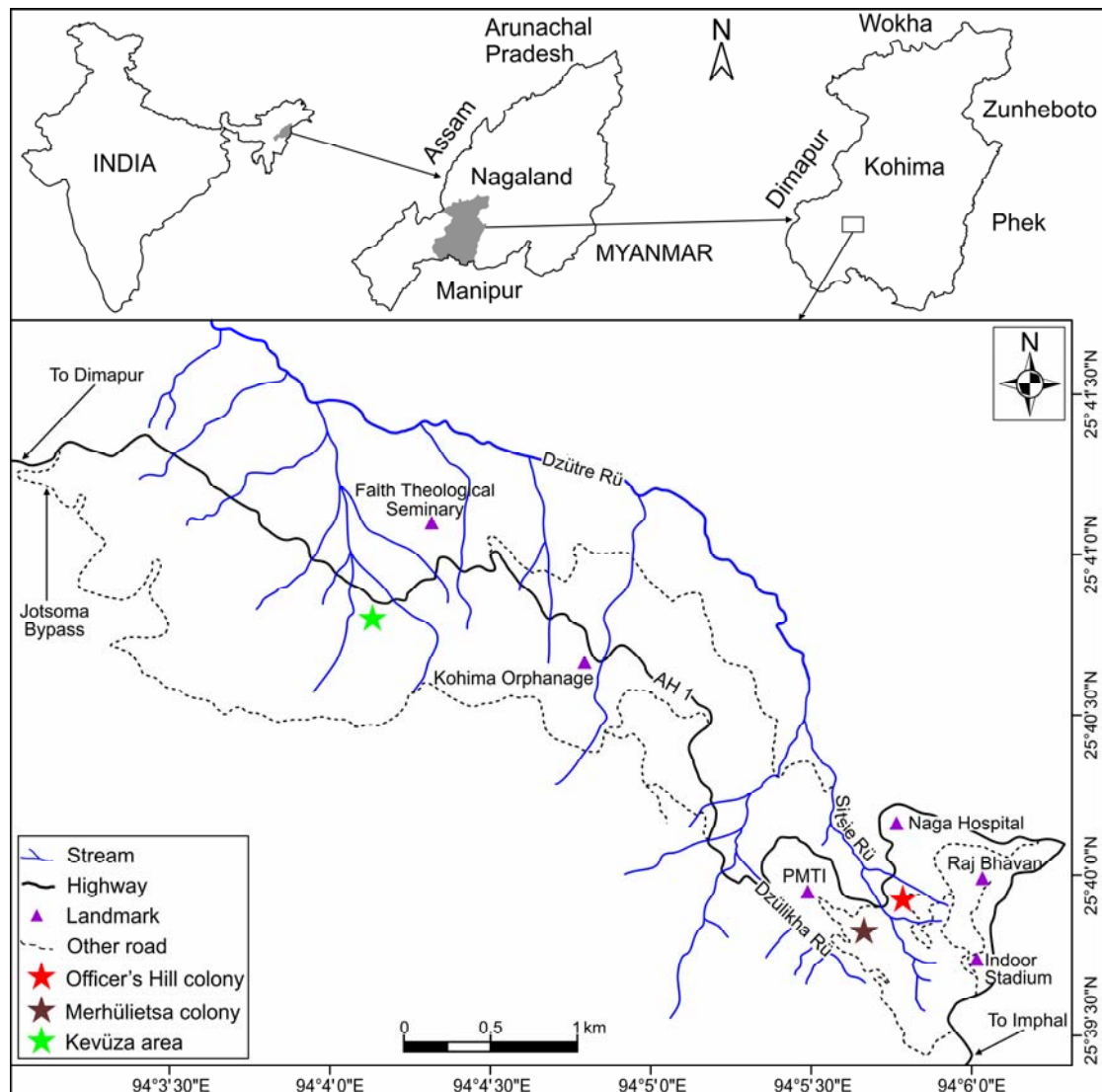


Fig. 1.1: Location map

The AH 1 which serves as the major supply route to most parts of Nagaland and Manipur runs through this area. It is part of the trans-Asian highway connecting India to the Southeast Asian countries through Myanmar. About 7.5 km stretch of the highway is encompassed in the study area.

1.2 Geomorphology

Kohima represents a rugged topography of highly dissected denudational hills, steep cliffs, narrow valleys and deep gorges. Mount Japfü is the highest peak with 3014 m and is located in the southern part of Kohima town. The hill ranges trend approximately NE-SW and are more or less parallel to each other. The western part of Kohima district is made up of low to moderate hills composed of sandstone, siltstone, shale, and mudstone. The northern central portion of the district is made up of high, linear structural hills and narrow valleys composed of semi-consolidated rocks. The southern central portion of the district is made up of curvilinear and irregularly shaped denuded structural hills with small valleys that are composed of hard compact sandstone, siltstone and shale. Kohima town lies at an average elevation of 1444 m above mean sea level (msl).

1.3 Climate and rainfall

The average annual rainfall of Kohima ranges between 1634 and 1817 mm, which falls in moderately high rainfall zone (Kusre and Singh, 2012). The minimum annual rainfall of 1075.6 mm recorded in Kohima was in 1985 and maximum of 2616.1 mm in 1993 (Directorate of Soil & Water Conservation, Nagaland). Kohima receives the highest rainfall during August and September, which is contributed by the southwest monsoon. The area enjoys a temperate climate with temperatures ranging from ~28°C in summer to ~6°C in winter.

1.4 Drainage

The drainage patterns in Kohima are mostly structurally controlled by joints and fractures through which groundwater in the area discharge. They are narrow, deep and asymmetrical. The study area is characterized by parallel drainage patterns comprising mostly 1st and 2nd order streams. Two minor streams, Sitsie Rü and Dzülíkha Rü along with several other tributaries merge into the major river Dzütë

Rü, in northwest. These highly erosive streams discharge abundant water during the monsoon.

1.5 Geological setting

Nagaland is a part of the northern extension of the Arakan-Yoma ranges representing orogenic upheavals during the Cretaceous and Tertiary. The region represents a fairly young mobile belt, which is subjected to orogenic/tectonic upheavals during different phases, mostly during the Tertiary. Nagaland is classified into four major morpho-tectonic divisions from west to east, i.e., Belt of Schuppen (BoS), Inner Fold Belt (IFB), Naga Hills Ophiolite and the Naga Metamorphics, which exhibit diverse structural parameters distinct from each other. The study area, lying at the northern edge of the Kohima Synclinorium, is part of the IFB of Nagaland (Fig. 1.2).

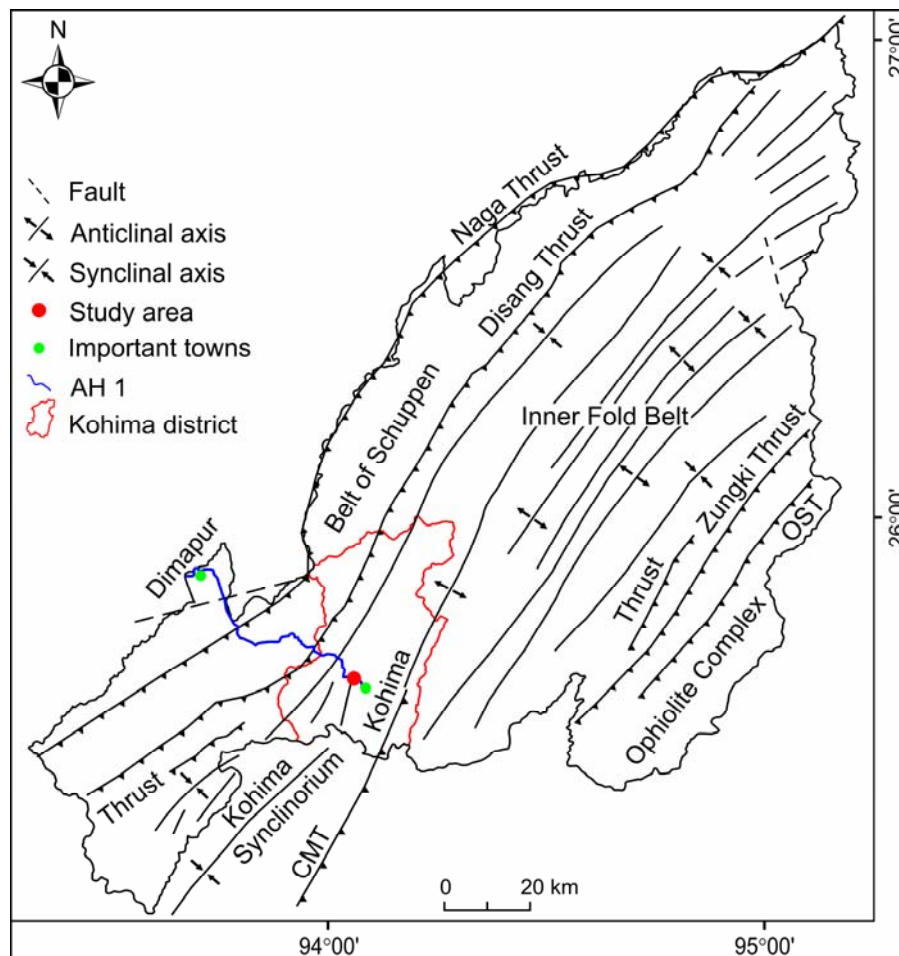


Fig. 1.2: Lineament map of Nagaland showing study area; modified after Nandy (2000) and Geological Survey of India (2011); CMT - Churachandpur-Mao Thrust; OST - Ophio-Sedimentary Thrust

The subduction of the Indian Plate beneath the Burma microplate has led to a NW-SE compression. The major lineaments of Nagaland trend approximately NE-SW, which is in agreement with the NW-SE compression. Thus, all compressional structures such as folds and reverse faults are parallel to the regional NE-SW trend. Tensile fractures and normal faults have developed parallel to the NW-SE compressional stresses. The region suffered three deformational episodes (F1, F2, F3), but only two of the post-collisional features (F2, F3) are imprinted in the rocks. The F₂ movements are responsible for thrusting in the region. The F₃ movements are attributed to ongoing Pliocene-Quaternary movements that have caused the development of minor folds and strike slip faults. The F₃ movements are responsible for numerous neotectonic signatures in the region, including the high degree of deformation of the rocks of the study area (Roy et al., 1986).

The study area is made up of rocks belonging to the Disang and Barail Groups of Eocene and Oligocene ages respectively (Mathur and Evans, 1964; Directorate of Geology and Mining, Nagaland, 1978). The Disang Group makes up the bulk of the rocks of study area. These are overlain by the Barail Group.

Disang Group

The Disang Group occupies a large area of the IFB. The Disang is predominantly represented by splintery shales, which are grey, khaki grey, or black in colour, with sandy and silty interbands at places, and thin, hard, interbedded sandstones. The formation is shaly towards the basal part while sandstone layers are more abundant higher up. The Disang shales are prone to spheroidal weathering and development of concretions. Shale pellets are seen parallel to the bedding (Devdas and Gandhi, 1985; Sarma, 1985). The contact of sandstone with shale is very sharp. The former stands out as prominent bands within the weathered shales.

Barail Group

The Barail Group is represented by the Laisong, Jenam, and Renji formations in the Assam Shelf, BoS, and IFB. They consist of medium grained sandstones with intercalations of shale. The Laisong Formation is exposed in the western part of Kohima. Kohima town consists essentially of folded and thrustured piles of monotonous shaly sequences of Disang flysch. The synclinal cores contain some Barail molasse. There exists a lithological gradation between the shaly sequence of the Disang Group

and the sand-dominated units of the Barail Group. The broad structural setup of this belt shows NNE-SSW trending folds which are generally open towards the west, but become tightly compressed towards the eastern boundary with the ophiolites. Folds in the arenaceous rocks of the Barail Group tend to be symmetrical and often form broad, open warps (Verma and Yedekar, 1983).

1.6 Objectives

The study area is marked by chronic slope instability, specially in the three locations, for many decades. The destruction of houses not only displaced many families, the regular obstruction of vehicular movement has caused huge economic losses, shortage of food and essential commodities, and immense hardship to travellers. This study therefore aims to -

- determine the mechanical properties of soils and rocks
- identify the possible modes of failure
- suggest preventive and/or mitigation measures

CHAPTER 2

LITERATURE REVIEW

2.1 Introduction

Landslide is a geological phenomenon that involves gravitational movement of rock, earth, or debris down a slope. Rockfalls, deep failure of slopes, and shallow debris flows are common types of ground movements. Gravity is the primary driving force of landslides other than the natural and anthropogenic factors. Major natural events (e.g. earthquakes, volcanic eruptions and cloud bursts) and anthropogenic activities (e.g. urbanization, deforestation and agriculture) have been attributed for landslide incidences in the past few decades.

2.2 Classification of landslides

Landslide classification is considered an important primary step to scientific investigation of landslides (Crozier, 1984; Msilimba, 2002). A classification is designed to reduce the multitude of different, but related phenomena to a few easily recognisable and meaningful groups on the basis of common attributes (Crozier, 1984). A summary of the criteria for landslide classification was given by Varnes (1978), and Cruden and Varnes, (1996) (Table 2.1). Landslide classifications were also given by Campbell (1951), Zaruba and Mencl (1969), Crozier (1973), Hutchinson (1978), Coch (1995), and Smith, (1996).

Table 2.1: Landslide classification according to Cruden and Varnes (1996)

Type of Movement		Type of Material		
		Bedrock	Engineering soils	
			Predominantly coarse	Predominantly fine
Fall		Rock fall	Debris fall	Earth fall
Topple		Rock topple	Debris topple	Earth topple
Slide	Rotational	Rock slump	Debris slump	Earth slump
	Translational	Rock slide	Debris slide	Earth slide
Spread		Rock spread	Debris spread	Earth spread
Flow		Rock flow	Debris flow	Earth flow (soil creep)
Complex		Combination of two or more types of movement		

Falls

Falls normally involve the free movement of rock material down steep slopes, with no permanent contact of the moving material to the slope surface (Crozier, 1984; Bryant, 1991; Alexander, 1993). The movement is turbulent and the reach of the rockfall is in close relation to the angle of internal friction of the moving material, and is defined by the energy line (Bryant, 1991).

Topples

Topples involve the outward rotation (or inward buckling and basal collapse) of angular blocks or rock columns that become detached from cliffs (Crozier, 1984; Alexander, 1993). These blocks or columns are usually defined by the intersection of joints or other fractures, and their basal stability is often disturbed by erosion (Ludman and Koch, 1982).

Slides

Slides are down-slope movements of rock and soil along a slip surface that are characterised by almost permanent contact between the moving mass and the slide surface (Crozier, 1984; Bryant, 1991; Alexander, 1993; Smith, 1996). The most common subgroups are *translational* and *rotational* slides. Translational slides are relatively flat, planar movements along surfaces. They generally have pre-existing slide planes that are activated during the slide event. In contrast, rotational slides have a curved surface of rupture and produce slumps by backward slippage (Alexander, 1993; Smith, 1996).

Flows

Flows are down-slope movements of fluidised soil and other materials acting as viscous masses. In a flow, the structure of the material changes into a quasi-fluid (Johnson and Rodine, 1984; Bryant, 1991). The most common type of flow is the debris flow (Corominas et al., 1996). It is the most dangerous type (Takahashi, 1991) due to the fact that debris flows often extend far beyond their sources, and their depositional areas often include inhabited sites. Other categories include solifluction, mudflows and debris avalanches (Coch, 1995).

Creep

One of the least destructive mass movement phenomena is *soil creep*, which tends to be slow, superficial, and predominantly seasonal (Hutchinson, 1978; Crozier, 1984; Alexander, 1993). However, many of the other forms of landslides initially start as creep to gradually cause serious damage.

2.3 Previous studies

Past workers on land instability of Nagaland include Sondhi (1941) who made the first attempt on landslide studies along the Dimapur-Manipur road. Slope classification maps of Kohima town and geotechnical reports were prepared by Sharda and Bhambay (1980). Some of the landslides of Kohima town were studied by Lotha (1994). Bhattacharjee et al. (1998) studied portions of the NH 39. The Central Road Research Institute (CRRI, 2000a) commented on some weak zones between Chumukedima and Maram. Aier (2005), Walling (2005), Sothu (2009), Supongtemjen (2013), and Khalo (2016) also carried out slope stability studies in and around Kohima town and the AH 1 and prepared landslide hazard zonation maps, and suggested remedial / mitigation measures. Jamir (2013) analysed slope stability and prepared a landslide susceptibility map of Mokokchung town. Kemas et al. (2004), Aier et al. (2005), Walling et al. (2005), Singh et al. (2008), Aier et al. (2009a), Aier et al. (2009b), Sothu et al. (2009), Aier et al. (2011b), Jamir et al. (2011), Sothu et al. (2011), Aier et al. (2012), Supongtemjen and Thong (2014), Supongtemjen et al. (2015), Khalo et al. (2016) and Walling et al. (2016) added to landslide literature of the region by their studies of surface instability in and around Kohima town.

2.4 Geological parameters

Slope morphometry

Slope morphometry includes the study of slope angles and relative relief of the area. An estimated 81% of landslides have occurred on slopes greater than 30°. Debris flows can occur on slopes greater than 30°. This is a lower limit that is somewhat shallower than slopes on which debris slides are generated (Terzaghi, 1950). The relative relief is a measure of the ruggedness of the terrain.

According to Piteau and Peckover (1989), the safety factor for a slope is the ratio of the sum of resisting forces that act to prevent failure to the sum of the driving forces that tend to cause failure. Unstable slopes involve downward and outward

movement of material. This is usually due to high pore pressure and large slope deformations in the terrain (CRRI, 2000b). Failure of natural slopes removes vegetation, thereby exposing the surface to further erosion (Choubey and Lallenmawia, 1987). Natural slopes become steeper when converted to cut slopes for construction of roads, bridges, dams and several other engineering structures (Das et al. 2010; Vishal et al. 2010). These slopes become more vulnerable to failure when proper scientific methods are not adopted.

Hydrogeology

Drainage is a function of slope, lithology, structure, weathering, soil content, vegetation and rainfall. During the dry season the groundwater table falls, so most areas are dry. However, certain areas are perennially wet, indicating high water tables. The high water tables indicate high absorption and very low drainage in such area, which causes water logging. During the monsoon however, most parts of Kohima town receives heavy rainfall and resulting infiltration to the soils bring up the water table. Some landslides in Kohima are triggered due to toe erosion by streams. However, majority of instability occurs on free slopes where the influence of streams is not the main causative factor (Walling, 2005).

Groundwater flow in clay-bearing rocks such as shales, intensify the rate of weathering process in the form of physical and chemical alteration. Shales which possess high total porosity but low effective porosity and permeability allows water to retain in the pores thereby leads to development of hydrostatic pressure (Singh et al., 2016).

Structure and lineaments

As described by Fookes et al. (1966) and Varnes (1978), geological and structural settings along the slopes play a key role in mass wasting processes. In slope deformation, favourable structures are characterized by a certain arrangement of rocks complexes, especially if they occur along slopes or ridges of local topography (Kandpal and Pant, 1995). The most important geologic discontinuities that affect slopes include bedding planes, joints and faults. Some authors have considered these structural features an important aggravating factors of landslides (Agliardi et al., 2013; Galeandro et al., 2013; Doglioni and Simeone, 2014).

Water infiltration along joints and bedding planes are commonly responsible for rock failures such as shale which has the tendency to swell in presence of water, and thereby exerting pressure in joints that are filled with clay. Tectonic fracturing of rocks may lead to deep fractures below the ground surface which can cause extensive damage of the rocks, as well as brittle and plastic deformation (Zischinsky, 1969; Ambrosi and Crosta, 2006; Willenberg et al., 2008; Jaboyedoff et al., 2011, 2013).

Numerous researchers have studied on the impact of faults on landslide and provided strong correlation between them (Densmore et al., 1997; Chen et al., 2014; Bucci et al., 2016; Carlini et al., 2016; Penna et al., 2016; Tsai et al., 2018). Sen et al. (2015) identified various types of movement in the form of debris flow, earth fall and rock slide located close to faults. A morphological reconstruction study in Tatun volcano group in northern Taiwan by Chang et al (2018) revealed landslide activity due to active normal faulting in the area. Chen et al (2019) studied on the influence of thrust faulting on deep-seated slope gravitational deformation based on the morpho-tectonic features, LiDAR derived DEM, aerial photographs and field observations.

Lithology

Different types of rocks and soils make up hill slopes. These rocks may be of different mineral assemblage with differing constituent strengths and bonds between minerals or rock grains. Probability of landslides are most common in fractured and weathered rocks. Weathering also greatly reduces the shearing strength resistance of rocks (Piteau and Peckover, 1989; Guo and Wang, 2017). The shear strength of a rock mass is also determined largely by the presence of the discontinuities as failure surfaces in rock masses tend to follow such pre-existing discontinuities. Clay minerals have a tendency to absorb and adsorb water on removal of the load. Water flows between clay causing large increases in volume and consequent reduction of the bonding forces between particles. Thus, clay studies are very important (Veder and Hilbert, 1980).

Rainfall

The relationship between climate and landslides has attracted much interest because rainfall is the most frequent landslide-triggering factor in many regions of the world (Corominas, 2001; Luino, 2005; Li et al., 2017; Roccati et al., 2019). The largest number of landslides occurs during and after long periods of relatively

continuous rainfall. Landslides occur more easily when the ground is damp and the water table is high. Areas with high mean annual rainfall are generally associated with abundant landslides. It has been noted that cloudbursts, particularly which occur in the rainy season, and those that follow prolonged wet spells, are the cause for some of the most damaging landslides in this region (Kemas et al., 2004; Thong et al., 2004; Aier, 2005).

2.5 Geotechnical parameters

Moisture content

The moisture content or water content (W_C) is defined as the ratio of the weight of water (w_l) to the weight of solid soil (w_d) in a given mass of soil. It is expressed as:

$$W_C = \frac{w_l}{w_d} \times 100 \quad (2.1)$$

The moisture content is generally expressed in terms of percentage. However, when formulae are used to give relationships between certain quantities, it may be expressed as fractions. The water content of a soil in its natural state is termed as *natural moisture content*. Knowledge of water content is necessary in soil compaction control, in determining consistency limits of soil, and for the calculation of stability of earth works and foundations.

Atterberg limits

The Atterberg or Consistency limits are a basic measure of the nature of a fine-grained soil. Depending on the water content of the soil, it may appear in four states as solid, semi-solid, plastic, and liquid. In each state, the consistency and behaviour of a soil is different and so are its engineering properties. Thus, the boundary between each state can be defined based on a change in the soil's behaviour. These limits were first proposed by Atterberg (1911).

In the remoulded state, the consistency of a clayey soil varies with the water content, which tends to destroy the cohesion exhibited by the particles of such soils. As the water content is reduced from a soil from the stage of almost a suspension, the soil passes through various states of consistency. The water contents at which the soil passes from one of these states to the next have been arbitrarily designated as Consistency limits, which include the liquid limit, plastic limit and shrinkage limit.

The consistency of a fine-grained soil is largely influenced by the water content of the soil. It helps in understanding the soil-water behaviour and consequently, its engineering properties.

Liquid limit

The liquid limit (W_L) is the water content corresponding to the arbitrary limit between the liquid and plastic states of consistency of a soil. It is the moisture content at which clay passes from the liquid to the plastic state. It is defined as the minimum water content at which the soil is still in the liquid state, but has a small shearing strength against flowing which can be measured by standard available means (Casagrande, 1932).

Plastic limit

The plastic limit (W_P) is the water content corresponding to an arbitrary limit between the plastic and the semi-solid states of consistency of a soil. Plasticity is the property of a soil which allows it to be deformed rapidly, without rupture, without elastic rebound, and without volume change. It defines the minimum water content at which a soil will begin to crumble when rolled into a thread. Plasticity is due to the presence of thin scale-like particles which carry electromagnetic charges on their surfaces.

Shrinkage limit

The shrinkage limit (W_s) is the arbitrary limit of water content at which a soil tends to pass from the plastic state to the semi-solid state of consistency, that is, it is the lowest water content between the semisolid and solid states. It can be defined as the maximum water content at which, a reduction in water content will not cause a decrease in the volume of the soil mass. When the moisture content exceeds the shrinkage limit of a soil, the soil will start swelling or change in volume, and the soil will be in a semi-solid state. Upon further wetting it will enter the semi-liquid state and eventually cause subsidence in the area.

The shrinkage limit is useful for the determination of the swelling and shrinking capacity of soils. Most soils experience periodic swelling and shrinkage during alternating wet and dry seasons. Due to shrinkage, soils decrease in height by

subsidence. On wetting, the soil increases in volume by swelling, the cracks close, and soil level rises.

Shear strength parameters

The shear strength of soil is the resistance to deformation by continuous shear displacement of soil particles upon the action of a shear stress (Punmia, 1994). A good understanding of the nature of shearing resistance is necessary to analyse soil stability problems such as bearing capacity, slope stability, and lateral pressure on earth-retaining structures. Shear strengths of soils may be determined in the laboratory by various methods, including direct shear test and triaxial compression test.

Types of shear tests based on drainage conditions

Before considering any method, it is necessary to consider the possible conditions before and during the tests since results are significantly affected. A cohesion-less or coarse-grained soil may be tested for shearing strength either in dry or saturated condition. A cohesive or fine grained soil is usually tested in the saturated condition. Depending upon whether drainage is permitted before and during the test, shear tests on such saturated soils are classified as unconsolidated undrained test, consolidated undrained test and drained test.

Unconsolidated undrained test

Drainage is not permitted at any stage of the test, that is, either before the application of the normal stress or during the test when shear stress is applied. Hence, no time is allowed for dissipation of pore-water pressure and consequent consolidation of the soil; no significant volume changes are expected. Undrained tests are often performed only on soils of low permeability. This is the most unfavourable condition which might occur in geotechnical engineering practice and hence is simulated in shear testing. Relatively small time is allowed for the testing till failure.

Consolidated undrained test

Drainage is permitted fully in this type of test during the application of the normal stress, and no drainage is permitted during the application of the shear stress. Thus, volume changes do not take place during shearing, and excess pore pressure develops.

Drained test

Drainage is fully permitted at every stage of this test. The soil is consolidated under the applied stress and is tested for shearing by applying shear stresses very slowly. Practically no excess pore pressure develops at any stage while volume changes take place.

Direct shear test

In the direct shear test, a soil sample of square or circular cross-section is compacted in a shear box split into two halves and allowed to fail along a pre-determined plane (Fig. 2.1). A graph is plotted for the applied normal stress and the corresponding shear stress for at least three to four tests at different values of normal stress. From the graph, cohesion (c) and internal friction angle (ϕ) is evaluated, and from which the shear strength of the soil is computed.

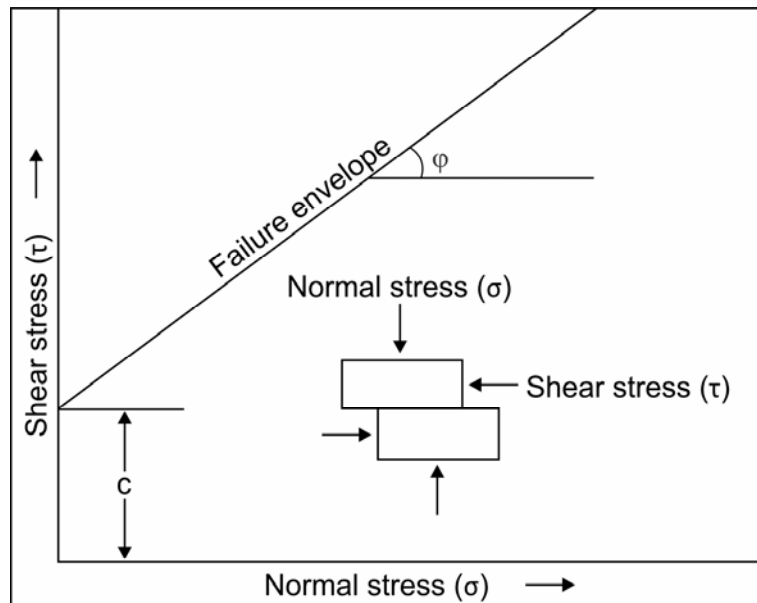


Fig. 2.1: Concept of shear strength in direct shear test

2.6 Rock mass rating and Slope mass rating

The rock mass rating (RMR) system is a geo-mechanical classification system for rocks developed by Bieniawski (1972, 1973). It combines the most significant geologic parameters of influence and represents them with one overall comprehensive index of rock mass quality.

The following five parameters are used to classify a rock mass using the RMR system:-

- a) Uniaxial compressive strength (UCS) of rock material
- b) Rock quality designation (RQD)
- c) Spacing of discontinuities
- d) Groundwater condition
- e) Condition of discontinuities

The rock strength can be determined can be carried out both in the field and laboratory using a Point Load Index Tester (PLIT) or a Schmidt's hammer. In PLIT, the rock sample is subjected to compressive stress between conical steel platens, until failure occurs. Depending upon the size and shape of test specimens, the point load index can be determined by diametral, axial, block or irregular lump tests.

The RQD was developed by Deere et al. (1967) which gives quantitative estimation of rock mass quality from drill core logs. RQD is core recovery that relies upon fracture frequency and softening of rock mass encountered during drilling. However, if the core drilling is not available, RQD can be estimated by volumetric joint count (J_v) using empirical relationship suggested by Palmström (1982),

$$RQD = 115 - 3.3J_v \quad (2.2)$$

where J_v is the sum of the number of joints per unit length for all joint (discontinuity) sets known as the volumetric joint count.

The stability of rock slopes is significantly influenced by structural discontinuities in rock in which the slope is excavated. A discontinuity is a planar surface that marks a change in physical or chemical characteristics in a soil or rock mass. Discontinuities such as orientation, persistence, roughness, and infilling are important properties in stability studies of jointed rock slopes. Persistence of discontinuities and their spacing together define the size of blocks that can slide from the face.

One of the important parameters for the assessment of stability conditions of a slope is groundwater condition. The presence of groundwater in the rock mass reduces the stability of the slopes by reducing the shear strength of potential failure surface. Water pressure in tension cracks or nearly vertical fissures reduces the stability by increasing the forces tending to induce sliding. Changes in water content of some rocks particularly shales can cause accelerated weathering with resulting decrease in its strength. Groundwater accounts for the influence of water pressure with particular reference to underground excavations.

The roughness of a joint surface is a measure of the inherent unevenness and waviness of the surface of discontinuity relative to its mean plane. The friction angle of a rough surface comprises two components - the friction of the rock material (ϕ) and the interlocking produced by the irregularities of the surface.

The slope mass rating (SMR) is a quantitative method applied on rock masses to evaluate stability conditions of rock slopes. Romana (1985) made an important contribution in applying rock mass classifications to the assessment of stability of rock slopes. SMR is empirically obtained from RMR by adding adjustment factors for the discontinuity orientation.

2.7 Kinematic analyses

Kinematics refers to the geometrically-possible motion of a body without consideration of the forces involved. Kinematic analysis is concerned with the direction of movement. With respect to slope stability, kinematic analysis generally is used to evaluate whether blocks or masses of rock may move along geologic structures and slide out of the face of a slope.

Plane failure

Plane failure is a translational failure. It occurs when a mass of rock in a slope slides down along a weak plane (Fig. 2.2a). A planar failure will have the failure plane sub-parallel to the slope.

For plane failure to occur, a cell must have both strike and dip components. For the strike component, the strike of the slope is compared to the strike of the bedding. If the strikes are within 20 degrees of each other, then the cell is identified as strike critical. To analyse the dip component, the slope dip is compared to the apparent dip of the bedding. If the apparent dip is less than the slope dip, the cell is identified as dip critical. Where a cell is both strike critical and dip critical, it is an area of potential plane failure.

Wedge failure

Wedge failure is another translational failure. Failure of a slope in the form of wedge can occur when rock masses slide along two intersecting discontinuities, forming the wedge-shaped block, dip out of the cut slope at an oblique angle. The

plunge of two intersecting discontinuities lies within the shade portion and is less than the dip angle of the slope face, but greater than the friction angle of the slope material (Fig. 2.2b).

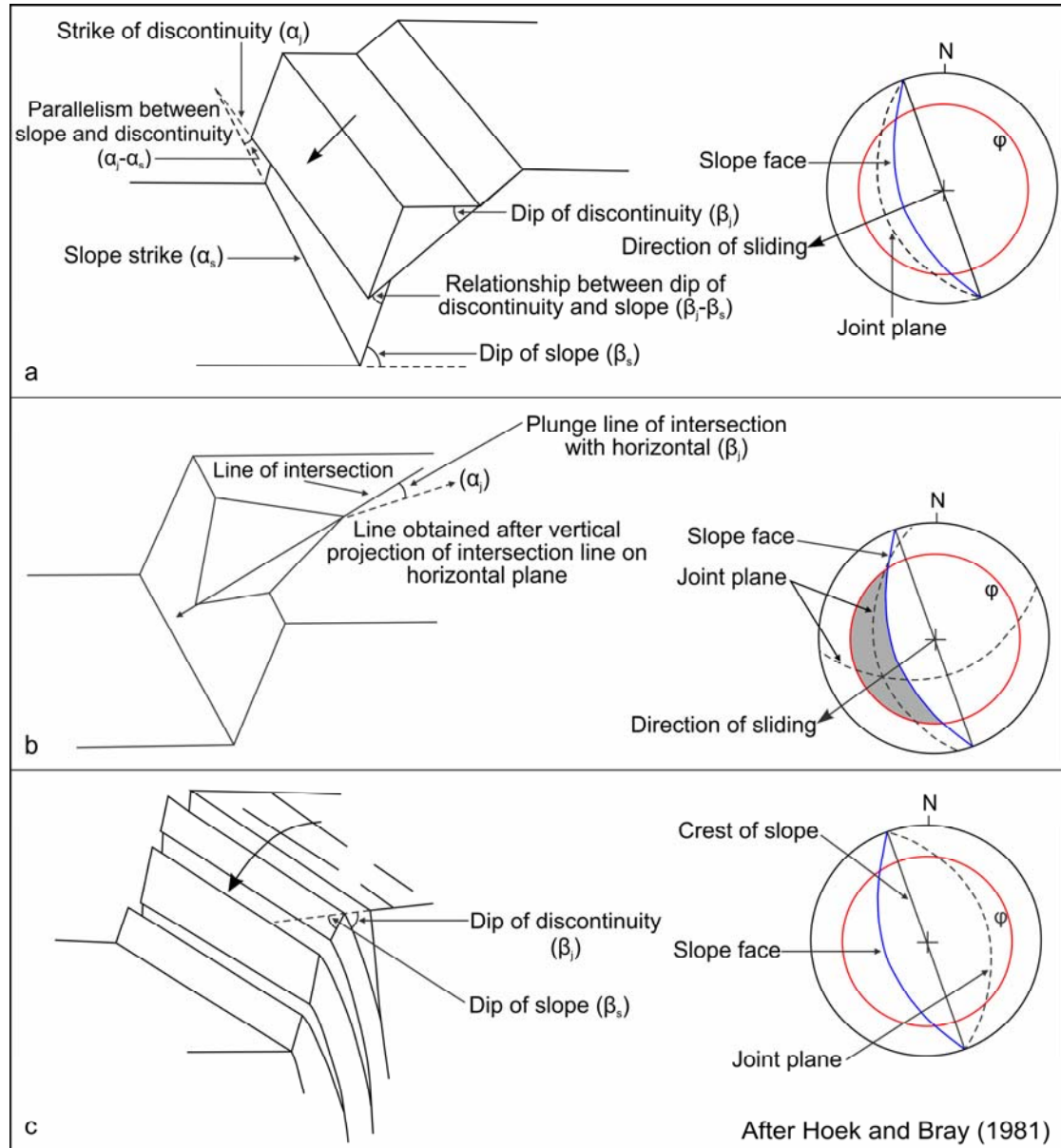


Fig. 2.2: Geometric representation and stereo-plots of structural discontinuities for (a) planar failure (b) wedge failure and (c) toppling failure; ϕ is the angle of internal friction

Toppling failure

Toppling is a failure in which the movement consists of forward rotation of a unit or units about a horizontal axis under the action of gravity and other forces. It

occurs when rocks along a slope are affected by closely spaced and steeply inclined discontinuities dipping into the slope (Fig. 2.2c).

Identification of mode of failure

The possible mode of failure is identified considering the type of slope materials involved in the slide. The geological materials can be broadly classified into two categories, the in-situ rocks and the overburden soil and debris. Rotational mode of failure is common in soil and debris, while translational and toppling modes of failures are common in in-situ rocks.

2.8 Electrical resistivity tomography (ERT)

The electrical resistivity method is based on the measurement and recording of changes in the mean resistivity or apparent specific resistance of various soils. The resistivity (ohm-meter) is usually defined as the resistance (ohm) between opposite faces of a unit cube (centimetre cube) of the material (Punmia, 1994). Each soil has its own resistivity depending upon water content, compaction, and composition; it is low for saturated silt and high for loose dry gravel or solid rock

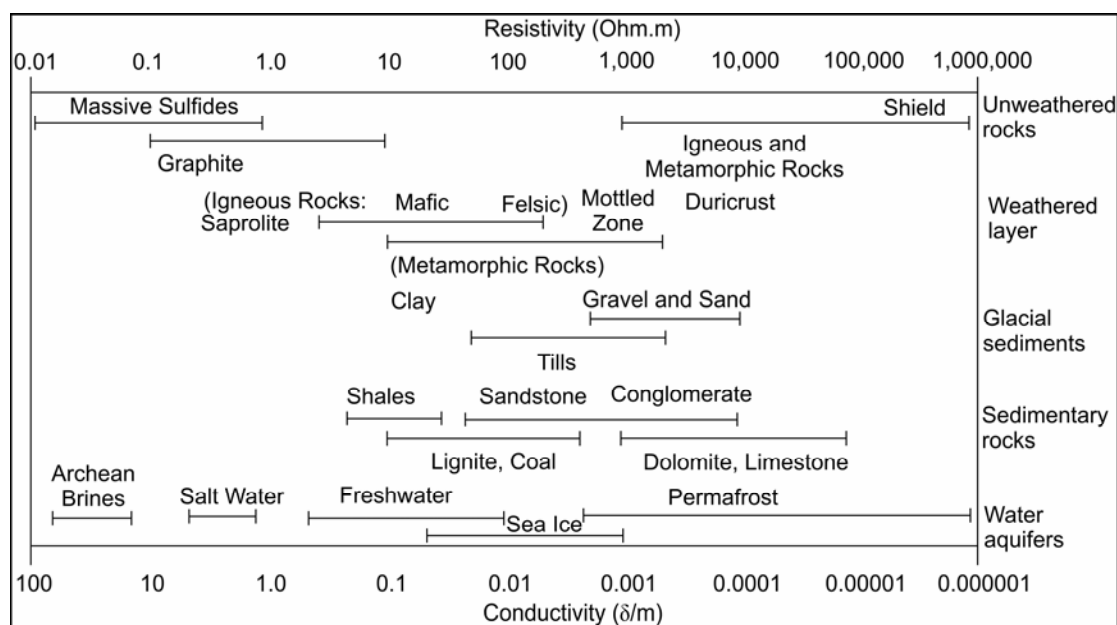


Fig. 2.3: Resistivity and conductivity values of common rocks and minerals; modified after Palacky (1987)

The resistivity of geological materials exhibits one of the largest ranges of all physical properties. There are a number of factors that influence resistivity. It is one

of the most variable material properties. Sedimentary rocks have low resistivity values due to high fluid content while igneous rocks tend to have high resistivity (Fig. 2.3).

Geoelectric analysis for prediction of inferred faults

In the determination of faults, it is important to observe changes in depth and thicknesses, and continuity or discontinuity of geological layers and evaluate the prospects of groundwater aquifers. Faults tend to follow certain trends, create permeability barriers, control the occurrence and flow of groundwater, and act as transmission routes for groundwater flow (Siddiqui and Parizek, 1971; Atre and Carpenter, 2010; Ammar and Kamal, 2018). Thus, the use of apparent resistivity helps in prediction of faults (Susilo et al., 2018). However, the difficulty in determining the expected locations of faults must be considered because of the restrictions in high accuracy measurements and interpretations. The final interpretation and output relies on available remote sensing, geological and hydrogeological data.

2.9 Factor of safety

The Factor of safety (FoS) describes the status of stability of a particular slope and is based on the concept of limiting equilibrium, that is, the condition at which forces tending to induce sliding are exactly balanced by those forces resisting. So, FoS can be defined as the ratio of total force available to resist sliding to total force tending to induce sliding:

$$FoS = \frac{\text{Total resisting force along plane of separation}}{\text{Total mobilizing force available to induce failure}} \quad (2.3)$$

When the slope is on the verge of failure, a condition of limited equilibrium exists in which the resisting and driving forces are equal, and in this condition it is considered that FoS=1. When the slope is stable, the resisting forces are greater than destabilizing forces, that is, FoS>1. Following the same logic, slopes with FoS<1 are unstable. Once the mode of failure and shear strength parameters are obtained, stability equations are worked out analytically by considering the resisting and mobilizing forces along the discontinuity to determine the FoS of that particular slope.

CHAPTER 3

METHODOLOGY

Thematic and metric information are extracted with the help of Survey of India (SOI) topographic sheets and remotely sensed data for input in Geographical Information System (GIS). The SOI topographic map No. 83 K/2/NW of scale 1:5,000 (1970-71 survey) was used as reference for Officer's Hill and Merhülietsa colony, and 1:25,000 (1982-83 survey) was used for Kevüza area. For preparation of thesis, input information was manually digitised and maps generated in ArcGIS 10.5 software. Besides satellite imageries, UAV (Unmanned Aerial Vehicle) mapping was carried out for detailed study in Kevüza area using a drone (DJI Phantom 4 Pro⁺). However, this could not be carried out in the other two study areas due to security reasons. A contour map was prepared on 1:500 scale with 50 cm contour interval using total station in the Officer's Hill colony. The buildings in the study area were translated onto the contour map from Google Earth (GE) imagery. A slope map was prepared from the contour map to classify slopes into five categories such as very gentle (0°-15°), gentle (16°-25°), moderate (26°-35°), steep (36°-45°) and very steep (>45°) following Bureau of Indian Standards - IS: 14496-2 (1998). Satellite-based precipitation data obtained from the Global Precipitation Measurement (GPM) mission has been used (Kirschbaum and Stanley, 2018) for the assessment of the landslides in Kevüza area.

3.1 Geotechnical parameters of soil

Soil samples were randomly collected from different sites of the study area. About 10 kilogram of samples was extracted with the help of a trowel, from pits excavated to depths devoid of organic matter. Small portions of samples were collected in a container and weighed in the field itself with the help of a portable weighing instrument. These were further analysed in the laboratory to determine the moisture content of the soil.

Sample preparation

Sample preparation was carried out in accordance with the American standards (ASTM D421-85, 2007). Soil samples were spread out and allowed to dry for a number of days depending on the amount of moisture content in the soil. The dried soil samples were pulverised and fractions passing through ASTM sieve no. 40 (425 μm) were used to determine the Atterberg limits, while those passing through ASTM sieve no. 10 (2 mm) were used for direct shear tests. For the experimental purpose, distilled water was used as the mixing substance. The purpose of using distilled water is that, it eliminates the risk of reaction with minerals present in the soil and hence minimise the risk towards the accuracy of the experiment. For consistency limit tests, soil in the mixed state is left for sufficient time (at least 24 hours) to ensure uniform moisture distribution.

Moisture content of the soils were determined by oven dried method. The initial weight of the container with the soil sample is noted. The samples are then kept in a thermostatically controlled oven at 104°C for 24 hours. The moisture content is determined by weighing the sample with the container again after drying to calculate the difference.

3.1.1 Atterberg limits

Liquid limit

The liquid limit was determined using Casagrande apparatus and Cone penetrometer method (IS: 2720-5, 1985). Casagrande apparatus was used for Officer's Hill colony and Merhülietsa colony, while Cone penetrometer for Kevüza area.

Casagrande method:

About 120 gram of air dried soil was thoroughly mixed with distilled water in an evaporating dish. A portion of the soil paste was placed in the Casagrande cup and trimmed to a depth of 1 cm at the point of maximum thickness. A groove was then made along the diameter of the soil. The cup was uniformly rotated at two revolutions per second and raised and dropped repeatedly until the two parts of the soil come in contact with the bottom of the groove along a distance of about 12 mm. Number of drops were recorded and small representative slice in which the soil flowed to close the groove was taken for moisture content determination expressed as a percentage of the oven dry weight.

Four tests were carried out for each soil sample by adjusting the water contents in such a way that the number of blows required to close the groove fall within the range of 15 to 35 blows. Water contents were plotted on the ordinate against the log of number of blows on the abscissa. The curve so obtained is known as the flow curve. The water content corresponding to 25 blows were determined from the flow curves to obtain the liquid limit of the soil.

Cone penetrometer method:

About 150 gram of the wet soil paste obtained from thoroughly mixed portion was transferred to the cylindrical cup and levelled up to the trough. It was then placed on the base of the cone penetrometer apparatus. The penetrometer was so adjusted that the cone point just touches the surface of the soil paste in the cup. The vertical rod was released so that the cone was allowed to penetrate into the soil paste under its weight for 5 seconds. A portion of the area penetrated by the cone (about 20 g) was taken for moisture content determination expressed as a percentage of the oven dry weight. The test was repeated so as to get a penetration range between 14 mm and 28 mm. Up to 4 readings were taken for this test. A graph representing water content and the cone penetration was plotted. The best fitting straight line was then drawn. The moisture content corresponding to cone penetration of 20 mm was taken as the liquid limit of the soil.

Plastic limit

Plastic limit was determined by rolling thread method (IS: 2720-5, 1985). About 8 gram of the soil was squeezed into a ball and hand-rolled on a glass plate into a thread of uniform diameter. At 3 mm diameter, the specimen was kneaded and rolled out again. The process was repeated till the thread crumbled at 3 mm diameter. The pieces of crumbled soil thread were collected in a container and the moisture content determined. This test was repeated to get at least three sets of values and the average was taken as the plastic limit of the soil. It is expressed in percentage.

Index properties

Plasticity index

The range of consistency within which a soil exhibits plastic properties is the plastic range. It is indicated by plasticity index (I_p) ranging from non-plastic to

extremely plastic (Table 3.1). The greater the difference between liquid and plastic limits, the greater is the plasticity of the soil. A cohesionless soil has a zero plasticity index. The plasticity index is defined as the numerical difference between the liquid limit (W_L) and the plastic limit (W_P) of a soil:

$$I_P = W_L - W_P \quad (3.1)$$

In the case of sandy soils, plastic limit should be determined first. When the plastic limit cannot be determined, the soil is non-plastic. When the plastic limit is equal to or greater than the liquid limit, the plasticity index is zero.

Table 3.1: Soil classification according to Plasticity Index (Anon, 1979)

Plasticity Index (%)	Description
< 1	Non-plastic
1 - 7	Slightly plastic
7 - 17	Moderately plastic
17 - 35	Highly plastic
> 35	Extremely plastic

Liquidity index

The liquidity index or water-plasticity ratio (I_L) is the ratio expressed as a percentage, of the water content (W_P) of a soil minus its plastic limit (W_P), to its plasticity index (I_P):

$$I_L = \frac{W_C - W_P}{I_P} \quad (3.2)$$

Consistency index

The consistency index or relative consistency (I_C) is the ratio of the liquid limit (W_L) minus the water content (W_C) to the plasticity index (I_P) of a soil:

$$I_C = \frac{W_L - W_C}{I_P} \quad (3.3)$$

The consistency index is useful in the study of the field behaviour of saturated fine grained soils. Thus, if the consistency index of a soil is equal to unity, it is at the plastic limit. Similarly, a soil with $I_C = 0$ is at its liquid limit. If I_C exceeds unity, the soil is in a semisolid state and will be stiff (Table 3.2). A negative consistency index indicates that the soil has water content greater than the liquid limit and hence behaves like a liquid. The liquidity index and consistency index are just opposite to each other. They indicate the state of the soil in the field.

Table 3.2: Values of I_L and I_c according to consistency of soil (Atterberg, 1911)

Consistency	Liquidity Index	Consistency Index
Semisolid or solid state	Negative	>1
Very stiff (moisture content = plastic limit)	0	1
Very soft (moisture content = liquid limit)	1	0
Liquid state (when disturbed)	>1	Negative

Plasticity chart

Fine grained soil can be classified according to the liquid limit and plasticity index properties of the soil using the plasticity chart. It has been observed that many properties of clays and silts, such as their dry strength, compressibility, and consistency near the plastic limit can be correlated with the Atterberg limits by means of the plasticity chart (Casagrande, 1932).

The Indian Bureau of Standards has adopted the Unified Soil Classification System (USCS) as their code of practice (IS: 1498, 1970) with some modification of the plasticity chart for the classification and identification of soils. The chart is divided into six regions by drawing vertical lines at liquid limits $W_L=35$ and $W_L=50$ (Fig. 3.1).

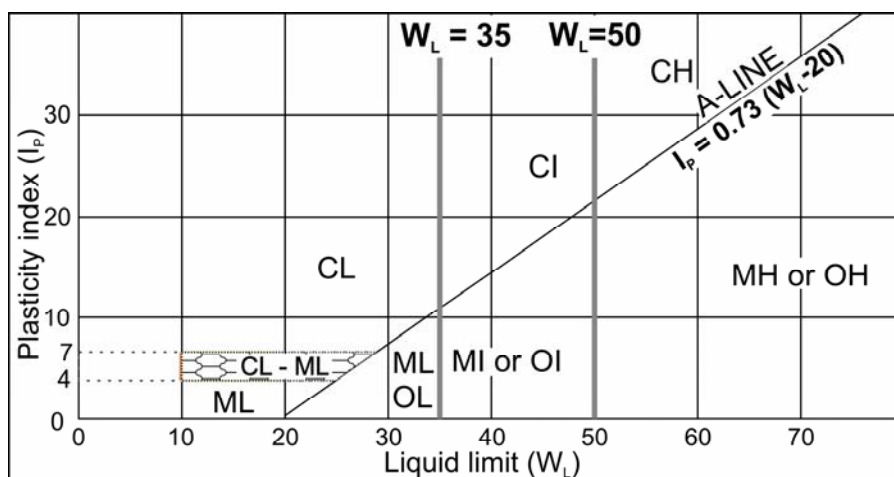


Fig. 3.1: Plasticity chart as per IS: 1498, 1970

The A-line divides clays of low ($W_L < 35$), medium ($35 < W_L < 50$), and high ($W_L > 50$) plasticity from inorganic silts or organic clays. Here, the ordinate represents the plasticity index and the abscissa, the corresponding liquid limit. Soils with plasticity index between 4 and 7 are classified as CL-ML. In accordance with the general classification, the following group symbols are used (Murthy, 2001):

CL, CI, CH = Inorganic clays of low, medium, and high plasticity respectively

ML = Inorganic silt of low plasticity

OL = Organic silts or organic silt-clays of low plasticity

OI = Organic clays of medium plasticity

MI = Inorganic silts or silty sands of medium plasticity

MH = Inorganic silts of high compressibility

OH = Organic clays of high compressibility or plasticity

The soils of a particular group may be admixtures of one or more components of other soils, including fine sand.

Shrinkage limit

About 30 g of soil was taken in an evaporating dish and mixed thoroughly with distilled water in an amount sufficient to fill the soil voids completely and to make the soil pasty enough to be readily worked into the shrinkage dish without entrapping air bubbles. The volume of the shrinkage dish, which is also the volume of the wet soil pat (V) was determined first. This was done by filling the shrinkage dish with mercury and weighing the mercury held in the shrinkage dish with the help of a measuring cylinder. The dish was completely filled with the soil paste and weighed (W). The dish was then dried at 105°C and cooled before measuring the weight of the mass of dry soil (W_o). The dried soil pat was taken and placed in a glass cup filled with mercury. The soil pat was immersed into the glass cup by pressing it with the help of glass plate. The displaced mercury was collected and its volume determined (V_o) and shrinkage limit was further estimated (IS: 2720-6, 1972). It is calculated from the following equation:

$$W_s = \left\{ \left(\frac{W - W_o}{W_o} \right) - \left(\frac{V - V_o}{V_o} \right) \right\} \times 100 \quad (3.4)$$

where,

W_s = shrinkage limit in percent

W = weight of the wet soil in gram

W_o = weight of dried soil in gram

V = volume of wet soil in ml

V_o = volume of dry soil in ml

3.1.2 Shear strength of soils

Direct shear tests were carried out to evaluate the cohesion (c) and internal friction angle (ϕ) for soils on remoulded samples of the study area. The consolidated drained test method was conducted for the purpose following standard procedure (IS: 2720-13, 1986). About 200 g of soil sample was thoroughly mixed with 20 ml of distilled water, compacted and placed in a shear box. The box was transferred into a water jacket filled with water and then mounted on the shearing machine to induce failure along a pre-determined horizontal plane between two halves of the shear box. The desired normal load in the range of 0.1 to 0.5 kg/cm² was applied through the loading frame. Readings were taken at intervals of 1 minute of shear displacement till failure. The sample was then removed and moisture content determined. Shearing was allowed at a low rate of constant strain (0.05 mm/minute) to permit complete drainage during shearing. The test was repeated with three more identical specimens under increased normal loads. Normal and peak shear stresses obtained from the tests were plotted in RocData software (Rocscience Inc., 2005) to obtain the cohesion (c), friction angle (ϕ) and σ_{ci} (UCS - unconfined compressive strength).

3.2 Rock mass rating and Slope mass rating

Field studies were carried out in detail to determine the lithology, structure and groundwater conditions. About 20-25 rock samples were collected from every rock exposure for point load test. Their averages were taken to determine the strength. Orientations of the exposed litho-units and structural features were measured using a Brunton compass. Numerous joint trends were taken to determine the rock and slope mass rating to help interpret the mode of slope failure in the area. Spacing of discontinuities were measured with the help of a ruler. Visual observations were made for estimating the groundwater conditions for the present work and accordingly their ratings estimated. It is classified as completely dry, damp, wet, dripping and flowing (Bieniawski, 1989). Joint roughness was felt by touch and estimated as very rough, rough, slightly rough, smooth, polished and slickenside surfaces. Altogether eight rock slopes were studied. They were selected based on the ideal conditions for large structural data collection in in-situ rocks.

The representative rock samples were determined under laboratory condition. For the present study, irregular lump test was conducted to determine the rock strength using a Point Load Index Tester in accordance with the Indian standard (IS:

8764, 1998). Rock blocks or lumps of size 50 ± 35 mm and of shape shown in fig. 3.2 are used for irregular lump tests. The ratio of D/W should be between 0.3 and 1.0, preferably close to 1. The distance 'L' should be at least $0.5D$. The specimen is inserted in the test machine and the platens closed to make contact with the smallest dimensions of the block or lump, away from the edges and corners. The distance 'D' between platen contact points is recorded to ± 2 percent. The smallest specimen width 'W' perpendicular to the loading direction is recorded to ± 5 percent. If the sides are not parallel, then 'W' is obtained from W_1 , W_2 and W_3 as given in fig. 3.2 and calculated as follows:

$$W = \frac{W_1 + W_2 + W_3}{3} \quad (3.5)$$

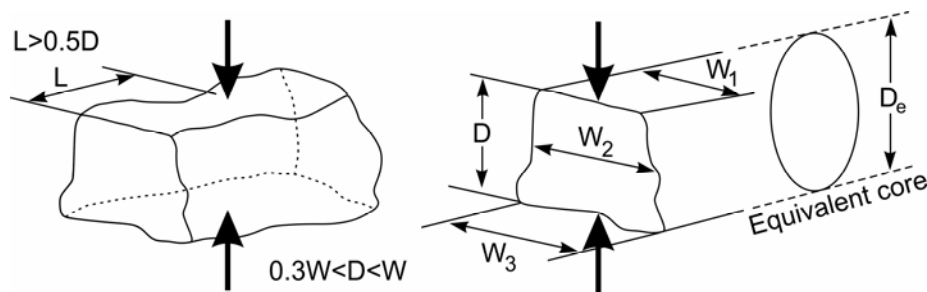


Fig. 3.2: Specimen shape requirement for irregular lump test

The load was then applied to the specimen such that failure occurs within 10-60 seconds and the failure load 'P' was recorded. The test should be rejected as invalid if the fracture surface passes through only one loading point.

Calculations:

Uncorrected point load strength (I_s) is calculated as P/D_e^2 where D_e , the “equivalent core diameter”, is given by:

$$D_e^2 = \frac{4A}{\pi} \quad (3.6)$$

Where,

$A = WD$ = minimum cross sectional area of a plane through the platen contact points

Size correction:

I_s varies as a function of 'D' in the diametral (core) test and as a function of D_e in irregular lump tests, hence size correction is applied to obtain a unique point

load strength value for the rock sample using the chart given in fig. 3.3. The size-corrected Point Load Strength Index $I_s(50)$ of a rock specimen or sample is defined as the value of I_s that would have been measured by a diametral test with $D = 50$ mm.

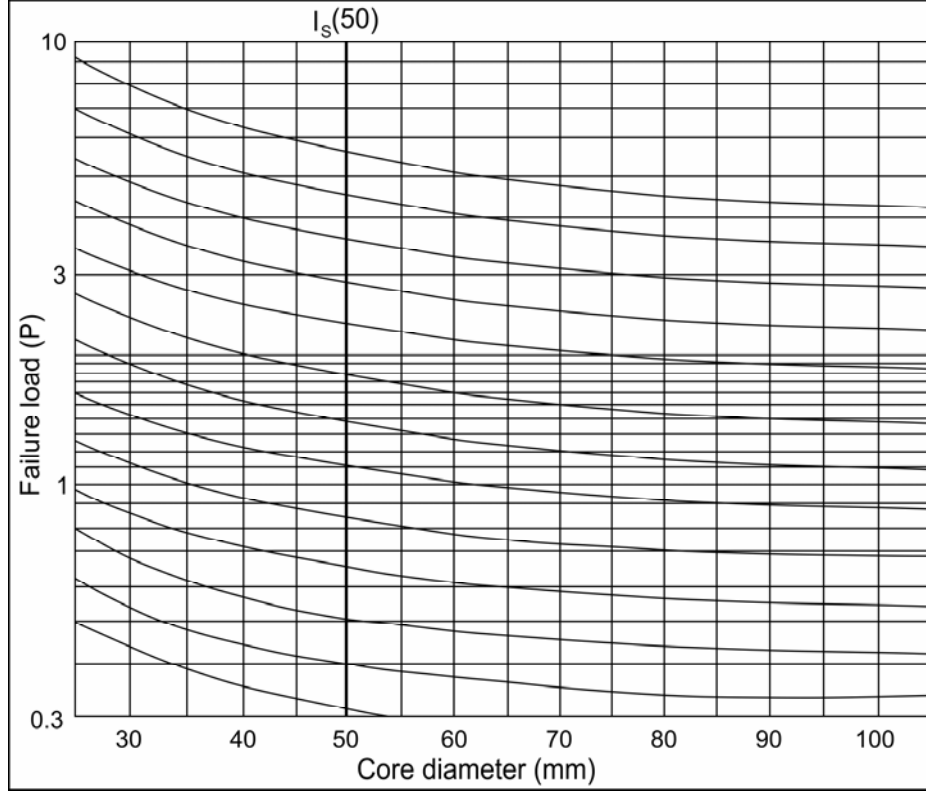


Fig. 3.3: Correction chart for point load strength test (Instrumentation & Technologies, Aimil Ltd., India, AIM-206-1)

Based on the Rock Mass Rating scheme (Bieniawski, 1989), if the point load index (PLI) is less than 1 MPa, UCS rather than the index strength is recommended. The correlating equation for UCS and PLI is given by,

$$\sigma_{ci} = K (PLI) \quad (3.7)$$

where K - conversion factor and PLI - point load index. A conversion factor of 14.4 was used for shale and 21.9 for sandstone after Singh et al. (2012).

Table 3.3 lists the discontinuity conditions and their relative ratings that are used to determine the RMR value of the rock mass in the study area. Rating numbers are applied to each parameter from the published chart of Bieniawski (1989). Ratings are added to obtain a total of RMR value. The final RMR value is classified into five classes (Table 3.3). Higher rock mass rating indicates better rock mass condition.

Table 3.3: The relative weight of observational and laboratory-determined parameters used to calculate RMR (after Bieniawski, 1989)

1	Strength of intact rock material (MPa)	Point load strength	>10	4-10	2-4	1-2			
		UCS	>250	100-250	50-100	25-50	5-25	1-5	<1
	Rating		15	12	7	4	2	1	0
2	RQD (%)		90-100	75-90	50-75	25-50	<25		
	Rating		20	17	13	8	3		
3	Spacing of discontinuity (m)		>2	0.6-2	0.2-0.6	0.06-0.2	<0.06		
	Rating		20	15	10	8	5		
4	Condition of discontinuity		Very rough, discontinuous, no separation, unweathered	Rough walls, separation <0.1 mm, slightly weathered	Slightly rough, separation <1 mm highly weathered	Slickensides or gouge, <5 mm thick or separation 1-5 mm, continuous	Soft gouge, >5 mm thick or separation >5 mm decomposed rock wall		
	Rating		30	25	20	10	0		
5	Groundwater conditions		Completely dry	Damp	Wet	Dripping	Flowing		
	Rating		15	10	7	4	0		
RMR value			>80	61-80	41-60	21-40	<20		
Class no.			I	II	III	IV	V		
Classification of rock mass			Very good	Good	Fair	Poor	Very poor		

The SMR was obtained from the RMR by adding a factorial adjustment factor depending on the joint-slope relationship and adding a factor related to the method of excavation using the following equation:

$$SMR = RMR + (F_1 \times F_2 \times F_3) + F_4 \quad (3.8)$$

- a) F_1 depends on parallelism between the strikes of joint (α_j) and the strike of slope face (α_s). Values range from 1.00 to 0.15. These values match the relationship $F_1 = (1 - \sin A)^2$, where A denotes the angle between the strikes of slope faces and joints.
- b) F_2 refers to joint dip angle in the planar mode of failure. Its value ranges from 1 - 0.15 and matches the relationship, $F_2 = \tan^2 \beta_j$, where β_j denotes the joint dip angle. For the toppling mode of failure F_2 remains 1.
- c) F_3 reflects the relationship between slope face (β_s) and joint dip (β_j).
- d) F_4 refers to the method of excavation of the slope, which ranges from +15 (natural slope) to -8 (poor blasting).

The values of adjustment factors F_1 , F_2 , F_3 and F_4 for the different joint orientations are given in table 3.4. The SMR classes are finally obtained by using the values of RMR and adjustment factors in equation 3.8. SMR values ranges from 0-100; stability classes are assigned accordingly (Table 3.5).

Table 3.4: Values of adjustment factors (after Romana, 1985)

Adjustment factors	Case of slope failure		Very favorable	Favorable	Fair	Unfavourable	Very unfavourable
F_1	Planar (P)	$ \alpha_j - \alpha_s $					
	Toppling (T)	$ \alpha_j - \alpha_s - 180 $	$>30^\circ$	$30^\circ - 20^\circ$	$20^\circ - 10^\circ$	$10^\circ - 5^\circ$	$<5^\circ$
	Wedge (W)	$ \alpha_j - \alpha_s $					
	P/W/T	Rating	0.15	0.40	0.70	0.85	1.00
F_2	Planar (P)	$ \beta_j $	$<20^\circ$	$20^\circ - 30^\circ$	$30^\circ - 35^\circ$	$35^\circ - 45^\circ$	$>45^\circ$
	Wedge (W)	$ \beta_j $					
	P/W	Rating	0.15	0.40	0.70	0.85	1.00
	T	Rating	1	1	1	1	1
F_3	Planar (P)	$ \beta_j - \beta_s $	$>10^\circ$	$10^\circ - 0^\circ$	0°	$0^\circ - (-10^\circ)$	$<-10^\circ$
	Wedge (W)	$ \beta_j - \beta_s $					
	T	$ \beta_j + \beta_s $	$<110^\circ$	$110^\circ - 120^\circ$	$>120^\circ$	-	-
	P/W/T	Rating	0	-6	-25	-50	-60
F_4	Natural slope	Pre-splitting	Smooth blasting	Normal blasting	Poor blasting		
	15	10	8	0	-8		

Table 3.5: Stability classes as per SMR values (after Romana, 1985)

Class No	V	IV	III	II	I
SMR value	0-20	21-40	41-60	61-80	81-100
Rock mass description	Very poor	Poor	Normal	Good	Very good
Stability	Very unstable	Unstable	Partially stable	Stable	Fully stable
Failures	Large planar or soil-like	Planar or big wedge	Planar along some joints, many wedges	Some block failure	No failure

3.3 Kinematic analyses

Angular relationships between discontinuities and slope surfaces were applied to determine the potential modes of failure following Kliche (1999). Joint trends were plotted in Rocscience software (Rocscience Inc., 1998) to generate pole density and contour diagrams to determine the dominant joint sets that control instability. These were used to generate stereographic projections to ascertain type of failure mode. Data generated from joint projections were used for kinematic analyses using Markland's test (Markland, 1972) that was modified by Hocking (1976), Cruden (1978), and Hoek and Bray (1981). Rose diagrams were constructed to understand the orientation of lineaments with respect to the general regional trend.

The friction angles were estimated using RocData software (Rocscience Inc., 2005). The input parameters include uniaxial compressive strength (UCS) based on field estimation (Table 3.6), geological strength index (GSI) (Fig. 3.4), material constant of the rock (M_i) estimated from a qualitative description of the rock material described in table 3.7. Disturbance factor (D_f), unit weight of rock and slope heights, which were estimated during field surveys. D_f depends on the degree of disturbance to which the rock mass has been subjected to, such as by blast damage and/or stress relaxation. It varies from 0 for undisturbed, in situ rock masses to 1 for very disturbed rock masses. The value assigned to $D_f = 0$, since blasting was not carried out in the area. Based on these inputs, the friction angles were automatically generated.

Table 3.6: Field estimates of UCS of intact rock (after Hoek and Brown, 1997)

Field estimate of strength	Examples	Strength (MPa)
Specimen can only be chipped with a geological hammer	Fresh basalt, chert, diabase, gneiss, granite, quartzite	>250
Specimen requires many blows of a geological hammer to fracture it	Amphibolite, sandstone, basalt, gabbro, gneiss, granodiorite, peridotite, rhyolite, tuff	100-250
Specimen requires more than one blow of a geological hammer to fracture it	Limestone, marble, sandstone, schist	50-100
Cannot be scraped or peeled with a pocket knife, specimen can be fractured with a single blow from a geological hammer	Concrete, phyllite, schist, siltstone	25-50
Can be peeled with a pocket knife with difficulty, shallow indentation made by firm blow with point of a geological hammer	Chalk, claystone, potash, marl, siltstone, shale, rocksalt	5-25
Crumbles under firm blows with point of a geological hammer, can be peeled by a pocket knife	Highly weathered or altered rock, shale	1-5
Indented by thumbnail	Stiff fault gouge	0.25-1

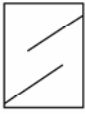
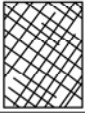




GEOLOGICAL STRENGTH INDEX FOR JOINTED ROCKS (Hoek and Marinos, 2000)		SURFACE CONDITIONS				
		VERY GOOD	GOOD	FAIR	POOR	VERY POOR
STRUCTURE		DECREASING SURFACE QUALITY ⇨				
	INTACT or MASSIVE - intact rock specimens or massive in situ rock with few widely spaced discontinuities	90 80 70 60 50 40 30 20 10 ⇩ DECREASING INTERLOCKING OF ROCK PIECES	/			
	BLOCKY - well interlocked undisturbed rock mass consisting of cubical blocks formed by three intersecting discontinuity sets					
	VERY BLOCKY - interlocked, partially disturbed mass with multi-faceted angular blocks formed by 4 or more joint sets		/			
	BLOCKY/DISTURBED/SEAMY - folded with angular blocks formed by many intersecting discontinuity sets. Persistence of bedding planes or schistosity					
	DISINTEGRATED - poorly interlocked, heavily broken rock mass with mixture of angular and rounded rock particles		/			
	LAMINATED/SHEARED - lack of blockiness due to close spacing of weak schistosity or shear planes					
		N/A	N/A	/	/	/

Fig. 3.4: General chart for GSI estimates from the geological observations

Table 3.7: Values of the constant M_i for intact sedimentary rock group (after Hoek and Brown, 1997)

Class	Group	Texture			
		Coarse	Medium	Fine	Very fine
Clastic		Conglomerates 21±3	Sandstones 17±4	Siltstones 7±2	Claystones 4±2
		Breccias 19±5		Greywackes 18±3	Shales 6±2
					Marls 7±2
Non-Clastic	Carbonates	Crystalline limestone 12±3	Spariritic limestones 10±2	Micritic limestones 9±2	Dolomites 9±3
	Evaporates		Gypsum 8±2	Anhydrite 12±2	
	Organic				Chalk 7±2

3.4 Structural analyses

Lineaments are linear or curvilinear surficial expressions caused due to subsurface bedrock deformities. These are identified on high resolution satellite imagery or aerial photographs as continuous or discontinuous features. In the present study, lineaments were mapped with the help of satellite imageries such as Cartosat-1 imagery, Linear Imaging Self Scanner (LISS-4) imagery and Google Earth imagery (Table 3.8). Some faults of the study area that were mapped, were validated in the field based on tectonic features such as slickensides preserved in the rocks. Slickenside is a non-penetrative type of lineation that is used as a kinematic indicator to determine the direction of fault slip (Ramsay, 1967; Hancock and Barka, 1987; Petit, 1987; Doblas, 1998; Mukhopadhyay et al., 2019). Features showing evidence of faulting were also verified and measured in the field using a handheld Global Positioning System (GPS).

Table: 3.8: Details of satellite imageries used in the study

Satellite data / Source	Date acquired	Spatial resolution (m)
Cartosat-1 (ISRO)	28 th November 2013	2.5
LISS-4 (ISRO)	7 th January 2019	5.8
Google Earth imagery	13 th November 2020	0.15-15

ISRO – Indian Space Research Organisation

3.5 Electrical resistivity tomography

The vertical electrical sounding (VES) method, which is based on the estimation of electrical resistivity of the medium, was used. In resistivity sounding, current is introduced into the ground through current electrodes at a known distance, and the resulting potential difference between two potential electrodes measured. The survey lines were selected ensuring that the surveys were conducted along straight lines and avoid underlying conductors. Among the several possible electrode arrangements employed to measure resistivity, the most common are the Wenner and Schlumberger configurations. The VES method following the symmetrical Schlumberger configuration (Fig. 3.5) was employed for the present study.

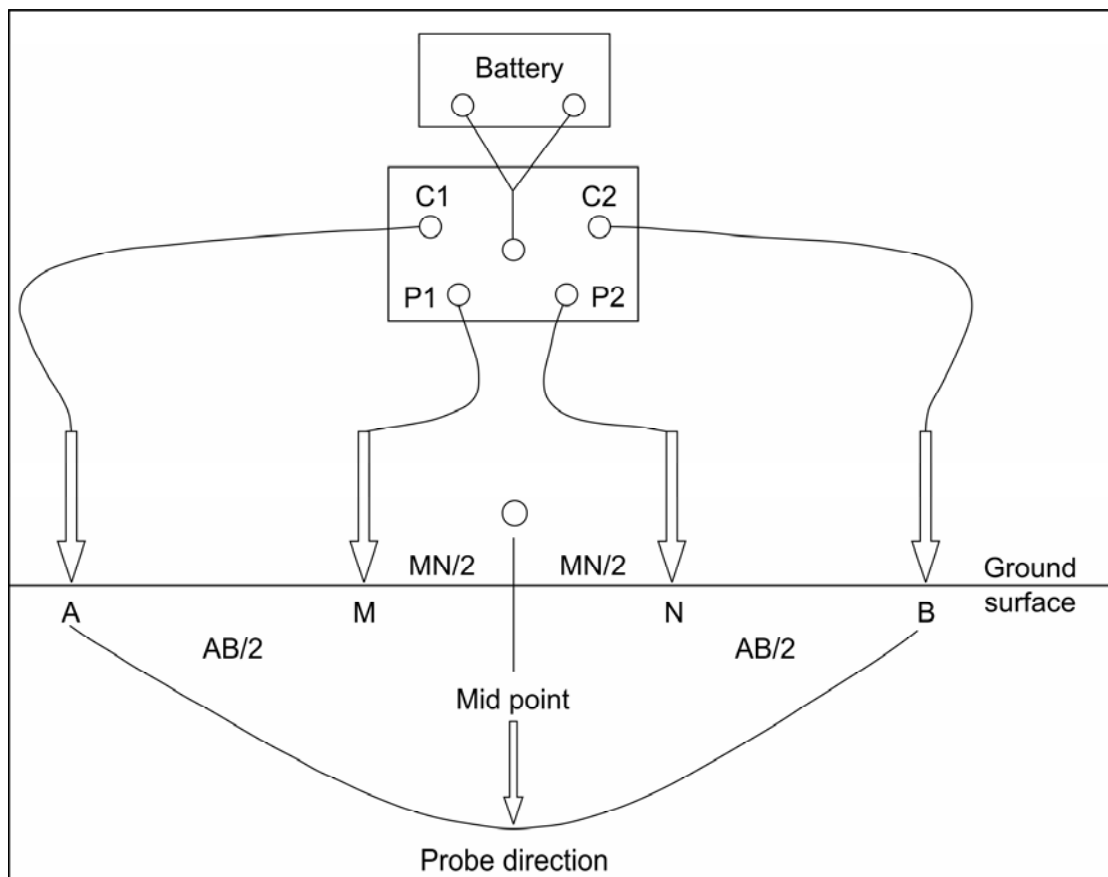


Fig. 3.5: Schematic diagram for the Schlumberger array field method

Here, current electrode spacing is greater than that of potential electrode by an order of 5 ($AB/2 \geq 5 MN/2$; AB - current electrode spacing and MN - corresponding potential electrode spacing). These sets of electrodes were connected to the respective terminals on the resistivity meter with the help of cables that were hammered into the ground for proper contact. Current 'I' is applied into the ground through the two

current electrodes (C1 and C2), then a potential difference ‘ δV ’ is induced, which is measured through the two potential electrodes (P1 and P2). The resistivity of the subsurface for each sounding was computed and displayed as a digital value by the resistivity meter.

For a heterogeneous medium, the apparent resistivity ‘ ρ_a ’ of a geologic formation (Telford et al., 1990), which is equal to the true resistivity for a given electrode configuration, is given by

$$\rho_a = K * \frac{\delta V}{I} \quad (3.9)$$

where $K = \frac{\pi}{2l} [L^2 - l^2]$, which is the geometric spacing factor ($AB = 2L$; $MN = 2l$),

The field data was quantitatively analysed using WINGLINK and IPI2win softwares to construct geoelectric cross-sections for the VES locations.

Depending on the resistivity values with depth, if ρ_1 , ρ_2 and ρ_3 are the resistivity of the subsurface layers, starting with ρ_1 at the top and followed by ρ_2 and ρ_3 , then the four basic categories of sounding curves types may be summarized as follows:

$\rho_1 < \rho_2 < \rho_3$: A-type

$\rho_1 < \rho_2 > \rho_3$: K-type

$\rho_1 > \rho_2 < \rho_3$: H-type

$\rho_1 > \rho_2 > \rho_3$: Q-type

Apparent resistivity curves obtained from two adjacent VES points were mapped together to predict the presence of faults, using the results from the pseudo cross-sections of apparent resistivities obtained along the VES stations and then by making use of two assumptions following Ammar and Kamal (2018):

1. Recorded subsurface layers may have a fault in between when the two adjacent VES curves intersect each other at a point. The point of intersection of the two curves may indicate the peak of the fault or depth of the fault from the surface (according to $AB/2$).
2. The recorded subsurface may not have a fault in between when the two adjacent VES curves follow a horizontal continuity by diverging away from each other.

A resistivity meter (SSR-MP-ATS) was used to obtain data for the Officer's Hill colony and Aquameter CRM 500 for Kevüza area. Resistivity survey could not be carried out at Merhülietsa colony due to dense settlement and other developmental structures.

3.6 Analysis of Factor of safety

The factor of safety was evaluated for the soil slopes of the study area. The following infinite slope stability equation after Brunsden and Prior (1984) was used to evaluate the FoS:

$$FoS = \left\{ \frac{[c + (\gamma - M\gamma_w) * (Z) * (\cos^2 \beta) * (\tan \phi)]}{[(\gamma) * (Z) * (\sin \beta * \cos \beta)]} \right\} \quad (3.10)$$

Here, c = Cohesion of the material

ϕ = Angle of internal friction

γ = Unit weight of the sample

Z = Landslide height

β = Inclination of slope

M = Saturation constant (1 - considering the slope as saturated)

γ_w = Unit weight of water in the soil (9.8 kN/m³)

Cohesion and internal friction angle was determined in the laboratory by direct shear test. Average value was used for the unit weight of the sample after Geotechnical Info (2012). The location and landslide features (height, width and angle) were established using topographic maps, Google Earth imageries and field surveys using a GPS.

CHAPTER 4

RESULTS AND DISCUSSIONS

4.1 Officer's Hill colony

This study area is situated in the lower portion of the Officer's Hill colony and lies between $25^{\circ}39'50''$ and $25^{\circ}40'01''$ N latitudes and $94^{\circ}05'39''$ and $94^{\circ}05'57''$ E longitudes (Fig. 4.1.1), occupying an area of roughly $92,000 \text{ m}^2$. The affected portion lies between 1310-1480 m above msl with some first and second order streams flowing through it and joining the main river Sitsie Rü.

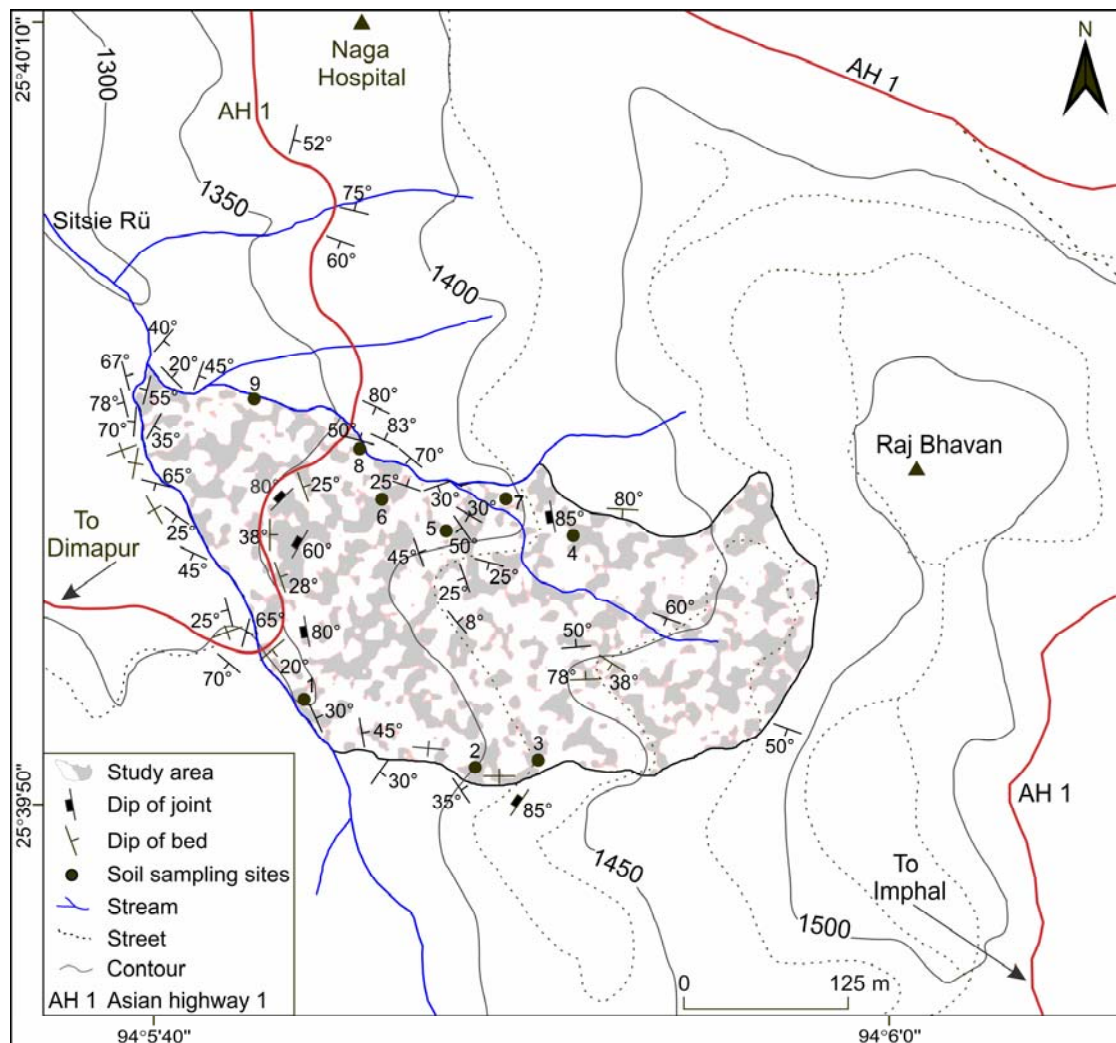


Fig. 4.1.1: Location map of Officer's Hill colony study area

A large portion of the colony was affected by continuing slope instabilities for several years destroying many houses, roads and other structures. The area is highly populated and densely settled with several large RCC buildings and roads, including the very vital highway, AH 1 (formerly NH 39), that passes through it near the lower boundary of the study area (Fig. 4.1.2). A massive landslide event occurred in the year 2005 where a landslide near the highway affected nearly 200 m section of the main highway as well as a portion of the colony road, cutting off connectivity of some households, severely disrupting the flow of traffic and causing great inconvenience to travellers. This instability continued for several years, growing in dimension and reach, affecting several more houses, different sections of roads and other structures.

The lithology in the area is predominantly the Disang Group of rocks, which are made up of shales intercalated with thin beds of sandstone and siltstone. The rock exposures in the vicinity of the slide zone are highly jointed, fractured and weathered. Large patches of sheared rocks and clay are also observed in the study area.



Fig. 4.1.2: Study area (yellow dotted line); arrow points to fault trace (Inset: Damaged highway)

The slope map (Fig. 4.1.3a) categorizes the study area into very gentle, gentle, moderate, steep, and very steep. The contours and field observations were used to develop a micro-slip map, demarcating two weak zones and movement viz., Slip zone 1 and Slip zone 2 (Fig. 4.1.3b) on the western portion of the study area. The AH 1 runs through these two weak zones.

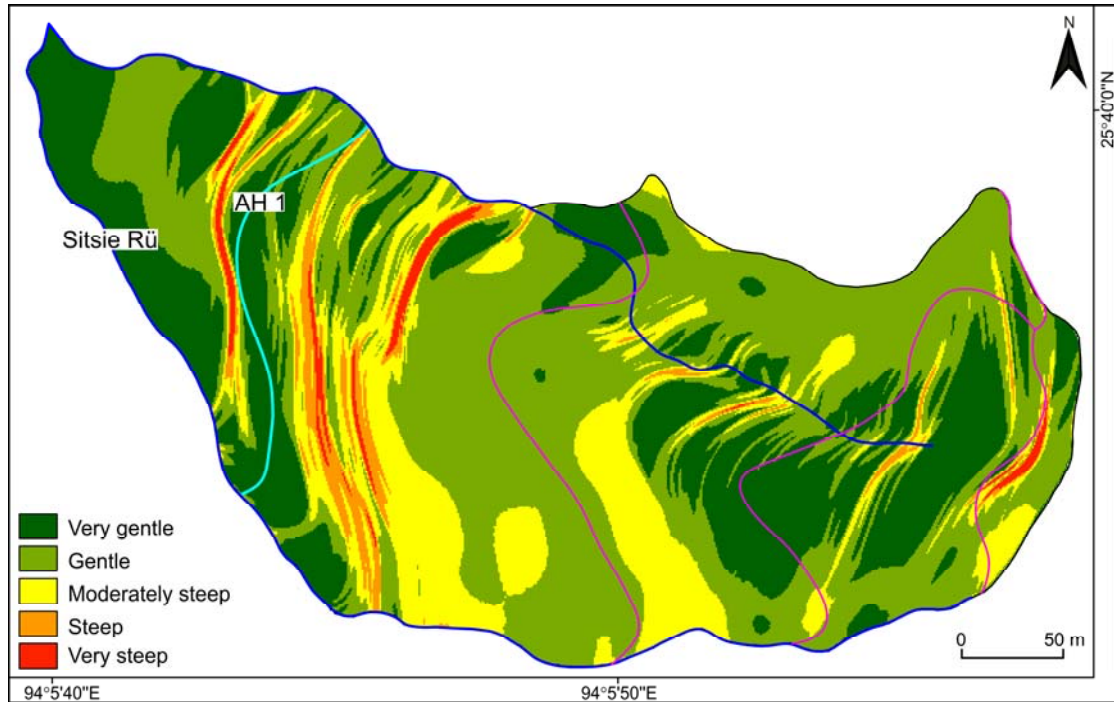


Fig. 4.1.3a: Slope map

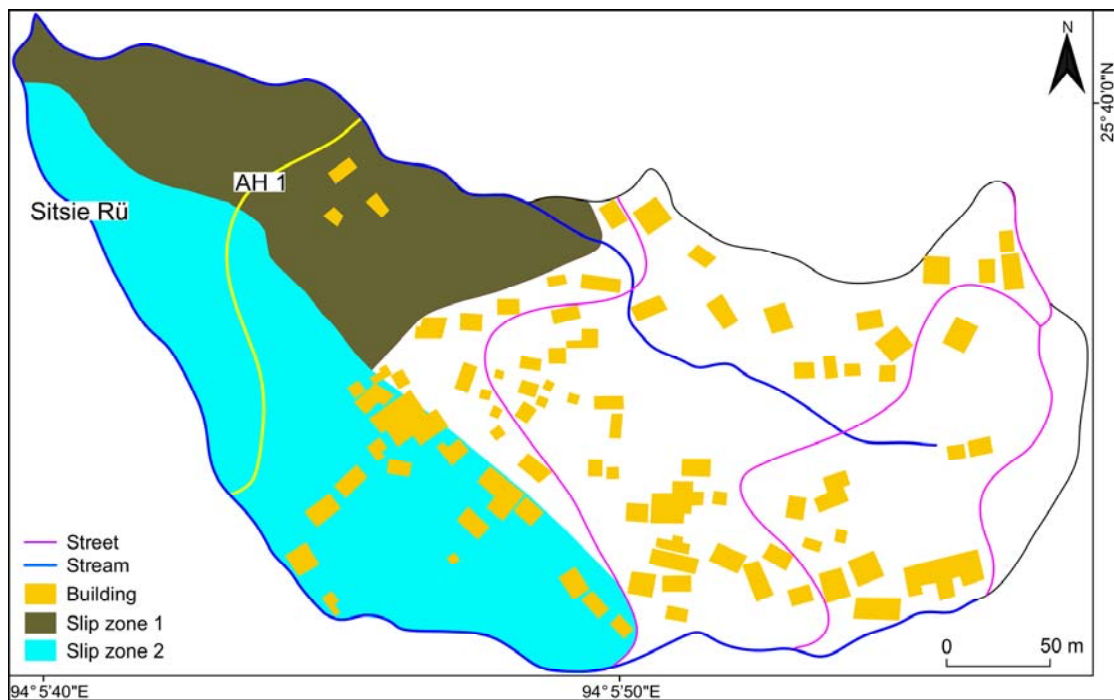


Fig 4.1.3b: Officer's Hill colony landslide map

Geotechnical analyses

Altogether nine soil samples were analysed to determine the moisture content and consistency limits, and six soil samples for determination of the shear strength.

Moisture content and Consistency limits

Soil samples were collected in the month of March. The moisture content of the soils ranges from 17.05 to 39.83% (Table 4.1.1). The liquid limit (W_L) varies from 30.9 to 53.5%. The water contents of samples 1, 2, 6, 7, 8 and 9 are higher than their corresponding plastic limit but lower than the W_L suggesting that the soils are in plastic state. In this state, soil deforms without the development of cracks. The consistency indices of samples 3, 4 and 5 are >1 which range from 1.05-2.47%. These values indicate that the soil samples at the time of sampling were below the plastic limit in their natural state. The plasticity index of the samples ranges from moderately to highly plastic.

Table 4.1.1: Moisture content and Consistency limits

Sample No	1	2	3	4	5	6	7	8	9
Water content (%)	27.51	39.83	21.47	17.05	20.81	38.53	21.48	29.29	19.05
Liquid limit (%)	41.50	50.60	53.50	46.00	39.50	42.40	30.90	32.00	32.50
Plastic limit (%)	23.74	21.53	23.00	34.30	26.71	16.34	15.00	21.16	17.11
Plasticity index (%)	17.76	29.07	30.50	11.70	12.79	26.06	15.90	10.84	15.39
Consistency index (%)	0.79	0.37	1.05	2.47	1.46	0.15	0.59	0.96	0.89
Shrinkage limit (%)	21.69	25.68	14.57	20.9	23.98	16.05	12.99	19.35	13.11

The shrinkage limit of samples 1, 2, 4, 5 are very high (20.9-25.68%), high in samples 6 and 8 (16.05-19.35%) and moderate in samples 3, 7, 9 (12.99-14.57%). Sample 7 displays the lowest shrinkage limit value (Table 4.1.1) whereas sample 2 the highest, suggesting the later will have higher volume change relative to water content (Hobbs et al., 2018).

From the plasticity chart (Fig. 4.1.4), it is observed that soil samples 7, 8 and 9 falls in the CL field indicating inorganic clays of low plasticity. Samples 1 and 6 falls in the CI field suggesting inorganic clays of moderate plasticity. Samples 2 and 3 falls in the CH field indicating inorganic clays of high plasticity. Samples 4 and 5 falls in the MI-OI field, which point to inorganic silts-organic clays of moderate plasticity.

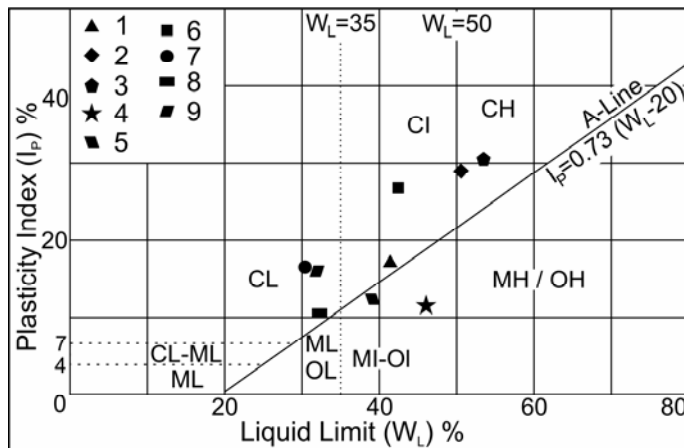


Fig. 4.1.4: Plasticity chart

Direct shear test

Shear strength parameters of c , ϕ and σ_{ci} (Table 4.1.2) were derived from the failure envelope by plotting normal stress against shear stress (Fig. 4.1.5). The σ_{ci} values obtained range from 46.8 to 67.29 kPa (Table 4.1.2) suggesting soils of weak to moderate strength (Das and Sobhan, 2018). Sample 1 displayed the lowest σ_{ci} of 46.8 kPa while sample 3 with 67.29 kPa shows the highest value, suggesting that the latter will have higher shearing resistance.

Table 4.1.2: Shear strength parameters of the soils obtained from direct shear test

Sample No.	Normal stress (kPa)	Shear stress (kPa)	c (kPa)	ϕ (°)	σ_{ci} (kPa)	Water content (W_c) %	Average W_c at failure (%)
1	9.89	19.02	17	18	46.8	22.35	25.78
	19.90	24.05				25.86	
	31.05	26.88				27.12	
	39.75	29.88				27.81	
2	10.14	25.33	23	13	57.83	26.85	29.87
	20.24	28.37				28.26	
	30.20	31.22				30.14	
	41.73	32.08				34.25	
3	9.96	30.18	24	19	67.29	25.74	31.21
	20.08	30.66				27.32	
	30.00	35.22				33.21	
	40.02	38.03				38.58	
4	10.27	23.05	21	17	56.76	27.58	29.59
	20.40	27.33				28.55	
	30.53	29.80				28.89	
	40.26	33.66				33.35	
5	10.11	19.96	17	21	49.47	21.85	26.58
	22.06	17.81				26.26	
	30.87	30.02				27.12	
	43.93	33.61				31.11	

	10.47	22.87				24.53	
6	22.06	28.98	19	22	56.34	29.59	28.58
	31.74	32.14				31.06	
	44.57	35.67				30.37	

It has been found that sample 2 and 3 possessing higher cohesion values, shows high W_L values (Table 4.1.1). This is indicative of high clay content in the soil and plasticity (sample 2 and 3), also classified in the Plasticity chart (Fig. 4.1.4). It has been observed that the water content determined at failure shows an increasing trend with respect to cohesion values (Table 4.1.2). This suggests that during the shearing process, soils with high cohesion absorb more water before deformation takes place due to more water retention capacity. Conversely, soils with lower cohesion such as sample 1 and 5 tend to fail at lower water content.

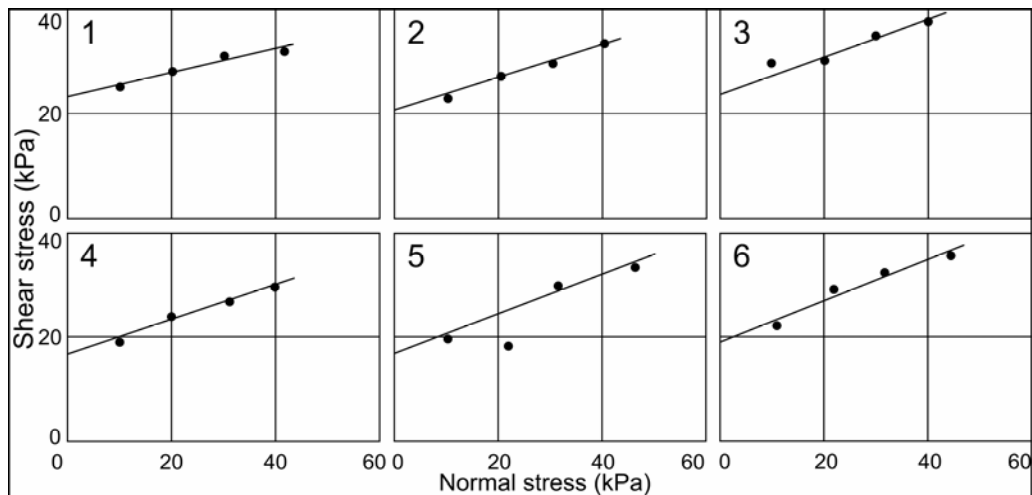


Fig. 4.1.5: Failure curves of samples

RMR and SMR

Slip zone 1 was devoid of undisturbed rock exposures and hence samples could not be collected. Twenty five rock samples from Slip zone 2 that were analysed for point load test gave an average strength of 2.18 MPa (Table 4.1.3). Sample 6 displayed the highest strength with point load index (PLI) value of 5.55 MPa, while sample 21 with 0.64 MPa exhibited the lowest. Sandstone samples showed higher strength with an average of 3.97 MPa. Siltstone and shale samples have an average values of 1.52 MPa and 0.82 MPa respectively.

Table 4.1.3: Results obtained from point load test

Sample No	Lithology	PLI (MPa)	Sample No	Lithology	PLI (MPa)
1	Sandstone (FG)	2.85	14	Siltstone (W)	1.55
2	Sandstone (FG)	4.88	15	Siltstone (W)	1.44
3	Sandstone (FG)	3.05	16	Siltstone (W)	1.47
4	Sandstone (FG)	2.94	17	Siltstone (W)	1.35
5	Sandstone (FG)	3.86	18	Shale (W)	0.94
6	Sandstone (FG)	5.55	19	Shale (W)	0.95
7	Sandstone (FG)	3.94	20	Shale (W)	0.69
8	Sandstone (FG)	4.32	21	Shale (W)	0.64
9	Sandstone (FG)	4.37	22	Shale (W)	0.85
10	Siltstone	1.38	23	Shale (W)	0.88
11	Siltstone	1.68	24	Shale (W)	0.83
12	Siltstone	1.73	25	Shale (W)	0.74
13	Siltstone	1.62			
Average strength = 2.18 MPa					

PLI - point load index; FG - fine grained; W - weathered

A rating of 37 is estimated for the RMR that classifies the rocks as Weak (Table 4.1.4). The SMR values for this slope fall in Class IV, which is indicative of unstable slope conditions.

Table 4.1.4: Slope mass rating

1. Point load strength (MPa)	2.18	7
2. RQD (%)	32.5	8
3. Spacing of joints (mm)	52	5
4. Condition of joints	Slickensided surface; joints separation 1-5 mm	10
5. Groundwater condition	Wet	7
RMR	= (1+2+3+4+5)	37
6. $F_1 = \alpha_j - \alpha_s$	26°	0.40
7. $F_2 = \beta_j$	34°	0.70
8. $F_3 = \beta_j - \beta_s$	-21°	-60
9. $F_4 =$ Adjustment factor	Pre-splitting	10
SMR = RMR+(F₁x F₂x F₃)+F₄	37+{0.40x0.70x(-60)}+10	30.2
10. Class	IV	
11. Description	Weak rocks; unstable slope prone to wedge failure	

Kinematic analyses

Kinematic analyses also could be performed only in the Slip zone 2 due to unavailability of undisturbed exposures in the Slip zone 1 (Fig. 4.1.3a). 127 joint attitudes were used to construct pole density (Fig. 4.1.6-a) and contour diagram (Fig.

4.1.6b), from which two dominant joint sets J_1 and J_2 were identified (Table 4.1.5). These were plotted in a stereographic projection (Fig. 4.1.6c) against the cut slope of the highway. The stereogram shows a distinct wedge towards WSW due to intersection of joints J_1 (34° due 286°) and J_2 (33° due 222°).

Table 4.1.5: Input data and mode of failure in kinematic analysis

No. of joints measured	127
Slope orientation	$55^\circ/260^\circ$
Orientation of principle joint sets	$J_1 = 34^\circ/286^\circ$ $J_2 = 33^\circ/222^\circ$
Internal friction angle (ϕ)	26°
Type of failure	Wedge
Data format	Dip / dip direction
Magnetic declination	-0.367 (west declination of the study area)

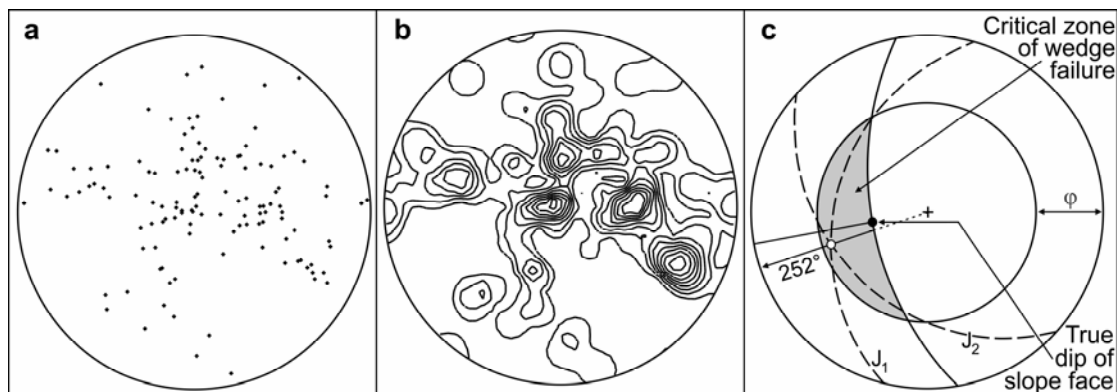


Fig. 4.1.6: **a** - Pole diagram; **b** - Contour diagram; **c** - Stereographic projection

Structural analyses

The rose diagram generated from the joints of the study area shows the development of a prominent NNE-SSW trend (Fig. 4.1.7), which is the approximate strike of the axes of the folds and thrusts of the region. The study area is crossed by lineaments trending in NE-SW, NW-SE, E-W and NNW-SSE directions (Fig. 4.1.8). Two minor NE-SW trending thrusts are seen in the central portion of the study area (Fig. 4.1.8). Sandstone beds

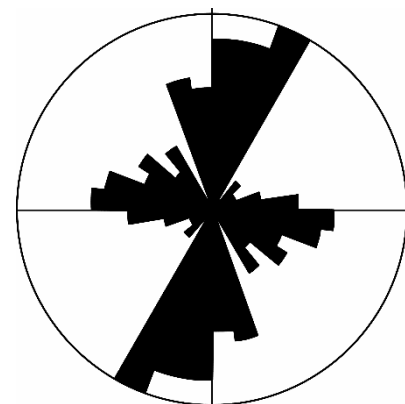


Fig. 4.1.7: Rose diagram

constituting the hanging wall block are seen overriding the footwall of shale (Fig.

4.1.9) in the vicinity, lending evidence of small-scale thrusting of the rocks. Rock exposure in the study area show a set of beds that has been affected by flexural folding, perhaps due to shearing stresses (Fig. 4.1.10). These folded beds bear a faulted relationship with the associated steeply inclined undisturbed beds.



Fig. 4.1.8: Google Earth image showing lineaments and photo locations

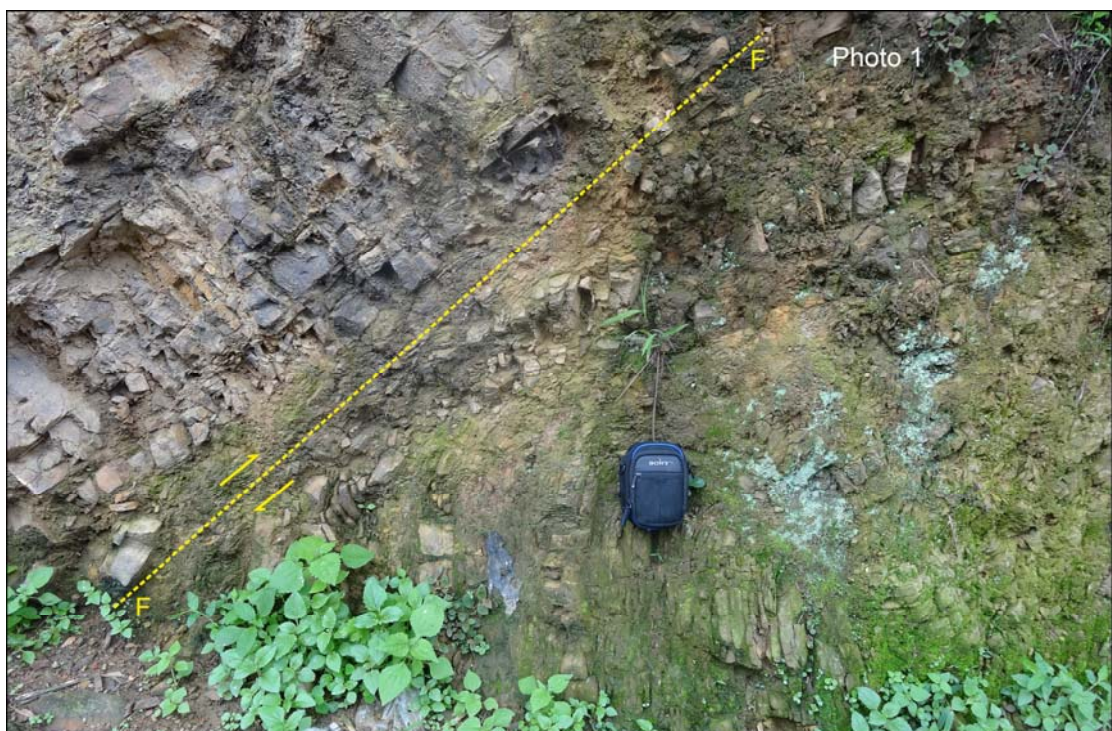


Fig. 4.1.9: Bedded sandstones overriding silty shales



Fig. 4.1.10: Flexure folds on left of fault plane

A fault trending NW-SE is observed at the northeastern edge of the study area (Fig. 4.1.8), that is parallel to the regional compression direction. This fault may be responsible for the shearing and fracturing of the bedrock (Fig. 4.1.11A) as well as controlling the stream channel flowing in the northwest. Elevated groundwater conditions have also led to intense weathering of the shale (Fig. 4.1.11B). The portion of the highway along this fault is prone to continuous damage (Fig. 4.1.2, inset). Another parallel lineament is noted ~50 m southwest of NW-SE trending fault (Figs. 4.1.2, 4.1.8). The disposition of the rocks indicates normal faulting (Fig. 4.1.12). The third lineament is observed near-vertical beds (Fig. 4.1.13A) along the southern boundary of the study area and trends E-W (Fig. 4.1.8). Slickenside preserved in the bedrock nearby (Fig. 4.1.13B) point to faulting of the rocks.



Fig. 4.1.11: A - Sheared rocks; B - Weathered shale with sulphur leaching (bleached)

The major stream Sitsie Rü carved its channel along the fault trending NNW-SSE ($\sim 340^\circ$). Antithetic shearing may be responsible for the large-scale fracturing of the rocks (Fig. 4.1.14). This fault is responsible for surface instability along its strike (Fig. 4.1.15). A slickenside trending 340° (NNW-SSE) noted here, which is parallel to the fault (Fig. 4.1.15 - inset), lends evidence of strike-slip faulting in the area (Fig. 4.1.8). The orientation of the slickenside implies diagonal-slip movement. The eastern bank of the river would therefore, represent the footwall of the fault, along which the area would slowly sink diagonally. This is probably the cause for general subsidence in the Slip zone 2 (Fig. 4.1.16), which has also affected the highway (Fig. 4.1.16A, B). The net effect of these stresses and weathering is the production and accumulation of thick piles of debris and weak soils that continuously fail particularly in the shale dominated areas (Fig. 4.1.17A). The soils and rock after saturation due to abundant subsurface water gets loosened and ultimately slide down as debris and mud flows (Fig. 4.1.17B).



Fig. 4.1.12: Normal fault in the study area

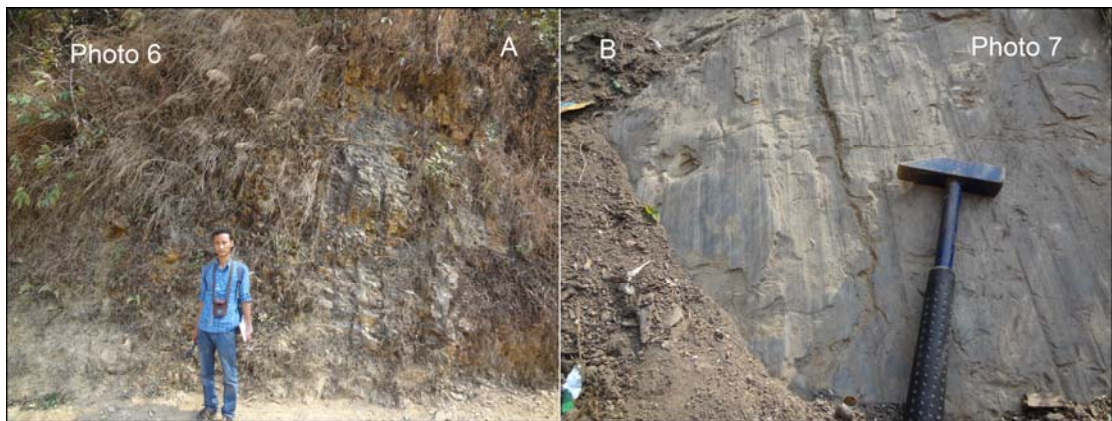


Fig. 4.1.13: A - Near-vertical beds in the study area; B - Slickenside in the bedrock

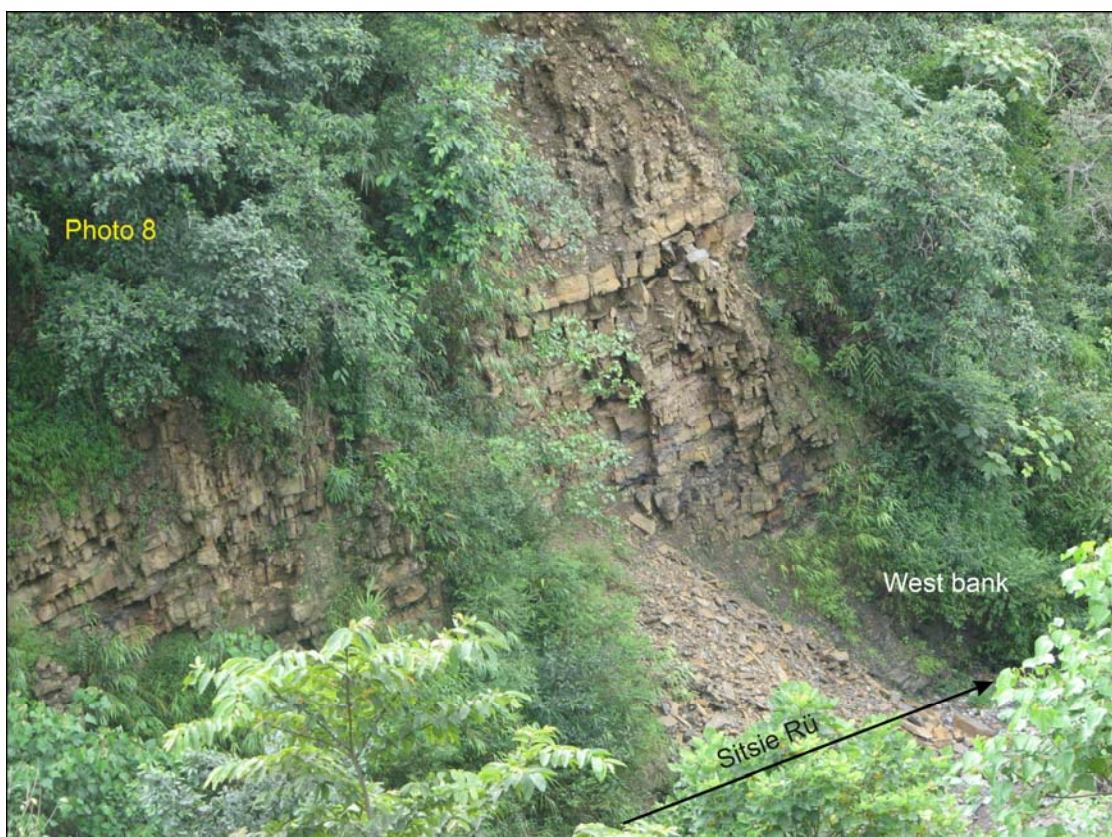


Fig. 4.1.14: Fractured and shattered rocks on the western bank of the Sitsie Rü



Fig. 4.1.15: Field photograph showing condition of slope due to strike-slip fault
(Inset: Slickenside on western bank of river)



Fig. 4.1.16: Field photograph showing subsidence on the eastern bank of the stream
(Inset: A - Subsidence of highway; B - Retaining walls for road support)



Fig. 4.1.17: A - Loose debris constituting slope material; B - Debris flows on unstable slope



Fig. 4.1.18: House damaged due to differential settlement (Slip zone 1)

Electrical resistivity tomography

Resistivity tomography was carried out along five (5) profile lines (Table 4.1.6) in the study area to produce a 2D image of a pseudo-section of VES stations with elevations (Fig. 4.1.19). In order to understand the underlying subsurface condition, the section AA' is plotted along the SE-NW direction (Fig. 4.1.19). Analytical data shows the presence of four (4) geoelectric layers for all the VES stations, with curve types of HA, KQ and KH (Table 4.1.7).

Table 4.1.6: Location of VES stations

Location	Latitude	Longitude	Elevation (m)
VES 1	25°39'57.03"	94°05'43.70"	1353
VES 2	25°39'56.72"	94°05'44.07"	1349
VES 3	25°39'57.43"	94°05'45.30"	1378
VES 4	25°39'56.73"	94°05'46.37"	1400
VES 5	25°39'56.39"	94°05'47.26"	1413

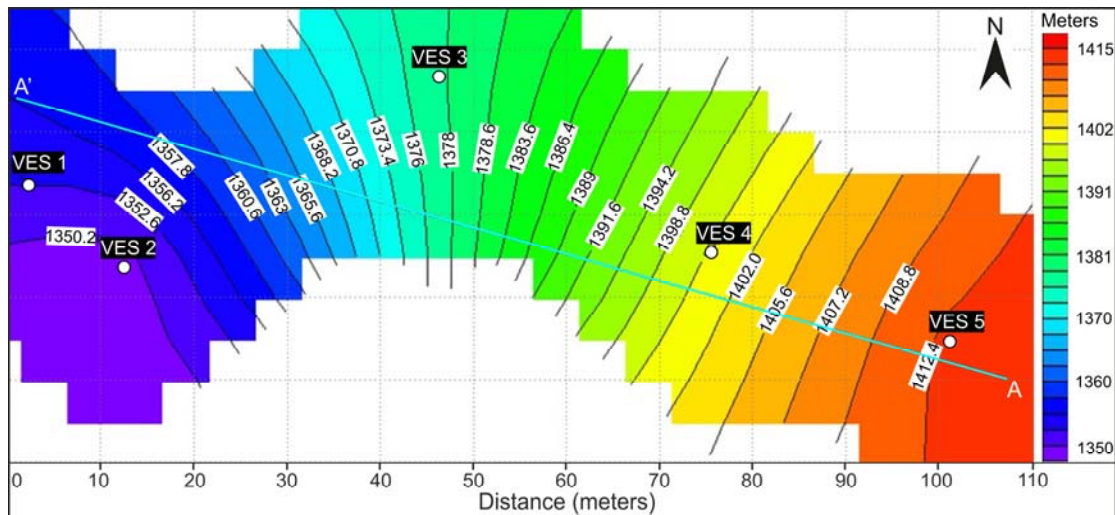


Fig. 4.1.19: 2D image showing pseudo-section of VES stations with elevations

Table 4.1.7: Layer parameters for the VES points

Station	Layer	Apparent Resistivity (Ohm-m)	Thickness (m)	Overburden Thickness	Interpreted Lithology	Curve Type
VES 1	1	53.20	3.34	3.34	Sandy clay/clayey sand	HA
	2	2.45	0.20	3.54	Clay	
	3	11.04	50.12	53.66	Fine sandstone	
	4	107.10	-	-	Sandstone	
VES 2	1	52.08	0.68	0.68	Sandy clay/clayey sand	KQ
	2	102.37	2.00	2.68	Sandstone	
	3	61.55	2.66	5.34	Weathered shale	
	4	40.00	-	-	Clay	
VES 3	1	157.15	0.44	0.44	Sandstone	KH
	2	665.18	0.97	1.41	Sandstone	
	3	39.87	1.02	2.43	Weathered shale (saturated)	
	4	139.78	-	-	Sandstone	
VES 4	1	119.76	0.21	0.21	Sandstone	KQ
	2	352.28	3.19	4.12	Shale	
	3	103.46	16.33	20.45	Shale and sandstone intercalations	
	4	20.29	-	-	Clay	
VES 5	1	82.81	0.60	0.60	Sandy clay/clayey sand	KH
	2	222.01	9.17	9.77	Sandstone	
	3	80.37	28.36	38.13	Clay	
	4	162.87	-	-	Sandstone	

The geoelectrical layers reveal that the area is composed of top soil, sandstone, shale, clayey sand, sandy clay and clay. KH curve type obtained for VES 3 and VES 5 suggests that these stations are occupied by weathered/fractured basement layers (Table 4.1.7). Curve type KQ for VES 2 and VES 4 suggest that the area contains fractured basement layers and clay as seen at the fourth layer. The KH and HA curve

types represents the presence of conductive layers followed by weathered/fractured basement layer resulting from probable fault activity.

A low resistivity zone of <15 ohm-m is seen at VES 1 at a depth of about 15 m (Fig. 4.1.20), which characterise an area of high water content. The zone of high conductivity is indicative of a fault, which is also identified as a thrust in the middle of the study area (Fig. 4.1.8). At the lower portions of the slope, deep cracks have developed on the surface (Fig. 4.1.21), representing the outer rim of the instability. Such fissured layer paves a pathway for water and infilling materials such as clays. When clays are saturated, ion-exchange takes place resulting in release of large number of ions. This process normally increases the ion concentration in pore water which therefore facilitated easy flow of electrical current, and the net result being an increasing conductivity (Ammar and Kamal, 2018).

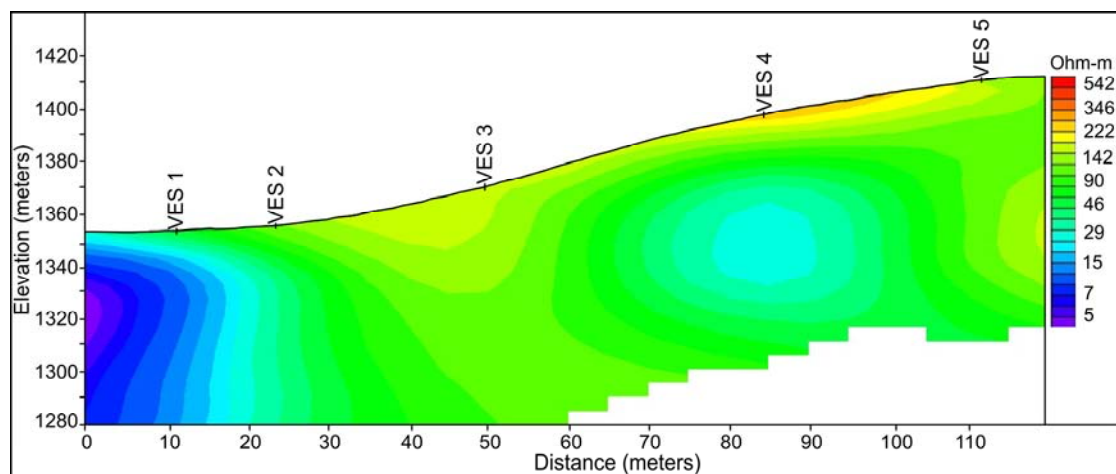


Fig. 4.1.20: 2D image showing a pseudo-section of the area with VES stations



Fig. 4.1.21: Tension fractures in the lower elevations of the study area

Factor of safety

The input values for the infinite slope stability equation for Slip zone 1 are as follows:

$$c = 18 \text{ kN/m}^2$$

$$\phi = 21.5^\circ$$

$$\gamma = 18 \text{ kN/m}^3 \text{ (unit weight of clayey soil)}$$

$$Z = 82 \text{ m}$$

$$\beta = 33^\circ$$

$$\text{Saturation constant (M)} = 1$$

$$\text{Unit weight of water in the soil, } \gamma_w = 9.8 \text{ kN/m}^3$$

For c and ϕ , averages have been taken from direct shear test results (Table 4.1.2: Samples 5 and 6). By assigning these values,

$$\begin{aligned} FoS &= \left\{ \frac{[18 + (18 - 1 * 9.8) * 82 * (\text{Cos}^2 33^\circ) * (\text{Tan} 21.5^\circ)]}{[18 * 82 * (\text{Sin} 33^\circ * \text{Cos} 33^\circ)]} \right\} \\ &= \left\{ \frac{[18 + (18 - 1 * 9.8) * 82 * 0.7 * 0.39]}{(18 * 82 * 0.54 * 0.84)} \right\} \\ &= \frac{201.57}{669.51} \\ FoS &= \mathbf{0.30} \end{aligned}$$

The factor of safety derived for Slip zone 1 is estimated at **0.30**, which indicates that the slope is very unstable.

4.2 Merhülietsa colony

The area of investigation is a zone of chronic slope instability at Merhülietsa colony on the western part of Kohima town. It lies between 25°39'35" - 25°40'07" north latitude and 94°05'15" - 94°05'50" east longitude (Fig. 4.2.1), occupying an area of about 3,45,200 m² and lying at an elevation between 1330-1460 m above msl. This study area consists of dense settlement with residential quarters, academic and government establishments, as well as the AH 1.

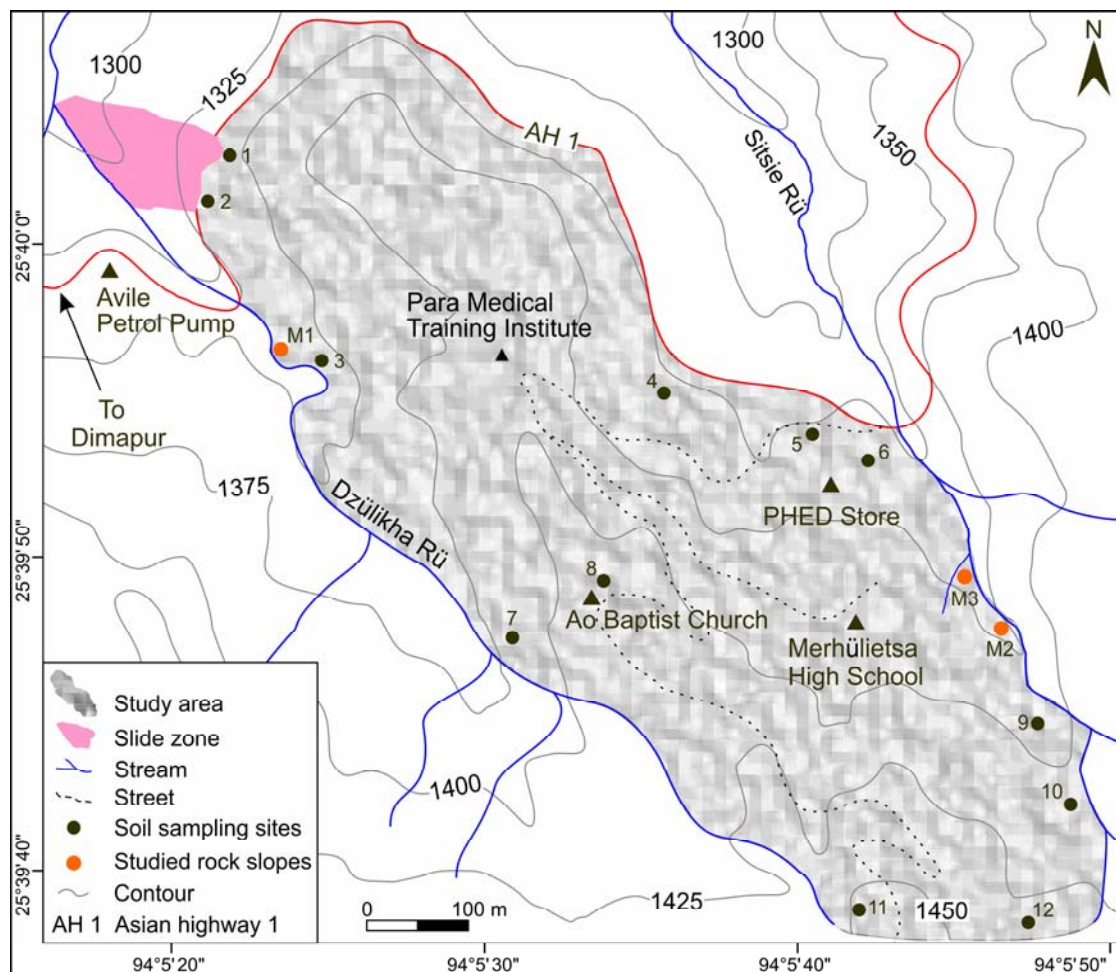


Fig. 4.2.1: Location map

Part of Merhülietsa colony was devastated by a landslide on May 13, 2007 located about 250 m west of the Para Medical Training Institute (PMTI). Some residential houses, hostel building, kitchen gardens, colony roads and about 100 m of the AH 1 were damaged. Another landslide occurred along this particular section of the highway on July 8, 2018 located 350 m northwest of PMTI (Fig. 4.2.1). This slide, about 160 m long and 90 m wide affected an area of ~10,800 m². About 70 m stretch

of the highway (Fig. 4.2.2) and some house also got damaged. Rotational failure is noted in the Slide zone. The materials comprise mixture of loose debris of soil, shales and mostly earth cut material. Incessant rains prior to landslide coupled with dumping of earth cut material by the side of the road were the primary cause of this event. This landslide also destroyed residential houses, affecting three families who had to be evacuated and relocated to safer location (Source: Nagaland Post - 9th July 2018). Hundreds of vehicles including several Manipur-bound trucks loaded with essential commodities were stranded for several days.

The study area continuous to see subsidence and minor creep in several areas notably below PHED store, in and around the Merhülietsa Ao Baptist church, and specially where the shear fractures cut across the highway (Aier, et al., 2012).



Fig. 4.2.2: Affected area along AH 1; (Inset - Water logged area)

The rocks in the study area are mostly observed along the stream sections and minor exposures in some road cuts. They comprise dominantly of shales that are black, buff and grey in colour. These rocks are interbedded with brown to reddish brown sandstones and minor siltstones. The sandstone beds are jointed, fractured and exhibit two to three sets of joints. The shales are highly crumpled and partially to completely weathered in many places.

The north-westerly Dzülikha Rü river flows through the western margin of the study area while the eastern margin is cut across by number of tributaries that drain

into NNW flowing Sitsie Rü. They are highly erosive and have dissected deep channels.

Geotechnical analyses

Twelve soil samples were analysed for determination of moisture content, consistency limits and shear strength.

Moisture content and Consistency limits

Soil samples were collected in the month of February and July. The moisture content of the soils ranges from 3.09 to 37.51% (Table 4.2.1). The liquid limit varies from 35.5 to 73.50% (Table 4.2.1), where sample 8 displayed the highest and sample 1 the lowest liquid limit values. The plastic limit and shrinkage limit of sample 1 is also comparatively lower. Soils possessing low consistency limits such as sample 1, are vulnerable to exceed their corresponding limits, i.e. from semi-solid to plastic and subsequently to liquid state, with increasing water content. In such cases, sudden disturbance will cause the slope soil to flow. For consistency index, it is observed that nine samples have values greater than 1, indicating that the soils are at semisolid state while sample 1, 2 and 12 have value <1 , which indicates plastic state. Majority of the samples display very high shrinkage limit value i.e. samples 3, 5, 6, 7, 8, 11, 12 (20.08-26.86%), high for sample 1, 2 and 4 (15.57-18.14%) and moderate for samples 9 and 10 (13.97-14.87%). Soils with high shrinkage limit according to Hobbs et al. (2018), tend to have higher change in its volume with increasing water content.

Table 4.2.1: Moisture content and Consistency limits

Sample No	1	2	3	4	5	6	7	8	9	10	11	12
Moisture content (%)	34.97	20.84	16.65	17.46	17.45	22.77	18.1	23.09	3.09	11.09	22.6	37.51
Liquid limit (%)	35.5	36	58.14	51.2	64	52	64.3	73.5	40	38.5	60.77	52
Plastic limit (%)	17.98	20.45	28.45	20.2	27.78	24.43	27.92	29.73	15.41	18.17	32.2	29.32
Plasticity index (%)	17.52	15.55	30.5	31	36.22	27.57	36.38	43.77	24.59	20.33	28.57	22.68
Consistency index (%)	0.03	0.97	1.39	1.09	1.29	1.06	1.27	1.15	1.5	1.35	1.34	0.64
Shrinkage limit (%)	15.57	18.14	20.08	17.35	21.43	21.9	24.29	23.24	14.87	13.97	26.86	20.38

From the plasticity chart (Fig. 4.2.3), it is observed that soil samples 1, 2, 9 and 10 falls under CI field indicating inorganic clay of moderate plasticity. Samples 3, 4, 5, 6, 7 and 8 falls under CH field indicating inorganic clay possessing high plasticity. Samples 11 and 12 fall under MH-OH field possessing high plasticity which depict organic clays.

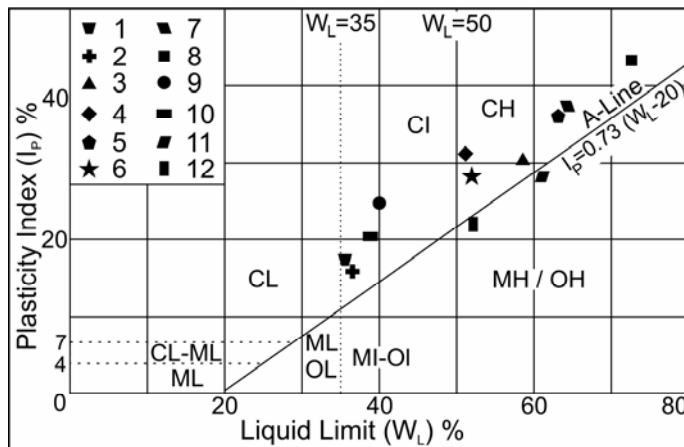


Fig. 4.2.3: Plasticity chart

Direct shear test

Shear strength parameters c , ϕ and σ_{ci} (Table 4.2.2) were derived from the failure envelope by plotting normal stress against shear stress (Fig. 4.2.4). The σ_{ci} values obtained range between 45.7 to 61.04 kPa suggesting soils of weak to moderate strength (Das and Sobhan, 2018). Sample 8 displayed the highest value (61.04 kPa), while sample 9 (45.7 kPa) the lowest (Table 4.2.2). The average W_c determined at failure varies from 25.06 to 31.28%.

Table 4.2.2: Shear strength parameters of the soils obtained from direct shear test

Sample No	Normal stress (kPa)	Shear stress (kPa)	c (kPa)	ϕ	σ_{ci} (kPa)	Water content (W_c) %	Average W_c at failure %
1	21.6	25.33	17.5	19	49.07	20.77	26.99
	33.17	28.17				27.42	
	45.37	34.15				28.56	
	56.07	36.27				31.22	
2	21.66	24.17	16.5	21	48.02	23.02	26.57
	34.98	34.27				23.55	
	44.43	34.22				29.47	
	55.68	37.22				30.27	
3	20.8	26.34	18	17	48.65	22.02	26.04
	33.55	27.06				23.6	
	44.43	33.22				28.33	
	55.53	35.07				30.24	

4	21.5	23.11	17	21	49.47	22.72	25.79
	30.22	29.88				22.16	
	44.43	33.61				28.55	
	53.21	39.05				29.74	
5	19.02	23.22	19	20	54.27	27.15	28.92
	36.22	33.21				28.18	
	44.43	33.22				28.83	
	54.21	38.22				31.52	
6	21.44	26.58	20	19	56.08	27.38	29.53
	32.08	33.57				28.68	
	43.21	32.28				28.91	
	53.07	39.21				33.17	
7	21.21	27.05	22	14.5	56.83	30.61	31.06
	33.67	31.25				28.79	
	45.08	34.56				29.57	
	54.38	35.75				35.28	
8	21.2	30.45	23	16	61.04	25.32	31.28
	34.89	32.01				28.17	
	43.57	37.25				33.77	
	54.22	38.99				37.87	
9	21.51	22.97	16	20	45.7	19.54	25.06
	33.29	28.87				23.66	
	44.08	32.81				27.42	
	54.27	35.14				29.63	
10	20.22	25.64	16.5	21	48.02	19.85	25.34
	32.88	28.58				22.73	
	44.43	35.08				30.11	
	54.66	36.85				28.67	
11	21.33	26.33	21	15	54.74	20.09	30.51
	34.05	31.02				28.61	
	44.43	33.22				35.42	
	54.29	35.07				37.95	
12	21.8	24.58	17.5	18	48.17	22.64	25.99
	33.08	26.04				22.91	
	43.21	32.07				29.67	
	54.21	34.91				28.74	

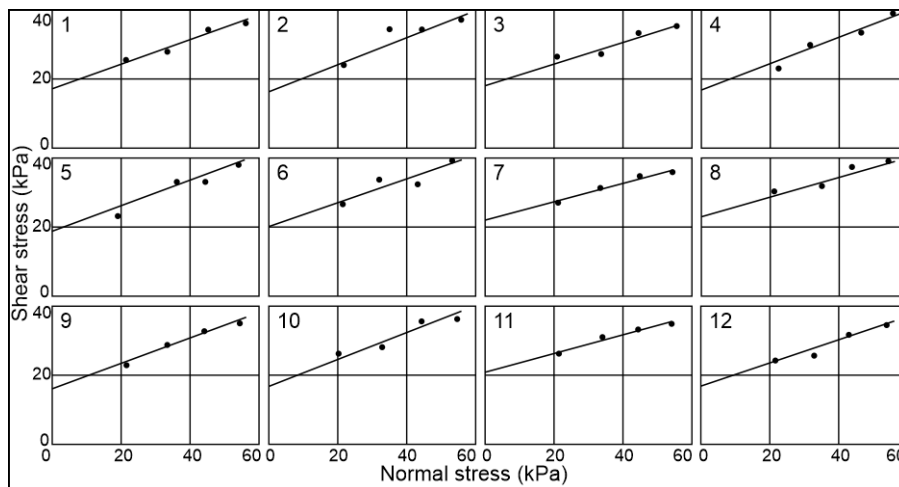


Fig. 4.2.4: Failure curves of samples

RMR and SMR

The data were collected mostly along the streams of Dzulikha Rü and Sitsie Rü from slope M1, M2 and M3 (Figs 4.2.1, 4.2.5). Sixty six rock samples were collected from undisturbed rock exposures for point load test. From the analyses, an average strength of 1.51, 1.2 and 2.71 MPa were obtained from slope M1, M2 and M3 respectively (Table 4.2.3). The point load index (PLI) of the rock samples obtained from all the sampling sites show higher strength in sandstones with an average of 2.73, 2.04 and 4.58 MPa, while that of low strength shales gave an average values of 0.28, 0.36 and 0.83 MPa respectively.



Fig. 4.2.5: Rock exposures of the studied slopes

The SMR values of 33 and 21.3 obtained from M1 and M2 respectively, falls in stability class IV which suggests unstable slope conditions (Table 4.2.4). Higher RMR and SMR values of 50 and 54 respectively are noted in M3. This slope falls in stability class III indicating partially stable slope.

Table 4.2.3: Results obtained from point load test

M1			M2			M3		
Sample No	Lithology	PLI (MPa)	Sample No	Lithology	PLI (MPa)	Sample No	Lithology	PLI (MPa)
1	Sandstone (FG)	2.28	1	Sandstone (FG)	2.08	1	Sandstone (FG)	3.94
2	Sandstone (FG)	3.12	2	Sandstone (FG)	1.51	2	Sandstone (FG)	4.67
3	Sandstone (FG)	2.34	3	Sandstone (FG)	2.61	3	Sandstone (FG)	4.37
4	Sandstone (FG)	2.85	4	Sandstone (FG)	2.05	4	Sandstone (FG)	3.92
5	Sandstone (FG)	3.07	5	Sandstone (FG)	2.85	5	Sandstone (FG)	5.74
6	Sandstone (FG)	3.03	6	Sandstone (FG)	2.11	6	Sandstone (FG)	4.86
7	Sandstone (FG)	3.14	7	Sandstone (FG)	1.46	7	Sandstone (FG)	3.91
8	Sandstone (FG)	4.05	8	Sandstone (FG)	1.94	8	Sandstone (FG)	4.82
9	Sandstone (FG)	1.37	9	Sandstone (FG)	1.86	9	Sandstone (FG)	4.04
10	Sandstone (FG)	2.81	10	Sandstone (FG)	2.11	10	Sandstone (FG)	5.31
11	Sandstone (FG)	2.05	11	Sandstone (FG)	1.86	11	Sandstone (FG)	4.83
12	Shale (W)	0.42	12	Shale (W)	0.61	12	Shale (PW)	0.81
13	Shale (W)	0.22	13	Shale (W)	0.45	13	Shale (PW)	0.95
14	Shale (W)	0.19	14	Shale (W)	0.37	14	Shale (PW)	0.74
15	Shale (W)	0.25	15	Shale (W)	0.25	15	Shale (PW)	0.75
16	Shale (W)	0.17	16	Shale (W)	0.53	16	Shale (PW)	0.86
17	Shale (W)	0.33	17	Shale (W)	0.19	17	Shale (PW)	0.88
18	Shale (W)	0.21	18	Shale (W)	0.33	18	Shale (PW)	0.83
19	Shale (W)	0.44	19	Shale (W)	0.26	19	Shale (PW)	0.79
20	Shale (W)	0.35	20	Shale (W)	0.49	20	Shale (PW)	0.94
21	Shale (W)	0.18	21	Shale (W)	0.26	21	Shale (PW)	0.85
22	Shale (W)	0.35	22	Shale (W)	0.22	22	Shale (PW)	0.81
Average strength = 1.51 MPa			Average strength = 1.2 MPa			Average strength = 2.71 MPa		

PLI - point load index; FG - fine grained; W - weathered; PW - partially weathered

Table 4.2.4: Slope mass rating

	M1		M2		M3	
1. Point load strength (MPa)	1.51	4	1.2	4	2.71	7
2. RQD (%)	48.22	8	47.09	8	38	8
3. Spacing of joints (mm)	55.91	5	58.65	5	30.2	5
4. Condition of joints	Slightly rough; highly weathered	20	Slightly rough; highly weathered	20	Slightly rough; highly weathered	20
5. Groundwater condition	Damp	10	Damp	10	Damp	10
RMR	$= (1+2+3+4+5)$	47	$= (1+2+3+4+5)$	47	$= (1+2+3+4+5)$	50
$F_1 = \alpha_j - \alpha_s $ (P/W)	-13°	1	15°	0.70	-160°	1
$ \alpha_j - \alpha_s - 180 $ (T)						
$F_2 = \beta_j$	28°	0.40	42°	0.85	80°	1
$F_3 = \beta_j - \beta_s $ (P/W)	-37°	-60	-38°	-60	115°	-6
$ \beta_j + \beta_s $ (T)						
$F_4 =$ Adjustment factor	Pre-splitting	10	Pre-splitting	10	Pre-splitting	10
SMR = $RMR + (F_1 \times F_2 \times F_3) + F_4$	$47 + \{1 \times 0.4 \times (-60)\} + 10$	33	$47 + \{0.70 \times 0.85 \times (-60)\} + 10$	21.3	$50 + \{1 \times 1 \times (-6)\} + 10$	54
Class Description	IV Weak rocks; unstable slope prone to wedge failure		IV Weak rocks; unstable slope prone to wedge failure		III Fair rocks; partially stable slope	

Kinematic analyses

Kinematic analyses were performed using 60, 227 and 80 joint attitudes from rock slopes M1, M2 and M3 respectively. From the joint analyses, pole diagrams (Fig. 4.2.6a) and contour diagrams (Fig. 4.2.6b) were constructed, from which dominant joints were identified. These were plotted against slope attitudes in stereographic projections (Fig. 4.2.6c). Two dominant joint sets are identified in M1 and M2, while only one set is registered in M3. In rock slope M1, the direction of the line of two intersecting discontinuity sets J_1 and J_2 are oriented 28° due 287° and 37° due 36° (Fig. 4.2.6c). This intersection produced a wedge trending NNW (337°). In slope M2, joint sets J_1 (42° due 55°) and J_2 (47° due 18°) intersect to produce wedge with NE (51°) trend. In slope M3, poles of discontinuities falling within the shaded portion have a chance of toppling failure whereas, those poles falling outside the shaded portion have less chance of toppling failure. The occurrence of toppling failure in this slope is certain due to the steeply inclined discontinuities (Fig. 4.2.5).

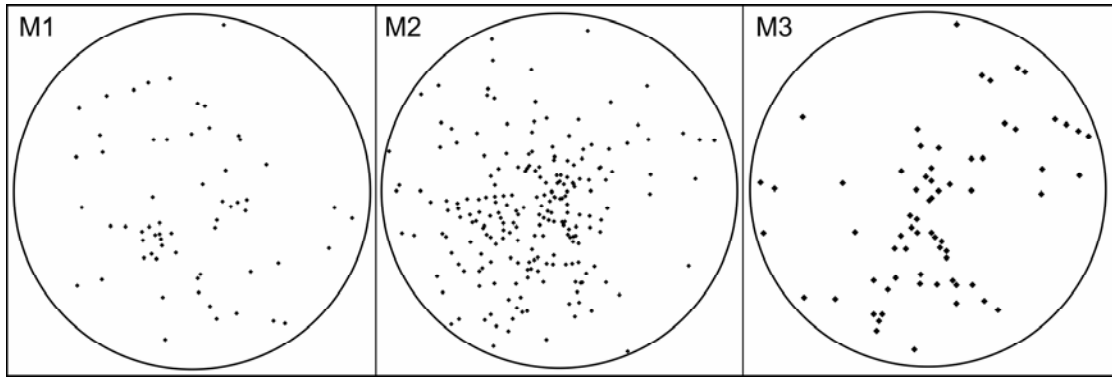


Fig. 4.2.6a: Pole diagrams

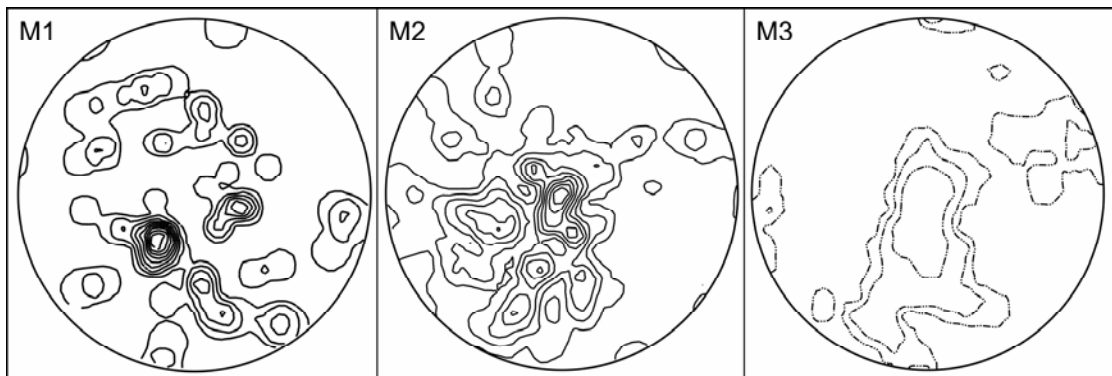


Fig. 4.2.6b: Contour diagrams

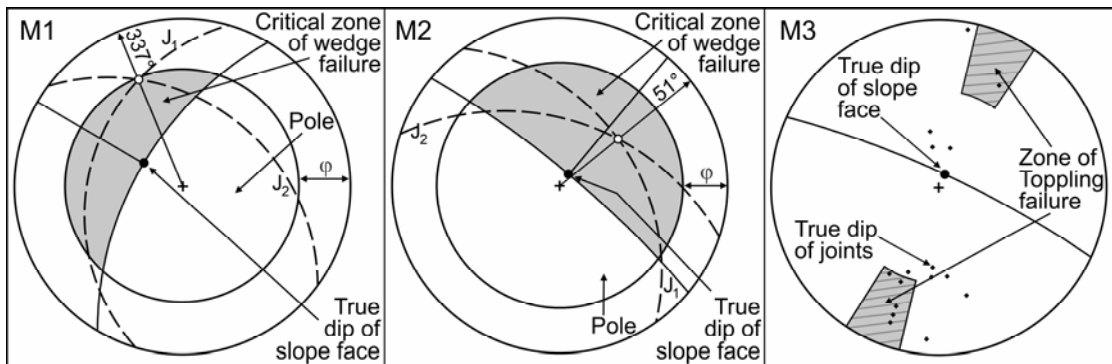


Fig. 4.2.6c: Stereographic projections

Table 4.2.5: Input data and mode of failure in kinematic analysis

Slope	M1	M2	M3
No. of joints measured	60	227	80
Slope orientation	65°/300°	80°/40°	80°/25°
Orientation of principle joint sets	J ₁ = 28°/287° J ₂ = 37°/36°	J ₁ = 42°/55° J ₂ = 47°/18°	J = 35°/45°
Internal friction angle (ϕ)	20°	18°	30°
Type of failure	Wedge	Wedge	Topple
Data format	Dip / dip direction		
Magnetic declination	-0.367 (west declination of the study area)		

Structural analyses

In rock slope M1, the rose diagram shows one dominant joint trend along NE-SW (Fig. 4.2.7), which is parallel to the regional trend that is related to F2 movements. Another set of joints trend NW-SE. These joints are due to tensile or shear stresses that are concentrated around the regional NW-SE compression corresponding to F3 movements (Roy et al., 1986). Slope M2 and M3 show joints with similar orientations along WNW-ESE and NNW-SSE where the dominant role of synthetic shearing of rocks and antithetic shears causes tensile fractures of the rock. Another joint trending ENE-WSW are observed at M2 and M3.

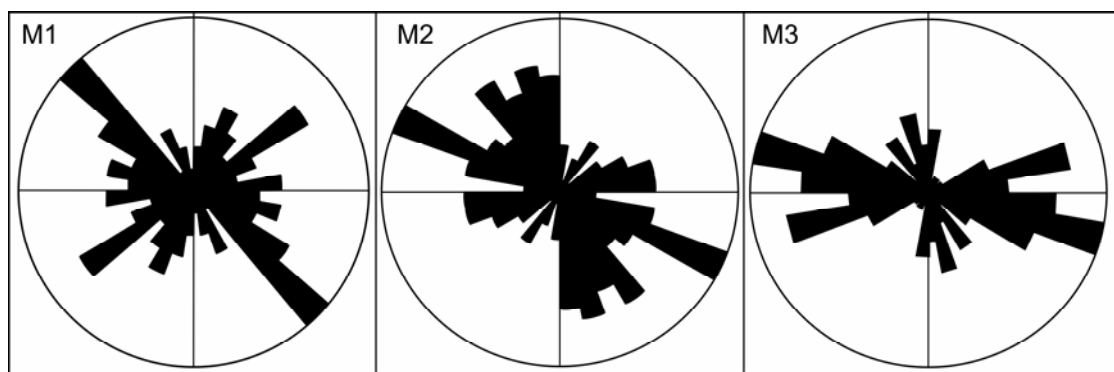


Fig. 4.2.7: Rose diagrams

The study area is crossed by lineaments trending NW-SE, NE-SW and NNW-SSE (Fig. 4.2.8). The NW-SE trending lineament runs almost parallel to highly erosive Dzulikha Rü (Fig. 4.2.9). Large-scale fracturing of the rocks is seen along its strike (Fig. 4.2.10). The basal erosion by the stream caused the slope to move downward as well as lend instability in the upper section in the form of tension cracks (Fig. 4.2.11A). This had further led to subsidence in the area (Fig. 4.2.11B). A NE-SW trending lineament cuts across almost perpendicular to the NW-SE trending lineament. Here, the slope materials have been intensely sheared and weathered to black clays (Fig. 4.2.12). Another NE-SW trending lineament may be responsible for some instabilities in the area (Fig. 4.2.13). A portion of the land that had been used for terrace cultivation composed of thick deposits of clay (Fig. 4.2.14A) occurs along the NNW-SSE trending lineament which runs parallel to Sitsie Rü. Water seepages are observed in such areas, specially near the lower part of the slope (Fig. 4.2.14B).



Fig. 4.2.8: Google Earth image showing lineaments and photo locations



Fig. 4.2.9: Toe erosion along Dzulikha Rü



Fig. 4.2.10: Jointed and fractured rocks on the western bank of Dzulikha Rü



Fig. 4.2.11: A - Tension crack developed on the slope; B - Road damaged due to subsidence



Fig. 4.2.12: Exposures of shale and clay along stream section



Fig. 4.2.13: A - Subsidence along the road section; B - Damaged house



Fig. 4.2.14: A - Slope material constituting clay deposits; B - Water seepages observed during dry season

Factor of safety

The input values for determination of factor of safety for the Slide zone are:

$$c = 17 \text{ kN/m}^2$$

$$\phi = 20^\circ$$

$$\gamma = 18 \text{ kN/m}^3 \text{ (unit weight of clayey soil)}$$

$$Z = 35 \text{ m}$$

$$\beta = 25^\circ$$

$$\text{Unit weight of water in the soil, } \gamma_w = 9.8 \text{ kN/m}^3$$

Here the slope is considered as saturated, so saturation constant (M) = 1

For c and ϕ , averages have been taken from direct shear test result from the slide zone itself, the values of samples 1 and 2 (Table 4.2.2) are used.

$$\begin{aligned} FoS &= \left\{ \frac{[17 + (18 - 1 * 9.8) * 35 * (\text{Cos}^2 25^\circ) * (\text{Tan} 20^\circ)]}{[18 * 35 * (\text{Sin} 25^\circ * \text{Cos} 25^\circ)]} \right\} \\ &= \left\{ \frac{[17 + (18 - 9.8) * 35 * 0.82 * 0.36]}{(18 * 35 * 0.42 * 0.906)} \right\} \\ &= \frac{101.72}{239.72} \\ FoS &= \mathbf{0.42} \end{aligned}$$

The FoS value of 0.42 is classified as low, which indicates that the slope is very unstable.

4.3 Kevüza area

This particular study is taken up in Kevüza area which is about 5 km west of Kohima town. The area lies between latitudes $25^{\circ}40'49.92''$ - $25^{\circ}41'34.07''$ N and longitudes $94^{\circ}03'47.49''$ - $94^{\circ}04'26.31''$ E (Fig. 4.3.1).

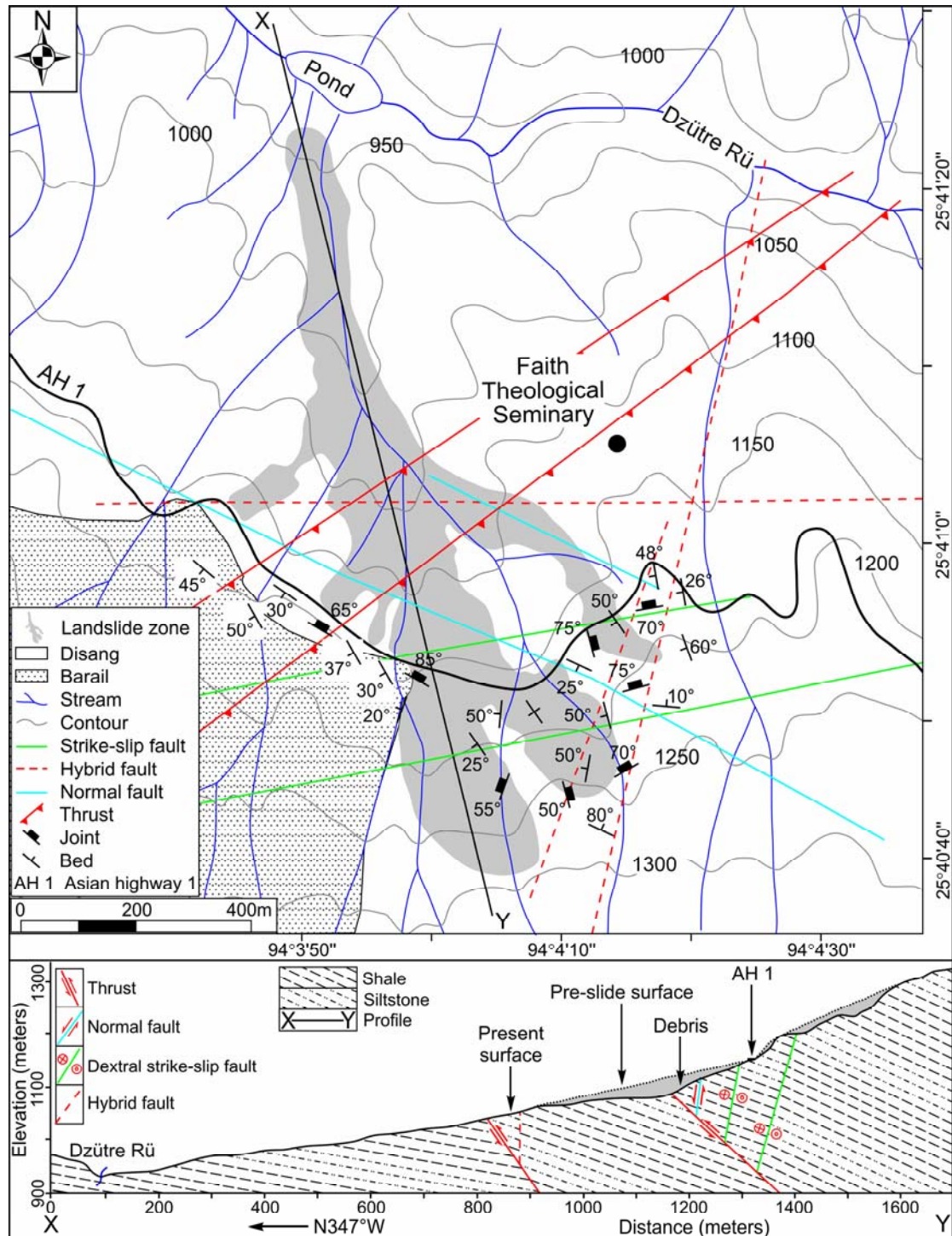


Fig. 4.3.1: Geological map of the Kevüza study area; Profile along X-Y (on map) depicting surface before and after the landslide event and subsurface geology

In Kevüza area, three landslide events have been reported so far. The first landslide incidence took place on June 2011 (Yano, 2017) where a major portion of the highway was completely washed away. The second event took place on 1st August 2018 where two portions of area including ~400 m of the highway was affected by a major landslide (Fig. 4.3.2c[S1, S2], e, f). This resulted in complete halt of vehicular movement for over a month. Another landslide occurred in the same area on 4th August 2019, which damaged portions of the highway (Fig. 4.3.3a) and electrical power structures (Fig. 4.3.3b), totally blocked vehicular traffic again for nearly a month.

The affected area lies at an altitude between 950 to 1300 m above msl with the slope angles ranging between 25° to 35°. Two landslide zones are identified for investigations in this area (Fig. 4.3.2c[S1, S2]). The first portion designated as Slide zone 1 is 270 m long, 60 m wide and 14 m deep. The other affected portion, Slide zone 2, is about 550 m long, 110 m wide and 8.5 m deep. The two slides altogether affected an area of ~60,000 m² and displaced ~2,90,862 m³ of material. The slide material is a mixture of dominantly clay with soil debris, siltstone and shale.

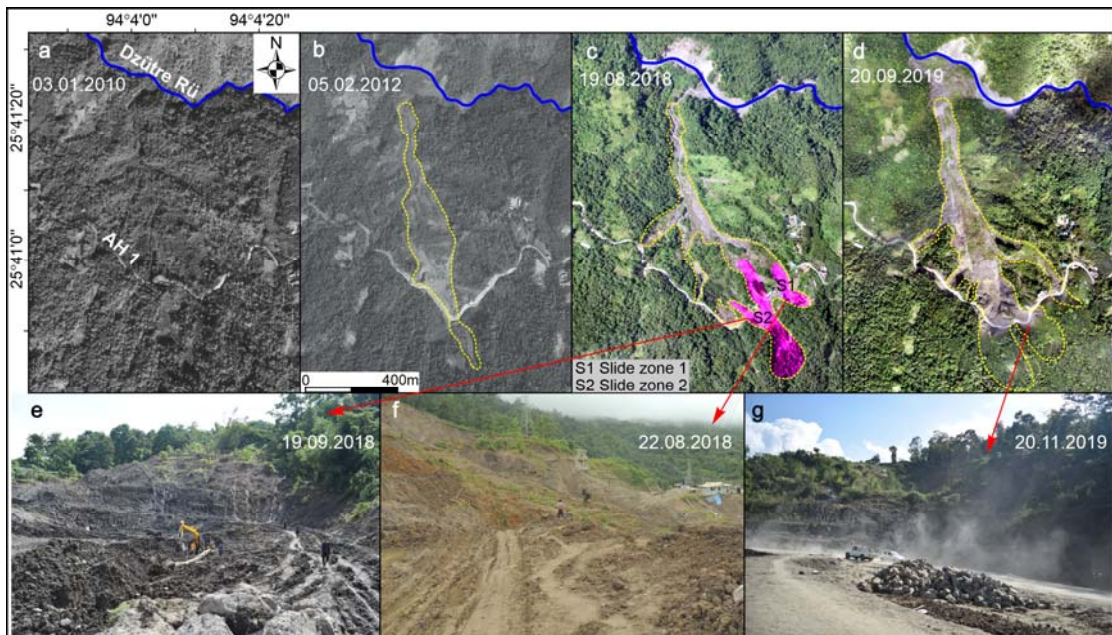


Fig. 4.3.2: **a** Google Earth (GE) image of 2010 before landslide; **b** GE image of 2011 landslide (yellow broken line - boundary of affected area); **c** Unmanned aerial vehicle (UAV) image showing landslides of 2018; **d** UAV image showing landslide of 2019; **e, f** Photos of damaged portions of highway at locations S1 & S2 due to landslides in 2018; **g** Photo of repaired highway after 2019 landslide event



Fig. 4.3.3: Effects of the landslides - **a** Large fissure on the highway at the eastern edge of the slide zone; **b** Collapsed pylon (major support for power cables to Kohima)

Rock exposures in the study area belong to the Disang and Barail Groups. These rocks, particularly the Disang, are highly fractured and crushed. The Disang consist predominantly of partially weathered shale with minor intercalations of thin-bedded siltstone. The outcrops vary in colour from reddish brown to grey; the shale and siltstone are dark grey. The rocks are crossed by three sets of joints. The Barail are exposed along the west and southwest of the highway. They are represented by massive sandstones with intercalations of thin papery shale. These brittle sandstones are crossed by three to four sets of joints; they are commonly shattered, which may be attributed to ongoing tectonic stresses. Some of the fractures in the rocks are as large as 15 mm (Fig. 4.3.4-K4). During heavy rainfall, and particularly during the monsoon, increased water infiltration into the pervious soils and rocks leads to elevated water tables that manifest as springs and seepages at different levels of the slopes.

This area is crossed by several 1st and 2nd order streams which merge into the major NW-flowing river, Dzütire Rü. These streams, which form parallel drainage patterns, vigorously dissect the weak rocks.

Remote sensing and UAV mapping

Remote sensing images of 2012, 2018 and 2019 show the gradual growth of the affected zone due to recurrence of landslides in the area (Fig. 4.3.2b, c, d). Aerial photography using a drone to study the landslide was undertaken to capture 484 images covering an area of ~2 km². Agisoft Metashape software was used to process the images using coordinate and projection system of WGS84/UTM zone 46N. This data was used to build an orthophoto and a digital elevation model (DEM) of the area which assisted in computing the landslide dimension and the total affected area. Based on the 1:25000 topographic map, another DEM of the same area was extracted using ArcGIS 10.5. The change in slope profile was estimated by comparing the two DEMs which represent the pre- and post-landslide surface profiles. The dimension, depth and volume of the landslides were calculated following Cruden and Varnes (1996) and Dewitte and Demoulin (2005), using the semi-ellipsoid equation of Jaboyedoff et al. (2020). It is expressed by the equation,

$$V = \frac{1}{8} \cdot \pi \cdot W \cdot L \cdot D \quad (4.3.1)$$

where V - volume of landslide, W - width of landslide surface, L - length of landslide-affected area and D - maximum vertical depth of the slide surface.

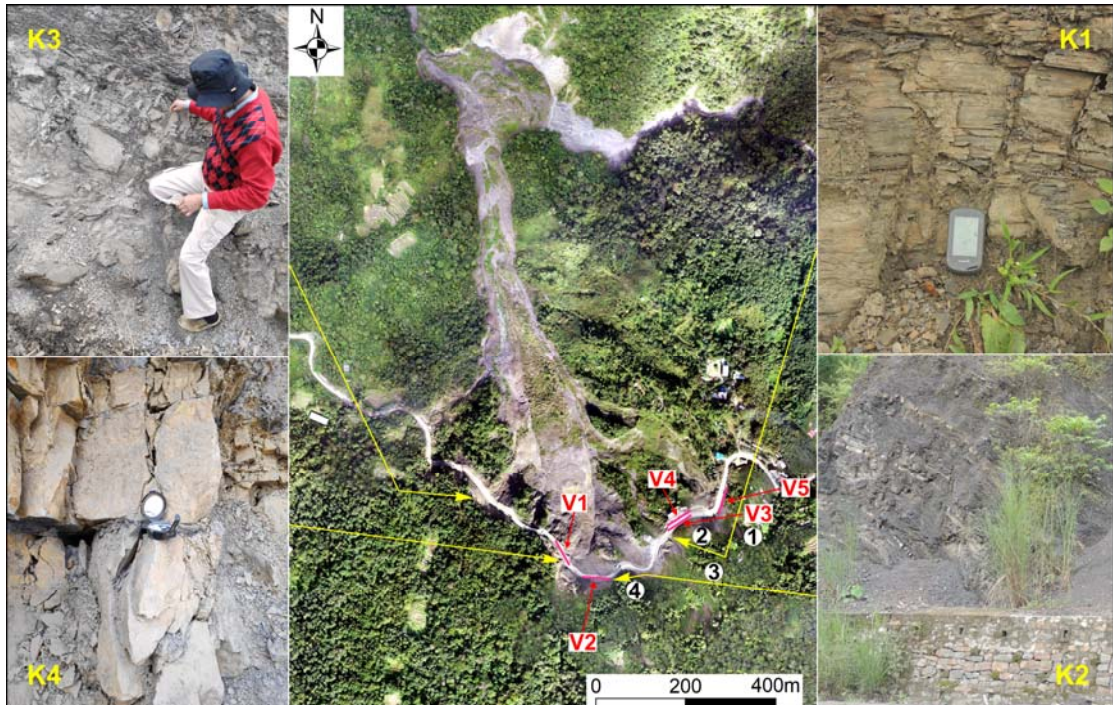


Fig. 4.3.4: **K1, K2, K3, K4** Rock exposures in the study area; **1, 2, 3, 4** Soil sampling sites for geotechnical analyses; **V1, V2, V3, V4, V5** Vertical electrical sounding sites (Pink lines) for resistivity survey profiles

Geotechnical analyses

Four soil samples were analysed to determine the moisture content, consistency limits and their shear strength properties.

Moisture content and Consistency limits

Soil samples were collected in the month of February. The moisture content of the soils ranges from 11.23 to 26.44% (Table 4.3.1). The liquid limit (W_L) of the soil samples range from 28.5 to 46%. The shrinkage limit of sample 1 (20.35%) is high and moderate in samples 2, 3 and 4 (range - 11.42 to 14.45%). The consistency index of samples 1, 2 and 4 have values greater than 1, indicating that the soils are at semisolid state while sample 3 is in plastic state.

Table 4.3.1: Moisture content and Consistency limits

Sample No.	Water content (%)	Liquid limit (%)	Plastic limit (%)	Plasticity index (%)	Consistency index (%)	Shrinkage limit (%)
1	12.66	44	25.56	18.44	1.69	20.35
2	18.75	46	22.86	23.14	1.17	11.42
3	26.44	28.5	14.54	13.96	0.14	13.17
4	11.23	29	14.04	14.96	1.18	14.45

The plasticity chart (Fig. 4.3.5) classifies the test samples as inorganic clays of low to moderate plasticity. The low plasticity of the soils may be due to the fine sands present in the mixture. The W_L of the soils indicate low to moderate compressibility (IS: 1498, 1970) with low to moderate swelling potential (Dumbleton, 1968). When surface-water percolation increases, very fine soil particles in the subsurface are carried away in suspension through the pervious crust and highly fissured subsurface rocks. This causes the retention of coarser particles such as silt and very fine sand, which leads to decrease in soil plasticity. This may be the reason for the lower swelling potential reported by other researchers (Al-Homoud et al., 1995). Stanchi et al. (2015) opine that soils possessing low W_L values, as noted in samples 3 and 4, are those where liquid limit can be reached more quickly, that is, the ability to change rapidly from semi-solid to liquid state with increasing moisture content. In such cases, any sudden disturbance would cause the soil to flow, making such slopes susceptible to failure. The frequent and cyclic wetting and drying during episodes of heavy precipitation and intermittent dry spells respectively, strongly influence the shrink-

and-swell behaviour of the soils in the study area. Such phenomenon can deform soils and damage man-made structures (Guney et al., 2007; Nowamooz and Masrouri, 2008).

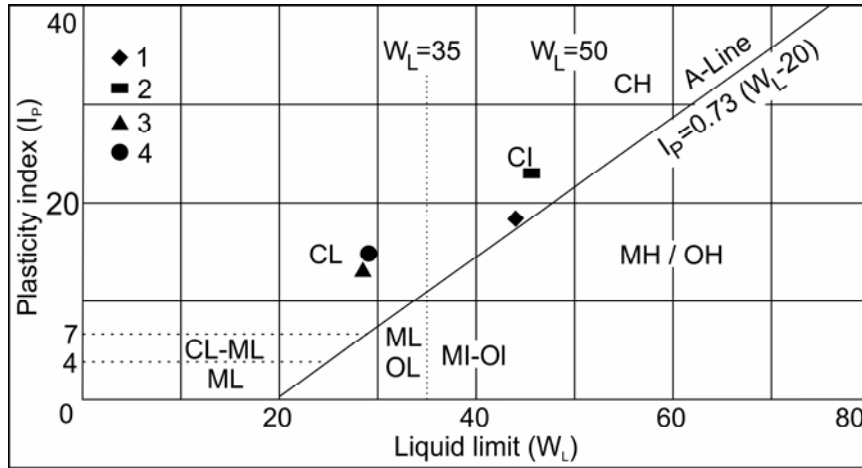


Fig. 4.3.5: Plasticity chart

Direct shear test

Shear strength parameters of c , ϕ and σ_{ci} (Table 4.3.2) were derived from the failure envelope by plotting normal stress against shear stress (Fig. 4.3.6). The σ_{ci} values obtained range from 33.43 to 49.26 kPa indicating soft and weak soils.

Table 4.3.2: Shear strength parameters of the soils obtained from direct shear test

Sample No.	Normal stress (kPa)	Shear stress (kPa)	c (kPa)	ϕ (°)	σ_{ci} (kPa)	Water content (W_c)	Average W_c at failure
1	21.87	24.55	16.41	21.65	48.34	25.66	27.34
	29.33	29.37				25.95	
	41.82	31.65				27.73	
	51.02	37.27				30.03	
2	21.93	25.37	17.74	20.08	49.26	26.02	28.92
	30.29	29.44				29.14	
	41.77	32.82				29.33	
	51.83	36.64				31.21	
3	21.93	18.51	14.87	15.72	39.27	21.87	23.76
	30.29	27.13				22.37	
	41.77	26.17				24.22	
	51.83	28.72				26.61	
4	21.18	20.03	11.95	18.88	33.43	20.69	22.88
	30.44	20.15				22.01	
	41.05	28.02				24.17	
	51.66	28.97				24.68	

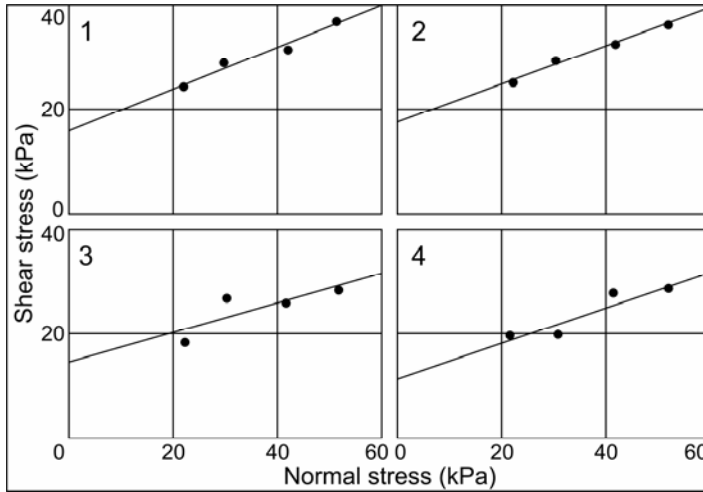


Fig. 4.3.6: Failure curves of samples

A decreasing trend of cohesion with respect to water content at failure is observed (Table 4.3.2). Samples 3 and 4, classified as soils of low plasticity and possessing low cohesion values, failed at lower water contents as compared to samples 1 and 2 of moderate plasticity (Fig. 4.3.5). This is due to the fact that soils with low plasticity consist of some coarser particles as well. Hence, water retention capacity is low in such cases, which therefore, tend to fail at lower water content. It has also been observed that there is a marked decrease in σ_{ci} from moderately plastic soils (samples 1 and 2) to those of low plasticity (samples 3 and 4), indicating decreasing compressive strength of the soil samples with decreasing plasticity. Similar trends have been observed by Malizia and Shakoor (2018).

RMR and SMR

The rocks exposed along the highway were evaluated for slope mass rating (Fig. 4.3.4). Eighty rock samples were collected from the 4 locations for point load test. Average point load index (PLI) values of 0.532, 0.383, 0.469 and 1.681 MPa were obtained for slope K1, K2, K3 and K4 respectively (Table 4.3.3). Since the index strength (average PLI) of K1, K2 and K3 are less than 1 MPa, as recommended by Bieniawski (1989), UCS was applied (Eq. 3.7). In order to maintain uniformity, index strength of K4 (1.681 MPa) was also converted to UCS (Table 4.3.4). Based on this rating scheme, it is found that the point load strength and UCS of K4 displayed the same rating even after conversion showing good correlation.

Table 4.3.3: Results obtained from point load test

K1			K2			K3			K4		
Sample No	Lithology	PLI (MPa)	Sample No	Lithology	PLI (MPa)	Sample No	Lithology	PLI (MPa)	Sample No	Lithology	PLI (MPa)
1	Shale (W)	0.58	1	Shale (W)	0.23	1	Shale (W)	0.38	1	Sandstone (FG)	1.49
2	Shale (W)	0.61	2	Shale (W)	0.17	2	Shale (W)	0.65	2	Sandstone (FG)	2.28
3	Shale (W)	0.58	3	Shale (W)	0.35	3	Shale (W)	0.57	3	Sandstone (FG)	2.08
4	Shale (W)	0.42	4	Shale (W)	0.24	4	Shale (W)	0.67	4	Sandstone (FG)	1.87
5	Shale (W)	0.69	5	Shale (W)	0.16	5	Shale (W)	0.39	5	Sandstone (FG)	2.16
6	Shale (W)	0.78	6	Shale (W)	0.29	6	Shale (W)	0.26	6	Sandstone (FG)	2.11
7	Shale (W)	0.65	7	Shale (W)	0.49	7	Shale (W)	0.38	7	Sandstone (FG)	1.36
8	Shale (W)	0.73	8	Shale (W)	0.27	8	Shale (W)	0.23	8	Sandstone (FG)	2.73
9	Shale (W)	0.67	9	Shale (W)	0.41	9	Shale (W)	0.27	9	Sandstone (FG)	2.09
10	Shale (W)	0.52	10	Shale (W)	0.31	10	Shale (W)	0.35	10	Sandstone (FG)	2.22
11	Shale (W)	0.33	11	Shale (W)	0.43	11	Shale (W)	0.24	11	Sandstone (FG)	1.87
12	Shale (W)	0.46	12	Shale (W)	0.33	12	Shale (W)	0.67	12	Sandstone (FG)	1.35
13	Shale (W)	0.42	13	Shale (W)	0.19	13	Shale (W)	0.73	13	Sandstone (FG)	0.93
14	Shale (W)	0.53	14	Shale (W)	0.39	14	Shale (W)	0.61	14	Sandstone (FG)	1.14
15	Shale (W)	0.53	15	Shale (W)	0.26	15	Shale (W)	0.6	15	Sandstone (FG)	2.08
16	Shale (W)	0.71	16	Shale (W)	0.17	16	Shale (W)	0.57	16	Sandstone (FG)	1.37
17	Shale (W)	0.27	17	Shale (W)	0.81	17	Shale (W)	0.31	17	Sandstone (FG)	1.27
18	Shale (W)	0.35	18	Shale (W)	0.65	18	Shale (W)	0.43	18	Sandstone (FG)	0.81
19	Shale (W)	0.55	19	Shale (W)	0.73	19	Shale (W)	0.55	19	Sandstone (FG)	1.33
20	Shale (W)	0.26	20	Shale (W)	0.78	20	Shale (W)	0.52	20	Sandstone (FG)	1.08
Average strength = 0.532 MPa			Average strength = 0.383 MPa			Average strength = 0.469 MPa			Average strength = 1.681 MPa		

PLI - point load index; W - weathered; FG - fine grained

Table 4.3.4: Determination of UCS from point load strength index using conversion factor

Location	Rock type	Conversion factor	Correlating equation	UCS (MPa)
K1	Shale	14.4	UCS = 14.4 PLI	7.66
K2	Shale	14.4	UCS = 14.4 PLI	5.52
K3	Shale	14.4	UCS = 14.4 PLI	6.75
K4	Sandstone	21.9	UCS = 21.9 PLI	36.8

The shale samples of slopes K1, K2 and K3 have low UCS values of 7.66, 5.52 and 6.75 MPa (Table 4.3.5) respectively, whereas the sandstones (slope K4) have higher UCS values (36.8 MPa). Slope K1 falls in stability classes V, K2 and K3 in class IV, while it is in class III in case of the slope K4.

Table 4.3.5: Slope mass rating

	K1		K2	
1. UCS (MPa)	7.66	2	5.52	2
2. RQD (%)	22.6	3	32.5	8
3. Spacing of joints (mm)	155	8	57	5
4. Condition of joints	Slickensided surface; joints separation 1-5 mm	10	Slightly smooth surface; separation 1-5 mm	10
5. Groundwater condition	Wet	7	Wet	7
RMR	$= (1+2+3+4+5)$	30	$= (1+2+3+4+5)$	32
$F_1 = \alpha_j - \alpha_s$	22°	0.4	-56°	1
$F_2 = \beta_j$	72°	1	55°	1
$F_3 = \beta_j - \beta_s$	-3°	-50	10°	-6
$F_4 = \text{Adjustment factor}$	Pre-splitting	10	Pre-splitting	10
SMR =	$30 + \{0.4 \times 1 \times (-50)\} + 10$	20	$32 + \{1 \times 1 \times (-6)\} + 10$	36
$\text{RMR} + (F_1 \times F_2 \times F_3) + F_4$				
Class	V		IV	
Description	Weak rocks; highly unstable slopes prone to soil-like failure		Weak rocks prone to wedge failure; unstable slopes	
	K3		K4	
1. UCS (MPa)	6.75	2	36.8	4
2. RQD (%)	16	3	9.4	3
3. Spacing of joints (mm)	75.5	8	163	8
4. Condition of joints	Slightly smooth surface; separation 1-5 mm	10	Slightly rough surface; highly weathered walls	20
5. Groundwater condition	Wet	7	Wet	7
RMR	$= (1+2+3+4+5)$	30	$= (1+2+3+4+5)$	42
$F_1 = \alpha_j - \alpha_s$	-15°	1	-36°	1
$F_2 = \beta_j$	65°	1	85°	1
$F_3 = \beta_j - \beta_s$	5°	-6	5°	-6
$F_4 = \text{Adjustment factor}$	Pre-splitting	10	Pre-splitting	10
SMR =	$30 + \{1 \times 1 \times (-6)\} + 10$	34	$42 + \{1 \times 1 \times (-6)\} + 10$	46
$\text{RMR} + (F_1 \times F_2 \times F_3) + F_4$				
Class	IV		III	
Description	Weak rocks prone to wedge failure; unstable slopes		Fairly stable rocks prone to wedge failure at places; partially stable slopes	

RMR values estimated for K1, K2 and K3 are 30, 32 and 30 respectively. The SMR values for slopes K1, K2 and K3 are 20, 36 and 34 respectively. Higher RMR and SMR values of 42 and 46 respectively are noted in slope K4. SMR values for slopes K1, K2 and K3 indicate unstable slope conditions. Clay-infilling is common within the rock masses due to easy infiltration of surface runoff into the numerous joints and fractures. Water seepages were observed at places during the dry season (10th April 2019; 3rd February 2020). The low UCS values of these rocks point to the effect of continuing weathering, which results from seasonal fluctuations of groundwater levels. The partially weathered shales, being highly sensitive to water, are prone to sudden drops in shearing strength in the presence of excess water, which reduces the stability of slopes. Erguler and Ulusay (2009) showed UCS reduction of up to 90% with increasing water content on clay-bearing rocks. Pellet et al. (2013) showed that both cohesion and internal friction angle of clay-infilled rocks decreased due to water saturation, causing reduction of strength by 50%. Higher RMR and SMR values of slope K4 indicate fairly stable rocks and partially stable slopes, which may be due to high frictional limit of the massive sandstones.

Kinematic analyses

Kinematic analyses were performed using 33, 203, 59 and 50 joint attitudes from rock slopes K1, K2, K3 and K4 respectively. From the joint analyses, pole diagrams (Fig. 4.3.7a) and contour diagrams (Fig. 4.3.7b) were constructed, from which dominant joints were identified. These were plotted against slope attitudes in stereographic projections (Fig. 4.3.7c). Three dominant joint sets have been identified in K1 and two each in K2, K3 and K4 (Fig. 4.3.7c). In slope K1, joint sets J₁ (72° due 342°) and J₂ (85° due 059°) intersect to produce a wedge with a NNW (344°) trend and the intersection between J₁ and J₃ (20° due 214°) produces a wedge trending WSW (256°). In slope K2, the direction of the line of two intersecting discontinuity sets J₁ (55° due 289°) and J₂ (45° due 316°) strike almost parallel ($\pm 6^\circ$) to the slope face trend (345°). This wedge has a NNW (339°) trend. In slope K3, the joint sets J₁ and J₂ trend 65° due 030° and 74° due 011° respectively. The two intersecting joint sets J₁ and J₂ are oriented 85° due 029° and 88° due 182° in slope K4.

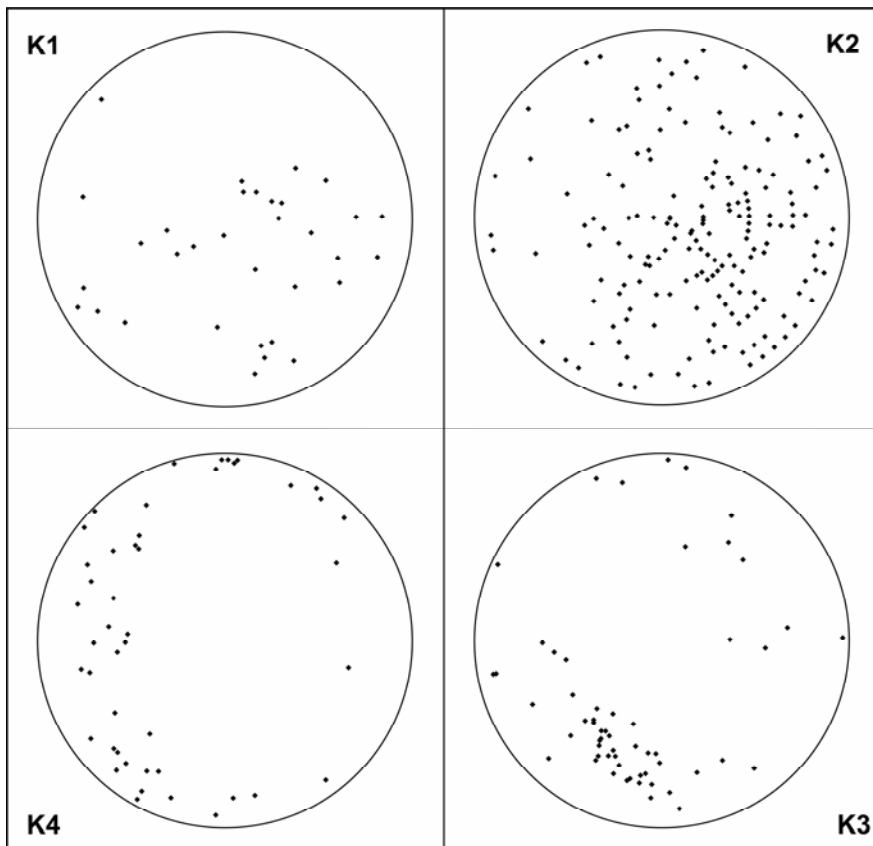


Fig. 4.3.7a: Pole diagrams

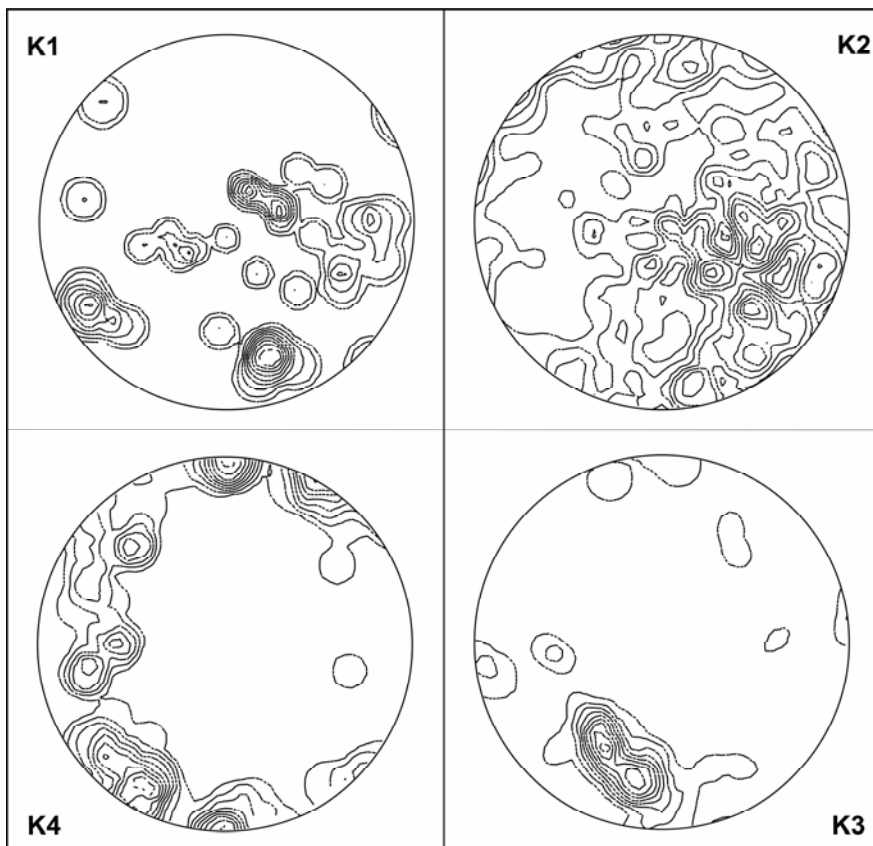


Fig. 4.3.7b: Contour diagrams

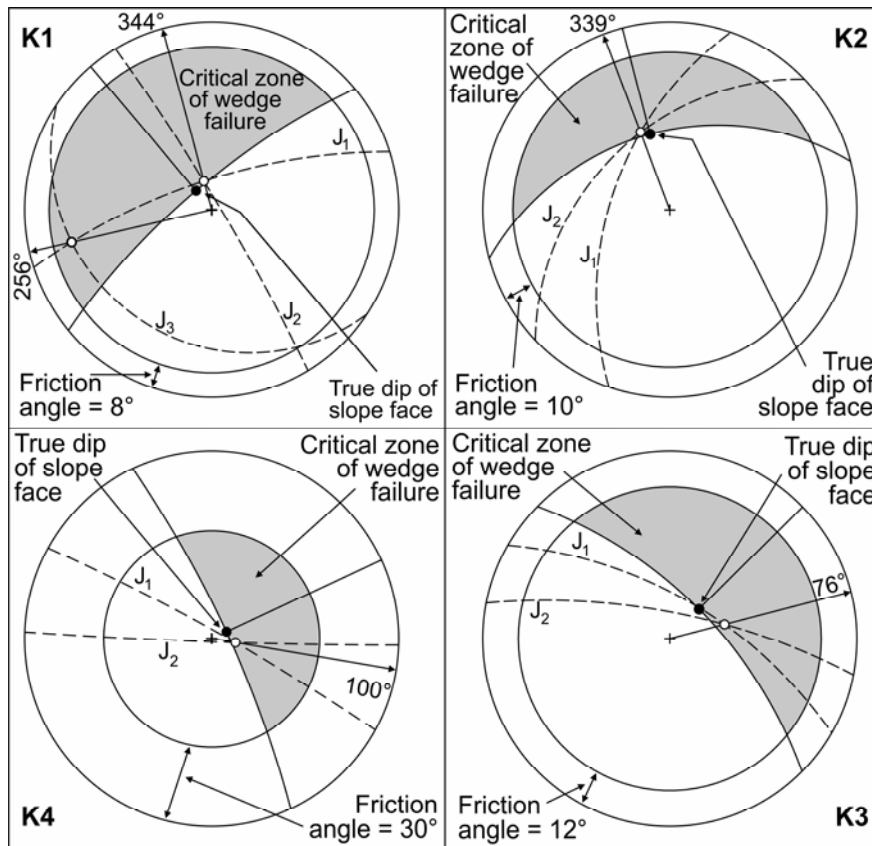


Fig. 4.3.7c: Stereographic projections

From input parameters (Table 4.3.6) the stereographic projections show wedge failure of the slopes (Fig. 4.3.7c). In slope K2, J_1 and J_2 form the perfect condition for wedge failure. In slope K3, the failure direction of the intersecting joint sets also indicates wedge failure along the ENE (076°) direction. The intersecting joint sets J_1 and J_2 in location K4 also provides conditions for wedge failure with an ESE (100°) trend.

Table 4.3.6: Input data and modes of failure in kinematic analysis

Slope	K1	K2	K3	K4
No. of joints measured	33	203	59	50
Slope orientation	$75^\circ/320^\circ$	$45^\circ/345^\circ$	$60^\circ/45^\circ$	$80^\circ/65^\circ$
Orientation of principle joint sets	$J_1 = 72^\circ/342^\circ$	$J_1 = 55^\circ/289^\circ$	$J_1 = 65^\circ/30^\circ$	$J_1 = 85^\circ/29^\circ$
	$J_2 = 85^\circ/59^\circ$	$J_2 = 45^\circ/316^\circ$	$J_2 = 74^\circ/11^\circ$	$J_2 = 88^\circ/182^\circ$
	$J_3 = 20^\circ/214^\circ$			
Internal friction angle (ϕ)	8°	10°	12°	30°
Type of failure	Wedge	Wedge	Wedge	Wedge
Data format	Dip / dip direction			
Magnetic declination	-0.367 (west declination of the study area)			

Structural analyses

The rose diagrams of the rock slopes (Fig. 4.3.8) show the orientations of the joints of the study area, which are aligned NW-SE, ENE-WSW, NE-SW, NNE-SSW, E-W and WNW-ESE. The study area also shows faults trending approximately NE-SW, WNW-ESE, WSW-ENE, E-W and NNE-SSW (Fig. 4.3.9). The rocks also show the presence of slickensides (Figs. 4.3.10[i], 4.3.10[ii]-h).

The NE-SW lineaments (Fig. 4.3.8-R2) in the study area conform to the regional trend of the thrusts and major fold axes of Nagaland. A thrust marked in the area trends approximately NE-SW along g-h (Fig. 4.3.9). An outcrop in the study area depicts the thrust relationship of the rocks (Fig. 4.3.10[ii]-g). Another thrust mapped (Fig. 4.3.9) trends almost parallel to the former. At the outcrop, lower beds are seen thrusting upward (Fig. 4.3.10[ii]-i) and deforming the upper beds in the process. A normal fault trending WNW-ESE crosses this area (Fig. 4.3.9). A waterfall in the area (Fig. 4.3.10[ii]-j) lies along this fault. Synthetic shearing is dominant in these rocks. Two faults trending WSW-ENE mapped by visual examination of satellite imagery (Fig. 4.3.9), are dextral strike-slip faults. The E-W and NNE-SSW lineaments may be hybrid faults generated due to multiple stresses acting in various directions. The intense deformation of the rocks (Fig. 4.3.11) and presence of slickenside point to multiple stresses in the area, and possible ongoing tectonism.

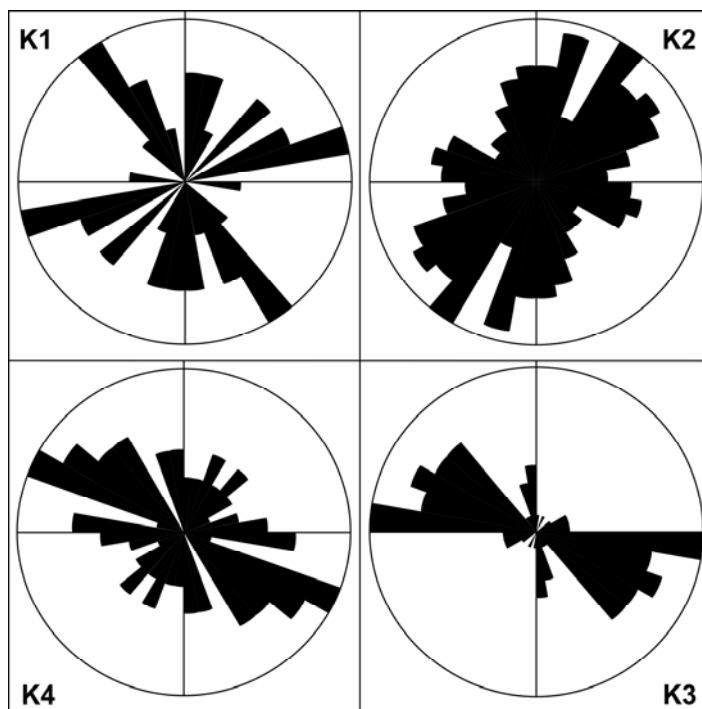


Fig. 4.3.8: Rose diagrams

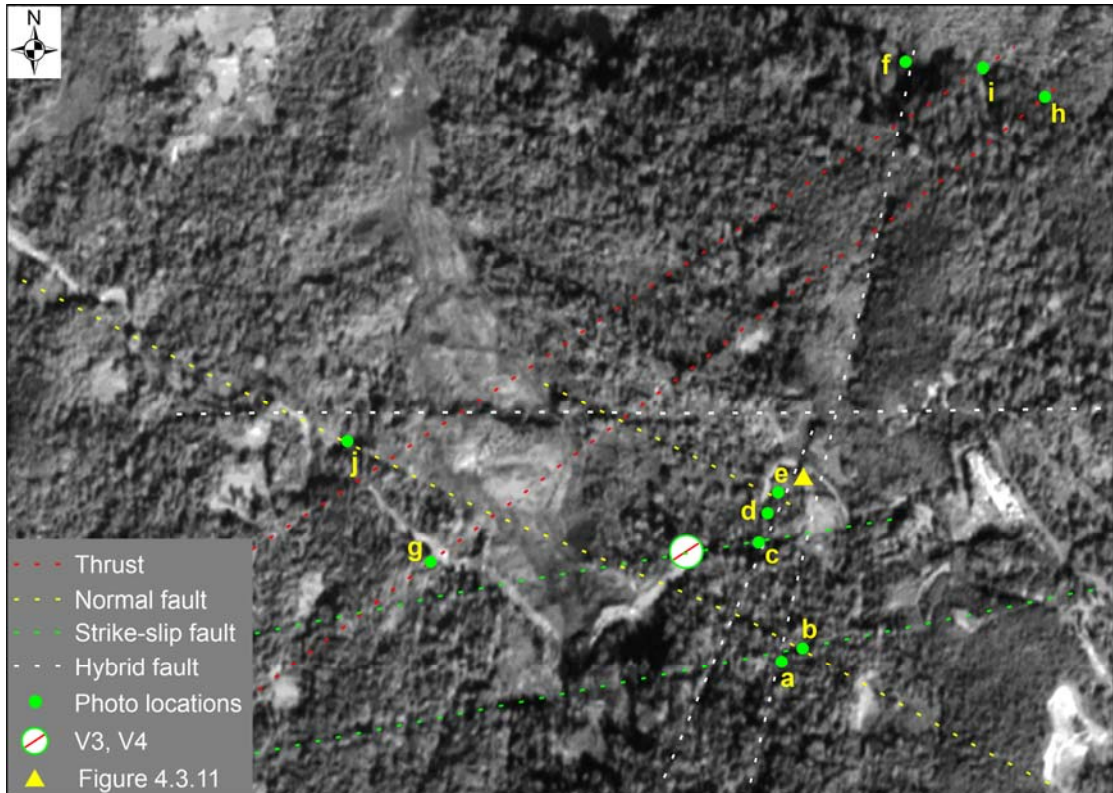


Fig. 4.3.9: Lineament map of the study area; Red line within green circle represents resistivity survey lines VES 3 and VES 4 (see fig. 4.3.4)

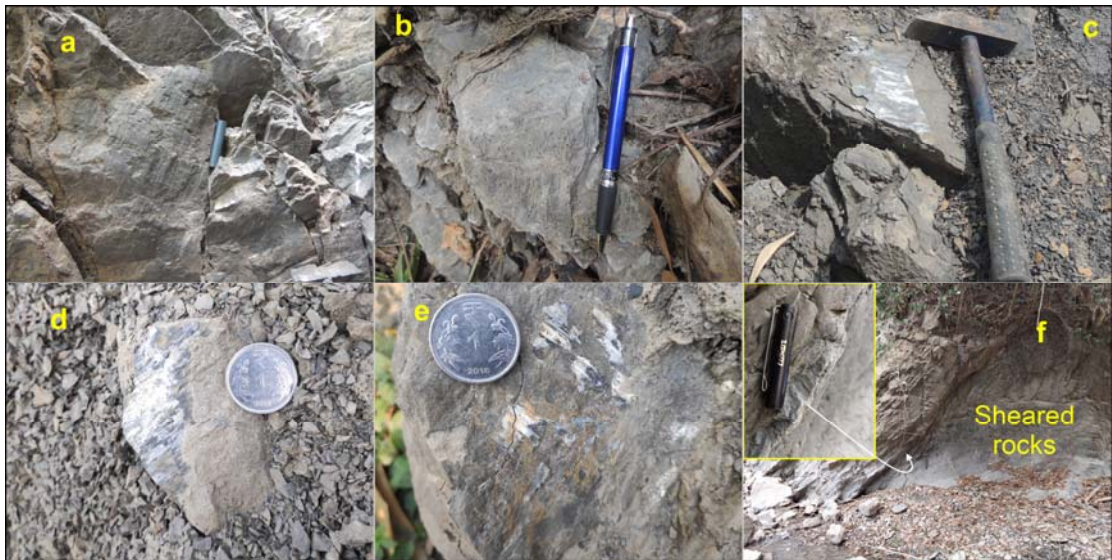


Fig. 4.3.10[i]: Slickensides along fault planes



Fig. 4.3.10[ii]: **g** Blocks displaced due to thrusting; **h** Slickenside along fault plane; **i** Steeply inclined beds thrust (red arrow) over younger rocks; **j** Waterfall along exposed scarp of normal fault



Fig. 4.3.11: Outcrop of intensely folded and sheared rocks (See fig. 4.3.9)

Precipitation analysis

GPM 3IMERGDF v06 data, with a temporal resolution of 24 hours and a spatial resolution of 0.1° (Acker, 2007), was used in this study. Precipitation data (mm per day) was obtained by calculating spatial averages over the study area in the desired date range to generate a time-series output (Huffman et al., 2019).

The area received heavy rainfall intermittently (Fig. 4.3.12), with a maximum of 39.05 mm on 24th July 2018 (Table 4.3.7), which continued during the following days till 30th July. Two major landslides occurred on 1st August 2018 (Fig. 4.3.2c[S1, S2]). Heavy rainfall of up to 31.29 mm again occurred in the area from 1st to 3rd August 2019 (Fig. 4.3.12). This event was followed by another major slide on 4th August (Fig. 4.3.2d).

Table 4.3.7: GPM precipitation data for the study area

Precipitation (mm)			Precipitation (mm)		
<i>Date</i>	<i>2018</i>	<i>2019</i>	<i>Date</i>	<i>2018</i>	<i>2019</i>
22 July	10.22	6.32	30 July	37.41	14.03
23 July	11.30	10.11	31 July	8.52	13.27
24 July	39.05	8.34	01 Aug	26.19	26.77
25 July	38.61	27.76	02 Aug	3.22	26.30
26 July	17.82	19.22	03 Aug	2.20	31.29
27 July	11.09	18.24	04 Aug	17.48	2.68
28 July	27.98	5.18	05 Aug	7.69	6.23
29 July	33.78	4.44	06 Aug	4.61	9.94

As regards the role of rainfall in the area, percolation of rain water through the porous soils may have led to the formation of weak zones due to saturation. During this stage, the saturated soils attains the plastic state, leading to plastic deformation. With further saturation, the water content exceeds W_L of the soil, which causes the soils to behave as viscous fluids. During these transitions, according to Lambe and Whitman (1979) there is significant decrease of cohesion, friction angle and bearing capacity of soils. In addition to the drop in strength, the weight of the soils further increase upon wetting. This would have led to extensive loading on the weak rocks, predominantly low-strength shales, and weak soils of the area, when the resistances offered by them are easily exceeded by downslope stresses. Under such conditions, slope failure is imminent.

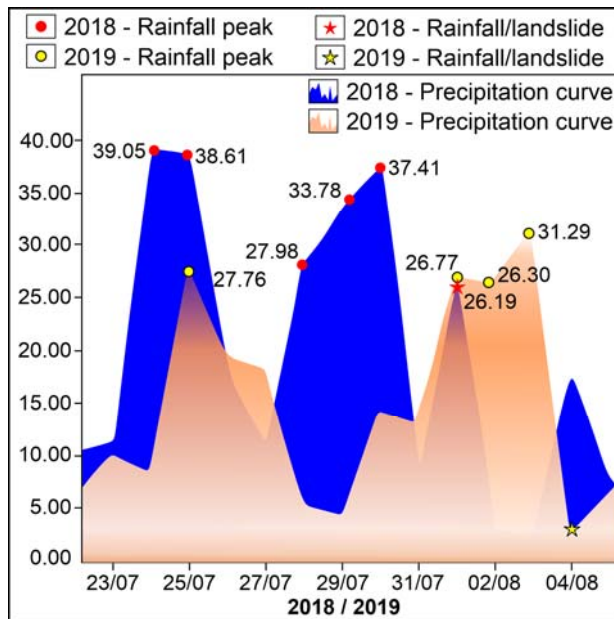


Fig. 4.3.12: Precipitation curves showing peak values and landslide occurrences

Electrical resistivity tomography

Five survey profile lines were carried out along the highway (Fig. 4.3.4-V1, V2, V3, V4, V5) to understand the subsurface and confirm the presence of a fault inferred from satellite imagery. Analyses of resistivity data collected for the five VES sounding points show three to five geoelectric layers (Table 4.3.8), namely top soil, weathered shale, wet weathered shale, fractured/weathered bedrock (shale with siltstone/sandstone intercalations) and groundwater. The sounding curves show HK, KHK and Q type patterns. Sounding data of VES 3, VES 4 and VES 5, obtained from Slide zone 1 (Fig. 4.3.4), show continuously decreasing resistivity values and three-layer models for each sounding ($\rho_1 > \rho_2 > \rho_3$), which indicate the predominance of Q-type curves in the area. Curve type KHK obtained at VES 2 is a five-layer model ($\rho_1 < \rho_2 > \rho_3 < \rho_4 > \rho_5$). It characterizes an abnormal distribution of electric layers with depth.

Table 4.3.8: Layer parameters for the VES points

Station	ρ_1	ρ_2	ρ_3	ρ_4	ρ_5	h1	h2	h3	h4	d1	d2	d3	d4	Curve type
	(Ωm)					(m)				(m)				
VES 1	55.32	49.98	146.90	30.45	-	0.90	4.98	9.13	-	0.90	5.88	15.01	-	HK
VES 2	51.41	62.28	31.93	43.87	4.68	0.90	1.26	3.04	7.3	0.90	2.16	5.20	12.5	KHK
VES 3	148.00	45.50	29.80	-	-	1.19	4.07	-	-	1.19	5.26	-	-	Q
VES 4	234.00	38.40	2.94	-	-	0.38	23.80	-	-	0.38	24.20	-	-	Q
VES 5	31.30	20.90	16.50	-	-	0.68	9.41	-	-	0.66	10.10	-	-	Q

ρ - layer resistivity; h - layer thickness; d - layer depth; Ωm - ohm meter; m - meter

The study area predominantly consists of Q-type curves; such curves indicate the presence of shear zones (Sultan and Santos, 2008). The weakness of such zones may be attributed to intense shearing of the rocks. Curve type KHK points to the presence of confined aquifers (Gouet et al., 2020), which is seen in the second and fourth layers with resistivity values 62.28 Ωm and 43.87 Ωm at depths of 2.16 m and 12.5 m respectively (Table 4.3.8). The slope along section VES 2 was affected by a major landslide in 2011. This particular section has been unstable since then. The highway along section VES 2 and Slide zone 2 (Fig. 4.3.2c) was severely damaged in 2018. The pressure generated by the two artesian aquifers and water seepage through the fractured rocks may have played a key role in slope failure.

Resistivity sounding along VES 1 can be explained by a four layer model ($\rho_1 > \rho_2 < \rho_3 > \rho_4$) with the HK-type curve. This type of curve indicates the presence of fractured and weathered horizons, which are noted at the third and fourth layers (Table 4.3.8). Such fractured and weathered horizons indicate the presence of aquifers.

The resistivity method employed for the present study to detect the presence of faults, revealed areas of high water content. Considering the two assumptions after Ammar and Kamal (2018), the presence of a fault is inferred at the intersection between sections VES 3 and VES 4 (Fig. 4.3.13). The arrow in the figure shows the intersection point, which indicates the presence of a fault zone at shallow depth. This is also reflected in the lineament map (Fig. 4.3.9) of the study area which indicates strike-slip fault trending WSW-ENE.

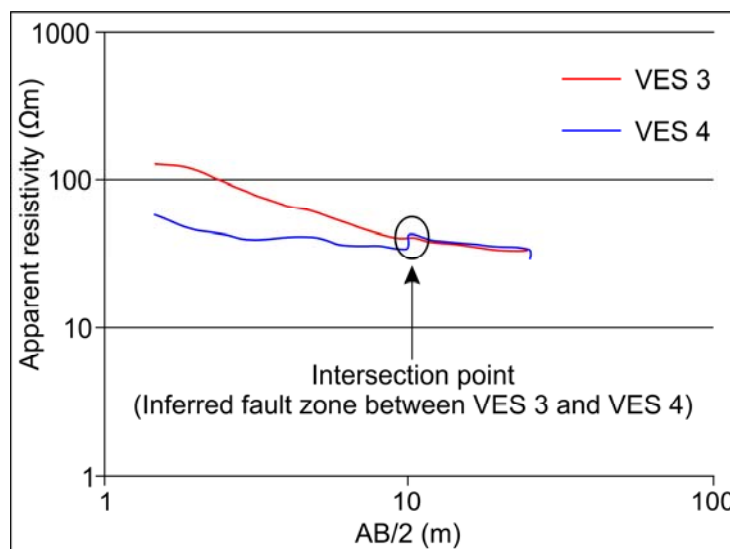


Fig. 4.3.13: Apparent resistivity curves showing an inferred fault

Results of the pseudo cross-sections of the geoelectric field data for the VES stations (Fig. 4.3.14) indicate the presence of weak zones between VES 2 and VES 4, located at shallow depths of 8 and 10 m from the surface. This can be seen by zones of high resistivity values separated by zones of lower resistivity from the surrounding areas. A low resistivity zone, observed in VES 5, up to a depth of 25 m below ground level, continues towards VES 4 and VES 2. This zone is a highly potential source for groundwater. Layers of high resistivity ($>70 \Omega\text{m}$) at VES 1 and VES 3 range in depths from 15 to 25 m and 1.5 to 2.5 m respectively. These are indicative of fractured and/or weathered horizons in the subsurface. Such weak zones, which are also observed along the tributaries of the Dzütre Rü flowing through the study area, point to the presence of faults (Lashari et al., 2019).

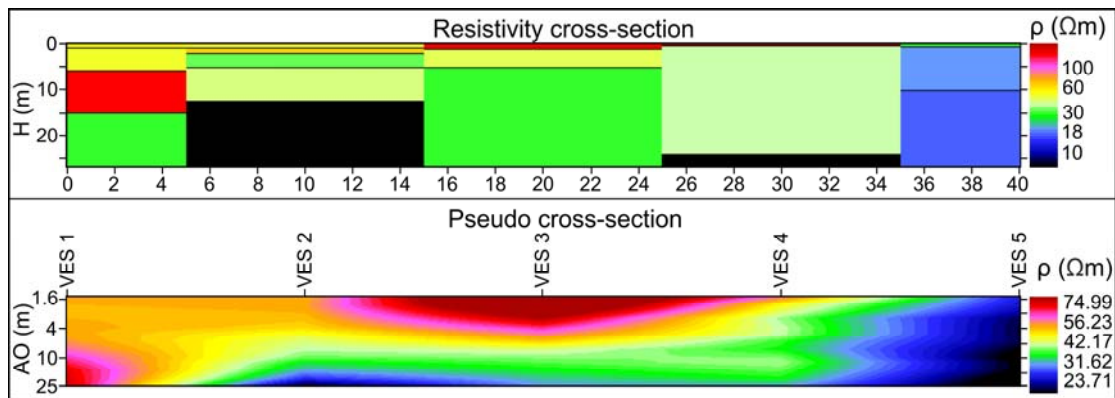


Fig. 4.3.14: Interpreted resistivity and pseudo cross-sections

Factor of safety

The input values for determination of factor of safety for Slide zone 1 are:

$$c = 17 \text{ kN/m}^2$$

$$\phi = 20^\circ$$

$$\gamma = 18 \text{ kN/m}^3 \text{ (unit weight of clayey soil)}$$

$$Z = 87 \text{ m}$$

$$\beta = 28^\circ$$

$$\text{Unit weight of water in the soil, } \gamma_w = 9.8 \text{ kN/m}^3$$

Here the slope is considered as saturated, so saturation constant (M) = 1

For c and ϕ , averages have been taken from direct shear test result from the Slide zone 1, the values of samples 1 and 2 (Table 4.3.2) are used.

$$\begin{aligned}
FoS &= \left\{ \frac{[17 + (18 - 1 * 9.8) * 87 * (\cos^2 28^\circ) * (\tan 20^\circ)]}{[18 * 87 * (\sin 28^\circ * \cos 28^\circ)]} \right\} \\
&= \left\{ \frac{[17 + (18 - 9.8) * 87 * 0.77 * 0.36]}{(18 * 87 * 0.47 * 0.88)} \right\} \\
&= \frac{214.75}{647.69} \\
FoS &= 0.33
\end{aligned}$$

The input values for determination of factor of safety for Slide zone 2 are:

$$c = 13 \text{ kN/m}^2$$

$$\phi = 17^\circ$$

$$\gamma = 18 \text{ kN/m}^3 \text{ (unit weight of clayey soil)}$$

$$Z = 160 \text{ m}$$

$$\beta = 25^\circ$$

$$\text{Unit weight of water in the soil, } \gamma_w = 9.8 \text{ kN/m}^3$$

Here the slope is considered as saturated, so saturation constant (M) = 1

For c and ϕ , averages have been taken from direct shear test result from the Slide zone 2, the values of samples 3 and 4 (Table 4.3.2) are used.

$$\begin{aligned}
FoS &= \left\{ \frac{[13 + (18 - 1 * 9.8) * 160 * (\cos^2 25^\circ) * (\tan 17^\circ)]}{[18 * 160 * (\sin 25^\circ * \cos 25^\circ)]} \right\} \\
&= \left\{ \frac{[13 + (18 - 9.8) * 160 * 0.82 * 0.31]}{(18 * 160 * 0.42 * 0.906)} \right\} \\
&= \frac{346.51}{1095.89} \\
FoS &= 0.31
\end{aligned}$$

Low FoS of **0.33** and **0.31** evaluated for Slide zone 1 and Slide zone 2 indicate that the slopes are very unstable.

CHAPTER 5

CONCLUSIONS AND RECOMMENDATIONS

5.1 Officer's Hill

Slope instability in parts of the Officer's Hill colony has been an issue for several years. The area hosts several vital establishments including the Raj Bhavan, office of the Superintendent of Police, some central agencies as well as the only highway connecting to mainland India, the AH 1. Field observation and electrical resistivity survey revealed that the area comprises fractured and weathered shale and clays with low resistivity. It also identified a thrust in the middle of the study area. The consistency limit shows clays possessing low, intermediate and high plasticity. The plasticity of the soils is attributed to concentration of clay, which controls water retention. The soils are found to have variable liquid limit. High liquid limits ($>50\%$) exhibit relatively higher cohesion, and therefore can be considered of better physical quality. Shear strength analyses revealed that soils with low cohesion are more susceptible to failure when subjected to water saturation. Slope stability analyses provided very important tools for assessing possible causative factors for slope failure. The RMR classified rocks of the Slip zone 2 under poor class. SMR values categorize the slope as unstable. The failure mode observed from kinematic analyses suggests wedge type. Lineament map shows the study area crossed by faults with close proximity to the landslide locations. The soil and rock slide down as debris and mud flows due to saturation by subsurface water in Slip zone 1. The combined effect of tectonic stresses and joint failures have led to continuous minor rock falls and differential subsidence in the Slip zone 2. The presence of local faults which are probably active, intersecting joints and fractures, high water table, shearing and weathering, pore-water pressure, and intense toe-erosion has made the area very weak and susceptible to slope failures. The study area can be thus categorised as a Complex type of landslide. Moreover, the area has a moderate settlement with numerous large and heavy residential buildings. The highway, being the lifeline for several districts of Nagaland and Manipur, facilitates heavy flow of traffic. Therefore, the weight of the heavy-laden vehicles and the vibrations caused by their movement must be another

factor for the abnormal and prolonged subsidence, along the particular stretch of the highway. Detailed studies may be required to determine the relation of vibration due to overloaded vehicles on instability along the highway.

The Border Roads Organisation (BRO), which is responsible for managing the highway have been kept busy over the years to ensure free movement in the highway as well as to reduce the impact on the upper residential portions of the area. To decrease the weight of the overburden and also to reduce the steepness of the slopes, benching has been carried out by the BRO (Fig. 5.1.1) in 2005 (Fig. 5.1.1A). This was followed by construction of roadside drains and short retaining walls at the base of the road cut slope. Pines (*Pinus patula*) were then planted on the benches in 2006 (Fig. 5.1.1B). It was suggested that such plantation should be replaced either by planting some grass species or undertake other measures since the rocks are highly fractured (Fig. 5.1.1C) and the area is very fragile. However, the pines were retained. These have now grown large and sturdy (Fig. 5.1.1B), which is a matter of concern. As they grow, their roots will grow thicker and longer, which will appreciably widen the fractured rocks, eventually causing their collapse.



Fig. 5.1.1: Previous mitigation measures in the weak zone (Inset: A - Landslide during 2005; B - Needle pine plantation; C - Open fissures)

All the landslide debris was spread over from the highway and towards the streamside below the highway. This accumulation caused the formation of a weak zone along the edges of the highway that led to sagging down under the load of unconsolidated overburden, thereby not only causing damage to the edges of the highway but also narrowing the road section. To address this erosion, extensive coir mats were nailed along the slopes to hold the slope material and vetiver grass planted (Fig. 5.1.2) in the hope that the grass would grow and bind the soil. The Sitsie Rü meanwhile continued to behave as a highly erosive stream, not only rapidly down-cutting the channel but also removing the loose debris and causing toe erosion.



Fig. 5.1.2: Mitigation measures taken up during 2005-06 (Inset: A - Soils dumped along the highway; B - Chute damaged)

This portion of the highway has become a common place for the public and some governmental agencies to transport and dump all unwanted excavated earth (Fig. 5.1.2A). Several pleas from the BRO and notices issued against this practice were in vain. This unrestrained practice is responsible for several instances of slope failure in this area. The initial treatment of coir mats and vetiver grass were covered up and washed away down due to continued dumping. The BRO also constructed a long chute (Fig. 5.1.2) to channelize the water along a portion of the weak section.

However, this treatment proved futile as it was removed due to combination of high velocity of water and erosion (Fig. 5.1.2B).

The results classify the study area into two distinct zones of movement with their associated lithological and slope conditions. Taking into consideration, the failures encountered with several past remedial measures, it is necessary to approach this complex landslide practically and cost effectively on the basis of their intrinsic conditions. The following recommendations are therefore proposed as reinforcement to mitigate the problem.

Slip zone 1

The presence of huge volume of subsurface water is a major problem in this area. This has led to differential settlements and subsidence of the road section, creating pore water pressure on the slope materials as well as erosion of finer materials. Perforated subsurface pipes (Fig. 5.1.3) are ideal under such circumstances to safely channelize this excess water away from the weak zones. These pipes can be made from any variety of materials including PVC (polyvinyl chloride), iron, cement and clay. They should have perforations and openings at the top through which the water can enter. The lower part must be properly lined so that the upslope water enters the pipe and are channelized away into the nearby streams.

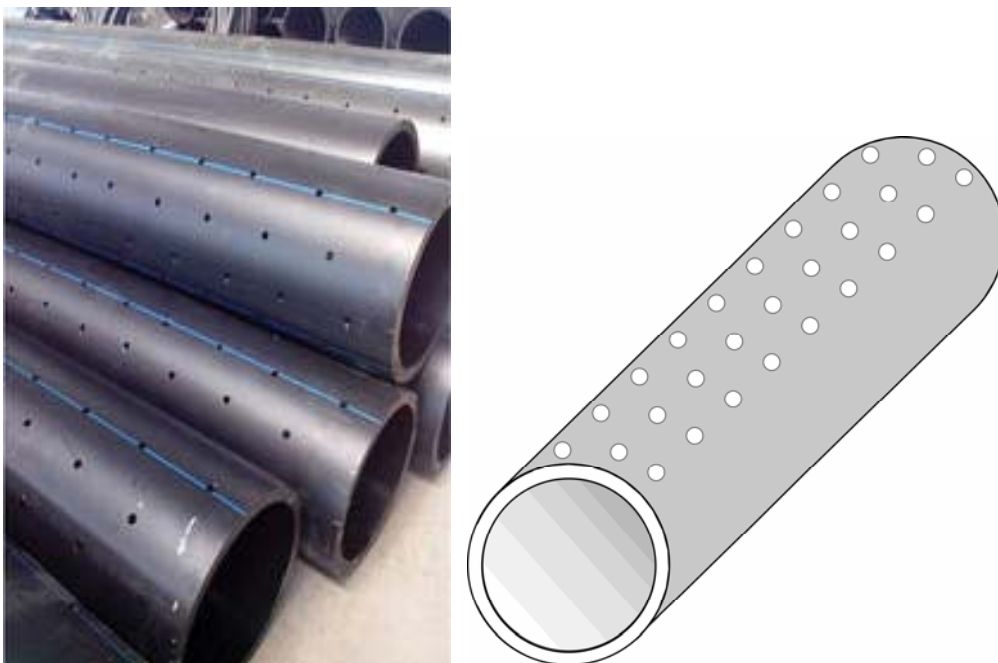


Fig. 5.1.3: Perforated pipes for subsurface use (Representational)

The stream channels in this weak zone, with the exception of Sitsie Rü, are narrow, highly erosive first order streams that are not lined by concrete. In such areas, treatment using old vehicle tyres is suggested over other structures that are made of rock and mortar. This approach lends credence to the fact that such rubber tyres are more resistant to erosion, lighter in weight and more elastic to any minor movement of the slope materials. Used tyres can be obtained in large quantities for throwaway prices (if not free) and therefore, their use would ensure a very inexpensive solution. A major impact on the environment is also averted using old tyres, which would otherwise be indiscriminately discarded to add to the pollution. The proper construction of a support wall involves filling the tyres with earth from the immediate surroundings. This earth is compacted into the tyre using a sledgehammer. This innovative method, started in Nagaland by Mr. Sukho Movi, Office Assistant in the Nagaland University, Kohima Campus. This method can be employed in the study area as embankment and retaining walls to control toe erosion by streams and ensure minimal loading on the fragile slope condition (Fig. 5.1.4).



Fig. 5.1.4: Used tyres forming a protective wall against toe erosion (Representational; Source: Mr. Sukho Movi)

Slip zone 2

This area is characterised by slope possessing lithology with numerous weak planes such as joints or vertical fractures and is thus associated with rockfall and rockslides endangering the life of commuters and properties alike. Here, rockfall protection systems must be installed after proper calculation and designed in such a way that it is capable of absorbing the impact of the falling rock and must also contain such moving rocks from venturing into the road. Draped wire-mesh and cable net slope protections using double twisted gabion wire mesh or high tensile wire mesh

(Fig. 5.1.5) are recommended along the highway section in the study area where the fractured rocks are exposed. These systems are typically galvanized or PVC coated.



Fig. 5.1.5: Wire-mesh slope protection / Cable-net slope protection (Representational)

Field observations and structural data show crushed and sheared rocks characterized by multiple joint sets. In such areas the best solution is to prevent any further development in this weak zone so that the situation is not aggravated. Moreover, to minimise the infiltration of water to subsurface, adequate drainage system is required. Such network of channels should be properly lined with concrete, with appropriate check dams to minimise water velocity and ensure timely clearing of any obstructions to avoid over spilling.

Things to avoid:

1. *Benching of slopes*: Further benching of slopes is not advisable because the rock masses are highly jointed. Benching clears the surface of natural vegetation, which permits water to freely flow into the subsurface to increase the pore pressure.
2. *Planting of large trees*: This practice should be avoided as their roots help widen the fractures developed in the rocks. Rather, it is advisable to plant shrubs and grasses.
3. *Dumping of earth*: The concerned authorities should ensure that soils from other areas are not dumped along the weak highway section.

5.2 Merhülietsa colony

The area consists of clayey soils with low to moderate shear strength. These soils formed as a result of weathering of shales are highly sensitive to water with high swelling potential. Such soils also shrink heterogeneously due to which desiccation cracks develop on the surface. The alternate wetting and drying phenomena during rainfall and dry days, induces deformation of the soils, causing destabilization of structures that are constructed in the area. The shales, which are the dominant rock type, are highly sheared, pulverized and weathered, making them very weak and vulnerable to erosion. RMR results categorize the study area under fair rock quality. However, SMR classes of M1 and M2 suggest unstable slope conditions. This can be attributed to the orientations of discontinuities with respect to slope surfaces, as displayed by the stereographic projections, which produce ideal conditions for the occurrence of wedge failure. Occurrence of such joint patterns suggests complex interplay, producing hybrid fractures, which caused the extensive deformation of the rocks. The FoS determined for the Slide zone indicates a very unstable slope. Besides weak soils, rocks found in the vicinity are fractured and sheared. They generally allow movement of sub-surface water, facilitating large amount of water through these fissures. Proper roadside drainage system in the area is lacking, leading to excessive percolation of surface runoff into this weak zone. This resulted in increased pore water pressure along the potential sliding surface, ultimately leading to failure. The presence of local faults, joints and fractures contributed to the instability of the slopes aided by uncontrolled surface runoff and infiltration into the subsurface. Erosional activities of Dzulikha Rü and Sitsie Rü have led to failure of the hillslopes and subsidence in some sections of the area. Developmental works related to urbanisation and other anthropogenic activities have also disturbed the natural environment, exposing the soil to accelerated erosion, weathering and slope instability.

The highway affected by landslide is attributed to heavy rainfall hence mitigation measures focussing on minimal infiltration of water entering the Slide zone should be taken up. First and foremost, proper roadside drain and regular maintenance are necessary. The residents living above the highway should also contribute by practising good civic sense and ensure proper disposal of domestic discharge into the natural streams. These techniques will prevent water logging and also control seepage into the vulnerable subsurface. Retaining walls with appropriate weep holes will

minimize pore pressure due to trapped subsurface water behind the walls. This will hold the slope material and should be placed at the toe of the slopes in areas that are affected by creep. Practice of dumping earth materials along the highway should be stopped.

For areas experiencing toe erosion, storm drain baffle (Fig. 5.2.1) and check dams (Fig. 5.2.2) can be constructed along the steeper gradient of stream channels to reduce the velocity of water during sudden storms. The concrete baffles will act as a barrier thereby prevent uncontrolled flows downstream and further counteract erosional activities.

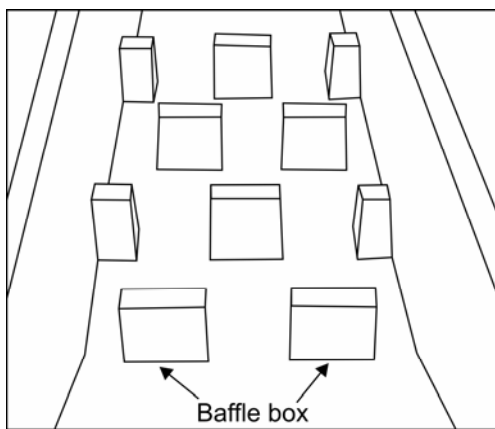


Fig. 5.2.1: Storm drain baffle

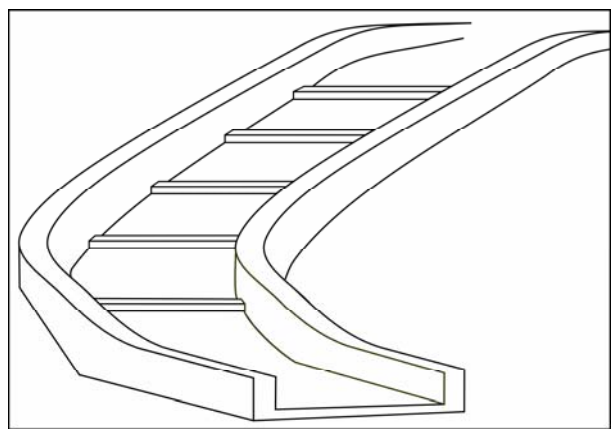


Fig. 5.2.2: Check dam

It is vital that surface and rainwater that are channelized through the drains are not impeded by obstructions that may lead to accumulation of waste materials and river load. Therefore, proper mechanisms for maintenance, cleaning and to avoid such accumulations should be kept in place. Construction of concrete drainage along sides of stable cut slopes and stream section will help drain the rainwater from soil slopes and, in turn, reduce the possibility of toe erosion. It is suggested that further developmental activities in the area, such as construction for heavy RCC structures should be discouraged without proper geological investigation.

5.3 Kevüza area

This study area is made up of geologically weak material that is prone to slope failure regularly. The rocks consist predominantly of shale and siltstone that have been extensively deformed and crossed by numerous joint planes and faults, and are differentially weathered to black and brown clays. Some faults cutting across the area have greatly pulverised the rocks. The roadside drains are devoid of concrete lining and are not properly drained out of the slide zone leading to erosion and infiltration. The section of highway along this landslide zone has been broadened by continuous excavation of the slopes to keep the road motorable, which has resulted in removal of the vegetative cover. The soils are classified as inorganic silts and clays of low to moderate plasticity that is characterized by rapid loss of consistency in response to water. The subsurface movement of water also causes the removal of finer materials, leading to enrichment of coarser particles, which explains the low plasticity of the soils in the study area. Direct shear tests of the samples give values between 33.43 to 49.26 kPa indicating the soils are of low shearing strength. RMR and SMR values categorize the area as partially stable to highly unstable slopes with dominant weak rocks. Groundwater in the area is also responsible for the reduction in shearing strength of the rocks with increasing water saturation. With the help of kinematic analyses, 2-3 dominant joint sets have been identified; their relationship has created ideal conditions for wedge failure. Lineament mapping supported by resistivity surveys point to the presence of a shallow fault and confined aquifers in the study area. The aquifers may be responsible for the extensive weathering of the pulverized rocks. The dominant Q-type sounding curves obtained from resistivity analyses also point to the presence of shear zones. The region receives heavy rainfall during the monsoon. Increased infiltration on inherently weak slopes materials led to elevation of the groundwater table and piezometric surfaces. Hence, seepages and small springs within the landslide zone are common. Consequently, the weak soil gets saturated, which led to increase in pore pressure and the weight of the slope material, thereby reducing the shearing strength of the soils resulting in the slope failure events of 2018 and 2019.

The slope materials display high degree of saturation, specially above the highway. In such scenario, the main aim would be to minimise the percolation of water from rainfall and surface run-off into the slope. Increased percolation of water

from rainfall and surface run-off would raise the water table and allow building up of hydrostatic pressure on the slope. Natural plants such as broom grass carpet, narrow leaf carpet grass and broadleaf carpet grass are recommended in such areas to restrict infiltration of such surface water. Opting for such light treatment methods would ensure very little amount of water percolating below as it will create a carpeting effect and surface water will easily flow over it, root system will bind and hold together the loose soil giving a more stable structure, and very importantly impose very negligible weight on the fragile slope material as compared to other heavy RCC structures. This slope protection and erosion control measures can be fortified by building adequate surface drainage. In areas where the slopes are stable, proper concrete lined nullahs can be laid out. However, in soft and unstable soils like clay, embankments and retaining walls built by using old vehicle tyres (Fig. 5.1.4) are suggested since such tyres will occupy comparatively more space and lighter in contrast to reinforced structures which will lead to undue loading in the fragile environment. The horizontal stress exerted by the upslope material as well as vertical load by passing vehicles can also be dissipated to some extent due to the elastic nature of the tyre material. Installation of French drain type will reduce water percolation into deeper horizons, prevent retention of water and drain out excess water during heavy rainfall. A French drain also known as Filter drain consist of a trench filled with gravel or rock containing a perforated pipe that redirects surface water and groundwater away from an area (Fig 5.3.1). The gravel and rock layer will allow easy flow of water. The water then, flows into perforated pipes at the bottom of the trench. From there it will eventually discharge to an outlet to a safer zone.

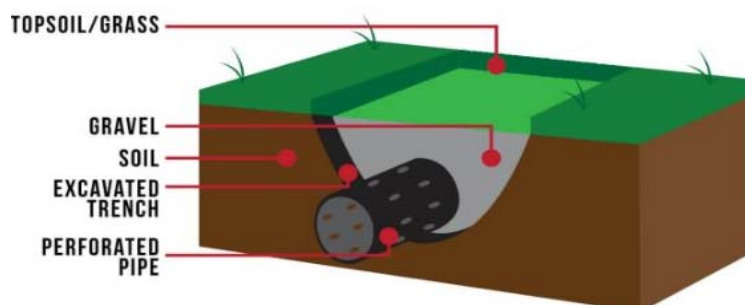


Fig 5.3.1: Typical French drain (Source: <https://northwestdrainage.com/wp-content/uploads/2020/09/northwest-french-drain-seattle-redmond-everett-drains.jpg>)

One effective way to lower the water table is dewatering of the area specially by construction of discharge wells at various levels of the slope. Dewatering by sump pumping and installation of tube well can be a very good option in this area as high water table is observed and ERT has identified an aquifer. Sump pumps are electric-powered pumps designed to discharge water accumulated in the sumps. When the water gets to a certain level, pressure sensor sends a signal to the pump and the float mechanism raises up which then turns the pump on and discharge the water (Fig. 5.3.2). These pumps may have an additional battery backup system.

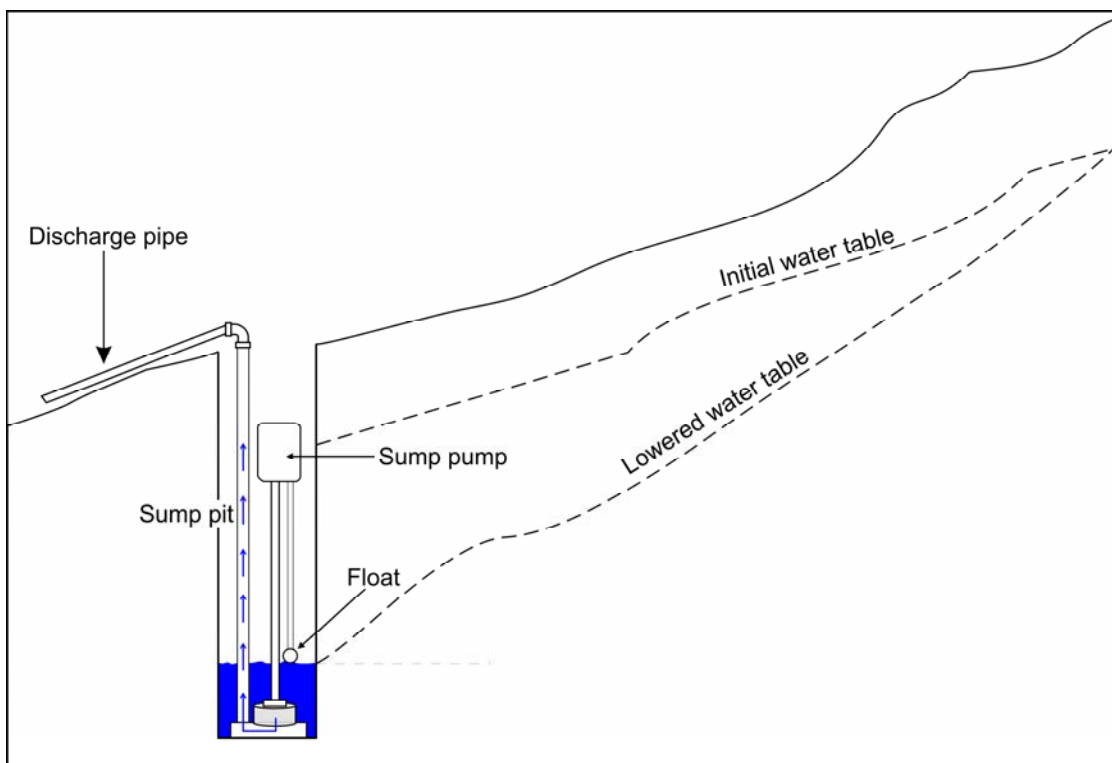


Fig. 5.3.2: Dewatering by Sump pumping method

This area has been extensively damaged due to the landslide event in 2018. Both temporary and long-term measures were provided to the Government of Nagaland. To open up the highway and keep motorable, some temporary measures were adopted during the monsoon of 2018 (Fig. 5.3.3). This approach has stabilized the area that is still maintaining its purpose till date.

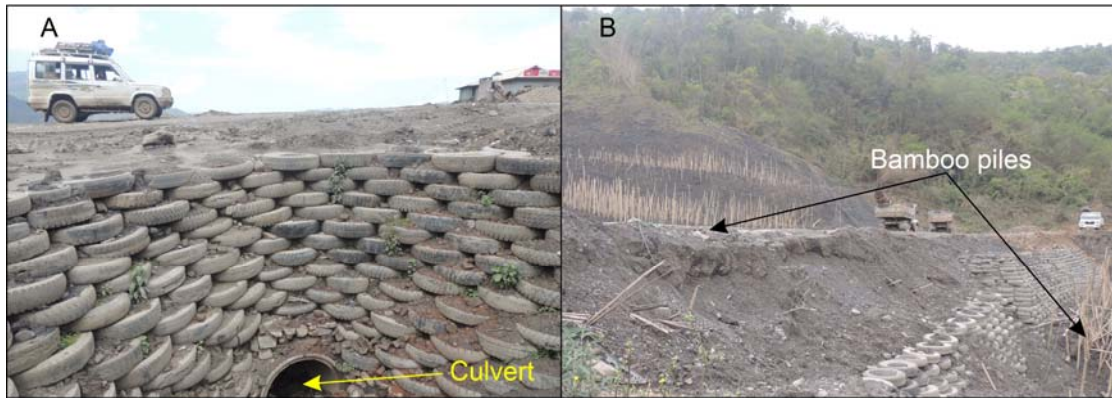


Fig. 5.3.3: Road made functional in Slide zone 1 - (A) Structures built with scrap tyres; (B) Upper and lower slopes temporarily stabilised using bamboo piles (Photo date: 10.04.2019)

Bioengineering intervention such as utilization of bamboo for piling along the slope are recommended as it will be cost effective, locally available, eco-friendly and offer more flexibility and strength in such a mobile scenario. These piles can be driven into the soil debris at regular intervals of the affected area (Fig. 5.3.3B). This will cause a binding effect of the loose materials and lend temporary support of shallow sliding along the slope. Bamboo crib walls (Fig. 5.3.4) can be used as structural elements to take load and resist the slope movement. This type of walls can be used as an alternative as they are lighter compared to gabions or masonry retaining walls.



Fig. 5.3.4: Crib wall retaining structure made of bamboo (Source: Rauch et al., 2002)

REFERENCES

- Acker, J.G., and Leptoukh, G., 2007. Online analysis enhances use of NASA earth science data. *Eos Trans Am Geophys Union*, vol. 88(2), pp. 14-17. <https://doi.org/10.1029/2007EO020003>
- Agliardi, F., Crosta, G.B., Frattini, P., and Malusà, M.G., 2013. Giant noncatastrophic landslides and the long-term exhumation of the European Alps. *Earth Planet Sci Lett*, vol. 365, pp. 263-274. <https://doi.org/10.1016/j.epsl.2013.01.030>
- Agliardi, F., Crosta, G.B., and Zanchi, A., 2001. Structural constraints on deep-seated slope deformation kinematics. *Eng Geol*, vol. 59, pp. 83-102. [https://doi.org/10.1016/S0013-7952\(00\)00066-1](https://doi.org/10.1016/S0013-7952(00)00066-1)
- Aier, I., 2005. Landslides along the Kohima-Dimapur road: their causes and possible remedial measures. Unpublished Ph.D. thesis, Nagaland University, Kohima.
- Aier, I., Luirei, K., Bhakuni, S.S., Thong, G.T., and Kothiyari, G.C., 2011a. Geomorphic evolution of Medziphema intermontane basin and Quaternary deformation in the schuppen belt, Nagaland, NE India. *Zeitschrift für Geomorphologie*, vol. 55, pp. 247-265. <https://doi.org/10.1127/0372-8854/2011/0055-0048>
- Aier, I., Singh, M.P., Thong, G.T., and Soibam I., 2012. Instability analyses of Merhülietsa slide, Kohima, Nagaland. *Nat. Hazards*, vol. 60, pp. 1347-1363. <https://doi.org/10.1007/s11069-011-9913-6>
- Aier, I., Supongtemjen, Khalo, M., and Thong, G.T., 2009a. Geotechnical assessment of the Mehrülietsa slide in Kohima, Nagaland. In: Kumar, A., Kushwaha, R.A.S. and Thakur, B. (Eds), *Earth System Sciences*, vol. 1, pp. 81-88. Concept Publishing Company, New Delhi.
- Aier, I., Supongtemjen, and Thong, G.T., 2009b. Slope mass rating and kinematic analyses along part of NH 61, Nagaland, NE India. *International Journal of Earth Sciences and Engineering*, vol. 2, pp. 520-526.
- Aier, I., Thong, G.T., and Supongtemjen, 2011b. Geological evaluation of surface instability along NH 39 (180 km), west of Raj Bhavan, Kohima, Nagaland. In: Singh, T.N. and Sharma, Y.C. (Eds), *Slope stability - Nat. and Man Made Slope*, pp. 192-201. Vayu Education of India, New Delhi.
- Aier, I., Walling, T., and Thong, G.T., 2005. Lalmati slide: Causes and mitigation measures. *Nagaland University Research Journal*, vol. 3, pp. 44-47.
- Alexander, D., 1993. *Natural Disasters*. University College Library Press Ltd., London.

- Al-Homoud, A.S., Basma, A.A., Malkawi, H., and Al-Bashabsheh, M.A., 1995. Cyclic swelling behavior of clays. *J. Geotech. Eng.*, vol. 121, pp. 562-565. [https://doi.org/10.1061/\(ASCE\)0733-9410\(1995\)121:7\(562\)](https://doi.org/10.1061/(ASCE)0733-9410(1995)121:7(562))
- Ambrosi, C., and Crosta, G.B., 2006. Large sackung along major tectonic features in the central Italian Alps. *Eng. Geol.*, vol.83, pp. 183-200. <https://doi.org/10.1016/j.enggeo.2005.06.031>
- Ammar, A.I., and Kamal, K.A., 2018. Resistivity method contribution in determining of fault zone and hydro-geophysical characteristics of carbonate aquifer, eastern desert, Egypt. *Appl. Water Sci.*, vol.8, pp.1-27. <https://doi.org/10.1007/s13201-017-0639-9>
- Anon, OH., 1979. Classification of rocks and soils for engineering geological mapping. Part I: Rock and soil materials. *Bull. Intl. Assoc. Engg. Geol.*, vol. 19, pp. 364-371.
- Aristizábal, E., García, E., and Martínez, C., 2015. Susceptibility assessment of shallow landslides triggered by rainfall in tropical basins and mountainous terrains. *Nat. Hazards*, vol.78, pp. 621-634. <https://doi.org/10.1007/s11069-015-1736-4>
- Aksoy, H., and Ercanoglu, M., 2007. Fuzzified kinematic analysis of discontinuity-controlled rock slope instabilities. *Eng. Geol.*, vol. 89, pp. 206-219. <https://doi.org/10.1016/j.enggeo.2006.10.007>
- ASTM D421–85, 2007. Standard Practice for Dry Preparation of Soil Samples for Particle Size Analysis and Determination of Soil Constants. ASTM Int. West Conshohocken, PA.
- Atterberg, A., 1911. Physical soil examination about the plasticity of the clays. *International Communications for Soil Science*, vol. 1, Berlin.
- Atre, S.R., and Carpenter, P.J., 2010. Identification of cross-valley faults in the Maynardville Limestone, Oak.
- Badger, T.C., 2002. Fracturing within anticlines and its kinematic control on slope stability. *Environ. Eng. Geosci.*, vol. 8(1), pp. 19-33. <https://doi.org/10.2113/gseegeosci.8.1.19>
- Bhattacharjee, C.C., 1991. The Ophiolites of northeast India: a subduction zone ophiolite complex of Indo-Burman Orogenic Belt. *Tectonophysics*, vol. 191, pp. 213-222.
- Bhattacharjee, C.C., Rahman, S., Sarmah, R.N., and Thong, G.T., 1998. Landslides and road instability along NH 39, between Kohima and Chumukedima, Nagaland. *Proc. Intl. Conf. Dis. Man.*, Guwahati, pp. 556-568.

- Bieniawski, Z.T., 1972. Propagation of brittle fracture in rock. In: Proceedings 10th Symposium on Rock Mech. (AIME), pp. 409-427.
- Bieniawski, Z.T., 1973. Engineering classification of jointed rock masses. Trans. South African Instt. Civil Engg., vol. 15, pp. 335-344.
- Bieniawski, Z.T., 1989. Engineering rock mass classifications. Wiley, New York, 251p.
- Brunsden, D., and Prior, D.B., (Eds.) 1984. Slope instability. Wiley, Chichester, 620p.
- Bryant, E. A., 1991. Natural Hazards. Cambridge University Press, Cambridge, 294p.
- Bucci, F., Santangelo, M., Cardinali, M., Fiorucci, F., and Guzzetti, F., 2016. Landslide distribution and size in response to Quaternary fault activity: The Peloritani Range, NE Sicily, Italy. Earth Surf. Process. Landf., vol. 41, pp. 711-720. <https://doi.org/10.1002/esp.3898>
- Butler, J., 1976. Natural Disasters. South Yarra, Victoria: Heinemann Educational Australia, 138p.
- Cai, X., Zhou, Z., Liu, K., Du, X., and Zang, H., 2019. Water-weakening effects on the mechanical behavior of different rock types: phenomena and mechanisms. Applied Science vol. 9. <https://doi.org/10.3390/app9204450>
- Campbell, D.A., 1951. Types of erosion prevalent in New Zealand. Assoc. Intl. d'Hydrologie Scientifique, Assemblee Generale de Bruxelles. Tome II.
- Cardinali, M., Ardizzone, F., Galli, M., Guzzetti, F., and Reichenbach, P., 2000. Landslides triggered by rapid snow melting: the December 1996 – January 1997 event in Central Italy. Proceedings 1st Plinius Conference on Mediterranean Storms. Claps P, Siccardi F (eds). Bios: Cosenza, pp. 439-448.
- Carlini, M., Chelli, A., Vescovi, P., Artoni, A., Clemenzi, L., Tellini, C., and Torelli, L., 2016. Tectonic control on the development and distribution of large landslides in the Northern Apennines (Italy). Geomorphology, vol. 253, pp.425-437. <https://doi.org/10.1016/j.geomorph.2015.10.028>
- Casagrande, A., 1932. Research on the Atterberg limits of soils. Public Roads, vol. 13, pp. 121-136.
- Census of India, 2011. Provisional Population Totals, Paper 2, vol. II. Rural-Urban Distribution, Nagaland. Series 14.
- Central Road Research Institute, 2000a. Preliminary report on correction of landslide at km-174 and km-180 on NH 39 in Nagaland, pp. 1-6.
- Central Road Research Institute, 2000b. Correction of landslides on NH 39 in Nagaland. Suppl. Rep.

- Chandrasekaran, S.S., Owaise, R.S., and Ashwin, S., 2013. Investigation on infrastructural damages by rainfall induced landslides during November 2009 in Nilgiris, India. *Nat. Hazards*, vol. 65, pp. 1535-1557. <https://doi.org/10.1007/s11069-012-0432-x>
- Chang, K.J., Chan, Y.C., Chen, R.F., and Hsieh, Y.C., 2018. Geomorphological evolution of landslides near an active normal fault in northern Taiwan, as revealed by lidar and unmanned aircraft system data, *Nat. Hazards Earth Syst. Sci.*, vol. 18, pp. 709-727. <https://doi.org/10.5194/nhess-18-709-2018>
- Chen, R.F., Lin, C.W., Lin, H.H., Hsieh, Y.C., Wang, C.L., Cheng, K.P., and Chen, T.C., 2019. The influence of thrust faulting on deep-seated slope gravitational deformation in southern Taiwan. *Proceedings of the XVII ECSMGE-Geotechnical Engineering foundation of the future*.
- Chen, A., Darbon, J., and Morel, J.M., 2014. Landscape evolution models: A review of their fundamental equations. *Geomorphology*, vol. 219(C), pp. 68-86. <https://doi.org/10.1016/j.geomorph.2014.04.037>
- Chen, L., Guo, Z., Yin, K., Shrestha, D.P., and Jin, S., 2019. The influence of land use and land cover change on landslide susceptibility: a case study in Zhushan Town, Xuan'en County (Hubei, China). *Nat. Hazards and Earth System Sciences* vol. 19, pp. 2207-2228. <https://doi.org/10.5194/nhess-19-2207-2019>
- Choubey, V.D., and Lallenmawia, H., 1987. Landslides and other mass movements in Aizawl, NE India, Mizoram state. 5th Intl. Conf., New Zealand, pp. 113-120.
- Coch, N. K., 1995. *Geohazards: Natural and Human*. Prentice Hall Inc., New Jersey.
- Coduto, D.P., 1999. *Geotechnical Engineering*. Prentice Hall, New Jersey, 481p.
- Corominas, J., 2001. Landslides and climate. In: Bromhead, E.N. (Ed), *Keynote lectures, 8th Intl. Symp. Landsl.*, Cardiff, pp. 1-33.
- Corominas, J., Remondo, J., Farias, P., Esterao, M., Zezere, T., Dias de Teran, J., Dikan, R., Schott, L., Moya, J., and Gonzalez, A., 1996. Debris flow. *Intl. Assoc. Geomorphologists*, vol. 5, pp. 61-180.
- Crosta, G.B., Frattini, P., Agliardi, F., 2013. Deep seated gravitational slope deformations in the European Alps. *Tectonophysics*, vol. 605, pp. 13-33.
- Crozier, M.J., 1973. Techniques for the morphometric analysis of landslips. *Z. Geomorph.*, vol. 17, pp. 78-101.
- Crozier, M.J., 1984. *Field Assessment of Slope Instability*. In Brunsden, D. and Prior, D. (Eds.), *Slope Instability*. John Wiley & Sons. New York.

- Crozier, M.J., 1986. Landslide: Causes, environments, and consequences. Croon Helm, London, 252p.
- Cruden, D.M., 1978. A method for distinguishing between single and double plane sliding of tetrahedral wedges: Discussion of G. Hocking's paper. *Intl. Jour. Rock Mech. Min. Sci. Geomech. Abstr.*, vol. 15, pp. 225-226. [https://doi.org/10.1016/0148-9062\(78\)91228-7](https://doi.org/10.1016/0148-9062(78)91228-7)
- Cruden, D.M., 1991. A simple definition of a landslide. *Bull. Intl. Assoc. Engg. Geol.*, vol. 43(1), pp. 27-29.
- Cruden, D.M., and Varnes, D.J., 1996. Slope movement types and processes. In: *Landslides - investigation and mitigation*. Spl. Rep. Natl. Acad. Press, Washington, vol. 247, pp. 36-75.
- Cui, Y., Cheng, D., Choi, C.E., Jin, W., Lei, Y., and Kargel, J.S., 2019. The cost of rapid and haphazard urbanization: lessons learned from the Freetown landslide disaster. *Landslides* vol. 16, pp. 1167-1176. <https://doi.org/10.1007/s10346-019-01167-x>
- Das, B.M., and Sobhan, K., 2018. *Principles of Geotechnical Engineering*, 9th edn. Cengage Learning, Boston, MA, 819p.
- Das, I., Sahoo, S., Van, Weston, C., Stein, A., and Hack, R., 2010. Landslide susceptibility assessment using logistic regression and its comparison with a rock mass classification system, along a road section in the northern Himalayas (India). *Geomorphology*, vol. 114, pp. 627-637. <https://doi.org/10.1016/j.geomorph.2009.09.023>
- Deere, D.U., Hendron, A.J., Patton, F.D., and Cording, E.J., 1967. Design of surface and near surface construction in rock. In: Fairhurst, C. (Ed.), *Failure and breakage of rock*. Proc. 8th US Symp. Rock Mech., New York. Soc. Min. Engg, Am. Inst. Min. Metal. Petro. Engg., pp. 237-302.
- Densmore, A.L., Anderson, R.S., McAdoo, B.G., Ellis, M.A., 1997. Hillslope evolution by bedrock landslides. *Science*, vol. 275(5298), pp. 369-72. <https://doi.org/10.1126/science.275.5298.369>
- Devdas, V., and Gandhi, P., 1985. Systematic geological mapping in Maromi-Akuluto-Suruhuto areas, Zunheboto district, Nagaland. GSI, Unpubl. Progress Report.
- Dewitte, O., and Demoulin, A., 2005. Morphometry and kinematics of landslides inferred from precise DTMs in West Belgium. *Nat. Hazards Earth Syst. Sci.* vol. 5, pp. 259-265. <https://doi.org/10.5194/nhess-5-259-2005>

- Ding, J.S., Wu, G. X., Wang, M., and Chen, L., 2010. Numerical stability analysis of the multi-layered high-filled embankment slope subjected to rainfall infiltration. In Proc. of 10th International Conference of Chinese Transportation Professionals (ICCTP), edited by H. Wei, pp. 3046-3054. Reston, VA: ASCE.
- Directorate of Geology & Mining, Nagaland 1978. Miscellaneous Publication, No 1.
- Doblas, M., 1998. Slickenside kinematic indicators. *Tectonophysics*, vol. 295, pp.187-197. [https://doi.org/10.1016/S0040-1951\(98\)00120-6](https://doi.org/10.1016/S0040-1951(98)00120-6)
- Doglioni, A., and Simeone, V., 2014. Geomorphometric analysis based on discrete wavelet transform. *Env. Earth Sc.*, vol. 71(7), pp. 3095-3108. <https://doi.org/10.1007/s12665-013-2686-3>
- Dou, J., Yunus, A.P., Xu, Y., Zhu, Z., Chen, C.W., Sahana, M., Khosravi, K., Yang, Y., and Pham, B.T., 2019. Torrential rainfall-triggered shallow landslide characteristics and susceptibility assessment using ensemble data-driven models in the Dongjiang Reservoir Watershed, China. *Nat. Hazards*, vol. 97, pp.579-609. <https://doi.org/10.1007/s11069-019-03659-4>
- Duc, D.M., 2012. Rainfall-triggered large landslides on 15 December 2005 in Van Canh District, Binh Dinh Province, Vietnam. *Landslides*, vol. 10(2), pp. 219-230.
- Dumbleton, M.S., 1968. The classification and description of soil for engineering purpose. A suggested classification of the British System RRL report, LR 182, UK.
- Erguler, Z.A., and Ulusay, R., 2009. Water-induced variations in mechanical properties of clay-bearing rocks. *Int. J. Rock Mech. Min. Sci.*, vol. 46, pp. 355-370. <https://doi.org/10.1016/j.ijrmms.2008.07.002>
- Fookes, P.G., and Wilson, D.D., 1966. The geometry of discontinuities and slope failures in Siwalik Clay. *Geotechnique*, vol. 16(4), pp. 305-320.
- Galeandro, A., Doglioni, A., Guerricchio, A., and Simeone, V., 2013. Hydraulic stream network conditioning by a tectonically induced giant deep seated landslide along the front of the chain and its influence on landslide and flooding hazard. *Nat. Hazards Earth Sys. Sci.*, vol. 13, pp. 1269-1283. <https://doi.org/10.5194/nhess-13-1269-2013>
- Galve, J.P., Cevasco, A., Brandolini, P., and Soldati, M., 2015. Assessment of shallow landslide risk mitigation measures based on land use planning through probabilistic modelling. *Landslides*, vol. 12, pp. 101-114. <https://doi.org/10.1007/s10346-014-0478-9>

- García-Ruiz, J.M., Beguería, S., Alatorre, L.C., and Puigdefàbregas, J., 2010. Land cover changes and shallow landsliding in the flysch sector of the Spanish Pyrenees. *Geomorphology*, vol. 124, pp. 250-259, <https://doi.org/10.1016/j.geomorph.2010.03.036>
- Geological Survey of India, 2011. Geology and Mineral resources of Manipur, Mizoram, Nagaland, and Tripura. Miscellaneous Publication, No 30, Part IV, vol. 1 (Part-2).
- Geotechnical Info, 2012. Soil unit weight [WWW Document]. URL http://www.geotechnicalinfo.com/soil_unit_weight.html
- Gofar, N., and Rahardjo, H., 2017. Saturated and unsaturated stability analysis of slope subjected to rainfall infiltration. MATCE web conferences 101, Sriwijaya International Conference on Engineering Science and Technology (SICEST), Les Ulis, France: EDP Sciences. <https://doi.org/10.1051/mateconf/201710105004>
- Gorsevski, P.V., Gessler, P.E., Boll, J., Elliot, W.J., and Foltz, R.B., 2006. Spatially and temporally distributed modelling of landslide susceptibility. *Geomorphology*, vol. 80(3-4), pp. 178-198. <https://doi.org/10.1016/j.geomorph.2006.02.011>
- Gorum, T., Fan, X., van Westen, C.J., Huang, R.Q., Tang, C., and Wang, G., 2011. Distribution pattern of earthquake-induced landslides triggered by the 12 may 2008 Wenchuan earthquake. *Geomorphology*, vol. 133(3), pp. 152-167. <https://doi.org/10.1016/j.geomorph.2010.12.030>
- Guney, Y., Sari, D., Cetin, M., and Tuncan, M., 2007. Impact of cyclic wetting–drying on swelling behavior of lime stabilized soil. *Building and Environment* vol. 42, pp. 681-688.
- Gouet, D.H., Meying, A., Nkougou, H.L.E., Assembe, S.P., Nouck, P.N., and Mbarga, T.N., 2020. Typology of sounding curves and lithological 1D models of mineral prospecting and groundwater survey within crystalline basement rocks in the east of Cameroon (Central Africa) using electrical resistivity method and Koefoed computation method. *Int. J. Geophys.* <https://doi.org/10.1155/2020/8630406>
- Guo, J., and Wang, J., 2017. Mechanism analysis of the failure for a safe jointed rock high slope: Tectonic structures and damage. *Geotechnical and Geological Engineering*, vol. 36, pp. 455-467. <https://doi.org/10.1007/s10706-017-0339-0>
- Hadi, A.I., Brotopuspito, K.S., Pramumijoyo, S., and Hardiyatmo, H.C., 2018. Regional Landslide Potential Mapping in Earthquake-Prone Areas of Kepahiang Regency, Bengkulu Province, Indonesia. *Geosciences* vol. 8(6): 219. <https://doi.org/10.3390/geosciences8060219>

- Hancock, P.L., and Barka, A.A., 1987. Kinematic indicators on active normal faults in Western Turkey. *J. Struct. Geol.*, vol. 9(5-6), pp. 573-584.
[https://doi.org/10.1016/0191-8141\(87\)90142-8](https://doi.org/10.1016/0191-8141(87)90142-8)
- Havenith, H.B., Torgoev, A., Schlögel, R., Braun, A., Torgoev, I., and Ischuk, A., 2015. Tien Shan geohazards database: landslide susceptibility analysis. *Geomorphology*, vol. 249, pp. 32-43.
<https://doi.org/10.1016/j.geomorph.2015.03.019>
- Hobbs, P., Jones, L., Kirkham, M., Gunn, D., and Entwisle, D., 2019. Shrinkage limit test results and interpretation for clay soils. *Quart. J. Eng. Geol. Hydrol.*, vol. 52(2): 220. <https://doi.org/10.1144/qjegh2018-100>
- Hocking, G., 1976. A method for distinguishing between single and double plane sliding of tetrahedral wedges. *Intl. Jour. Rock Mech. Min. Sci. Geomech. Abstr.*, vol. 13, pp. 225-226.
- Hoek, E., and Bray, J.W., 1981. *Rock slope engineering* (3rd ed.). The Institute of Mining and Metallurgy, London, 358p.
- Hoek, E., and Brown, E.T., 1980. Empirical strength criterion for rock masses. *Journal of Geotechnical and Geoenvironmental Engineering* 106 (ASCE 15715).
- Hoek, E., and Marinos, P., 2000. Predicting tunnel squeezing problems in weak heterogeneous rock masses. *Tunnels and Tunnelling International*, vol. 132 (11), pp. 45-51
- <https://civilmint.com/wp-content/uploads/2021/06/Open-Sump-Pumping.jpg>
- <https://northwestdrainage.com/wpcontent/uploads/2020/09/northwest-french-drain-seattle-redmond-everett-drains.jpg>
- Huffman, G.J., Stocker, E.F., Bolvin, D.T., Nelkin, E.J., Jackson, and Tan., 2019. GPM IMERG final precipitation L3 1 day 0.1 degree x 0.1 degree V06. Savtchenko A, Greenbelt, MD (Ed.) Goddard Earth Sci. Data Inf. Serv. Cent. (GES DISC) (Accessed 24.03.2020).
<https://doi.org/10.5067/GPM/IMERGDF/DAY/06>
- Hutchinson, J.N., 1978. *A geotechnical classification of landslides*. Imperial College, London.
- Iadanza, C., Trigila, A., and Napolitano, F., 2016. Identification and characterization of rainfall events responsible for triggering of debris flows and shallow landslides. *Journal of Hydrology*, vol. 541, pp. 230-245.
<https://doi.org/10.1016/j.jhydrol.2016.01.018>

- IS: 14496, Part 2 1998. Preparation of landslide hazard evaluation and zonation maps in mountainous terrain – Guidelines. Bureau of Indian Standards, New Delhi, India.
- IS: 1498, 1970. Classification and identification of soils for general engineering purposes. Bureau of Indian Standards, New Delhi, India.
- IS: 2720, Part 13, 1986. Method of test for soils: Direct Shear Test. test (Second Revision, Reaffirmed 2002). Bureau of Indian Standards, New Delhi, India.
- IS: 2720, Part 5, 1985. Method of test for soils: Determination of liquid and plastic limit (Second Revision, Reaffirmed 2006). Bureau of Indian Standards, New Delhi, India.
- IS: 2720, Part 6, 1972. Method of test for soils: Determination of shrinkage factors (First Revision, Reaffirmed 2001). Bureau of Indian Standards, New Delhi, India.
- IS: 8764, 1998. Method for determination of Point load strength index of rocks (First Revision, Reaffirmed 2008). Bureau of Indian Standards, New Delhi, India.
- Iverson, R.M., and Ouyang, C., 2015. Entrainment of bed material by Earth-surface mass flows: Review and reformulation of depth-integrated theory. *Rev. Geophys.*, vol. 53(1), pp. 27-58. <https://doi.org/10.1002/2013RG000447>
- Jaboyedoff, M., Carrea, D., Derron, M.H., Oppikofer, T., Penna, I.M., and Rudaz, B., 2020. A review of methods used to estimate initial landslide failure surface depths and volumes. *Eng Geol* vol. 267: 105478. <https://doi.org/10.1016/j.enggeo.2020.105478>
- Jaboyedoff, M., Crosta, G.B., and Stead, D., 2011. Slope tectonics: a short introduction. In: Jaboyedoff, M. (Ed.), *Slope Tectonics*. Geological Society, London, Special Publications, vol. 351, pp. 1-10. <https://doi.org/10.1144/SP351.1>
- Jaboyedoff, M., Penna, I., Pedrazzini, A., Baroň, I., and Crosta, G.B., 2013. An introductory review on gravitational-deformation induced structures, fabrics and modeling. *Tectonophysics*, vol. 605, pp. 1-12. <https://doi.org/10.1016/j.tecto.2013.06.027>
- Jamir, N., 2013. Landslide investigation and susceptibility mapping of Mokokchung town, Nagaland. Unpublished Ph.D. thesis, Nagaland University, Kohima.
- Jamir, N., Aier, I., Supongtemjen, and Thong, G.T., 2011. An appraisal of the debris slide in Artang Ward, Mokokchung Town, Nagaland, NE India. *Proceedings of the National Seminar on Geodynamics, Sedimentation and Biotic Response in the context of India-Asia Collision*, Mizoram University. *Memoirs of the Geological Society of India*, vol. 77, pp. 259-268.

- Jenelius, E., and Mattsson, L.G., 2012. Road network vulnerability analysis of area-covering disruptions: A grid-based approach with case study, *Transport. Res. A.-Pol.*, vol. 46(5), pp. 746-760. <https://doi.org/10.1016/j.tra.2012.02.003>
- Johnson, A.M., and Rodine, J.R., 1984. Debris flow. In: *Slope Instability*, Brunsden, D. and Prior, D.B. (Eds.). Wiley, United Kingdom, pp. 257-361.
- Kainthola, A., Singh, P.K., Wasnik, A.B., and Singh, T.N., 2012. Distinct element modelling of Mahabaleshwar Road cut hill slope. *Geomaterials*, vol. 2(4), pp. 105-113. <https://doi.org/10.4236/gm.2012.24015>
- Kandpal, G.C., and Pant, G., 1995. Geological evaluation of instability along Balia Nala, Dist. UP. *Symp. Rec. Adv. Geol. Studies, NE Himalayas*, Lucknow, pp. 21-23.
- Karsli, F., Atasoy, M., Yalcin, A., Reis, S., Demir, O., and Gokceoglu, C., 2009. Effects of land-use changes on landslides in a landslide-prone area (Ardesen, Rize, NE Turkey). *Environmental Monitoring and Assessment*, vol. 156, pp. 241-255. <https://doi.org/10.1007/s10661-008-0481-5>
- Kellogg, K.S., 2001. Tectonic controls on a large landslide complex: Williams Fork Mountains near Dillon, Colorado. *Geomorphology*, vol. 41(4), pp. 355-368. [https://doi.org/10.1016/S0169-555X\(01\)00067-8](https://doi.org/10.1016/S0169-555X(01)00067-8)
- Kemas, K., Thong, G.T., and Walling, T., 2004. Chokidzü debris slide - A case study. *Nagaland University Research Journal*, vol. 2, pp. 89-94.
- Khalo, M., 2016. Slope stability investigations between Kohima and Mao with special reference to NH-39. Unpublished Ph.D. thesis, Nagaland University, Kohima.
- Khalo, M., Soibam, I., Supongtemjen, and Thong, G.T., 2016. Geotechnical studies of the Viswema slide, Kohima, Nagaland. *Indian Landslides*, vol. 9, pp. 1-8.
- Khatsu, P., and Van Westen, C.J., 2005. Urban multi-hazard risk analysis using GSI and remote sensing: A case study from Kohima town, Nagaland, India. In: *Proceeding of ACRS, Hanoi, Vietnam*, pp.1-9.
- Kirschbaum, D.B., and Stanley, T., 2018. Satellite-based assessment of rainfall-triggered landslide hazard for situational awareness. *Earth's Future*, vol. 6(3), pp. 505-523. <https://doi.org/10.1002/2017EF000715>
- Kliche, C.A., 1999. *Rock slope stability*. Society for Mining, Metallurgy, and Exploration, Inc.: Littleton, CO, USA, 253p.
- Kemas, K., Thong, G.T., and Walling, T., 2004. Chokidzü debris slide - A case study. *Nagaland University Research Journal*, vol. 2, pp. 89-94.

- Knapen, A., Kitutu, M.G., Poesen, J., Breugelmans, W., Deckers, J., and Muwanga, A., 2006. Landslides in a densely populated county at the foot slopes of Mount Elgon (Uganda): Characteristics and causal factors. *Geomorphology*, vol. 73, pp. 149-165.
- Kojima, S., Nagata, H., Yamashiroya, S.I., Iwamoto, N., and Ohtani, T., 2015. Large deep-seated landslides controlled by geologic structures: prehistoric and modern examples in a Jurassic subduction–accretion complex on the Kii Peninsula, central Japan. *Eng. Geol.*, vol. 186, pp. 44-56. <https://doi.org/10.1016/j.enggeo.2014.10.018>
- Korup, O., 2004. Landslide-induced river channel avulsions in mountain catchments of Southwest New Zealand. *Geomorphology*, vol. 63(1-2), pp. 57-80. <https://doi.org/10.1016/j.geomorph.2004.03.005>
- Korup, O., Clague, J.J., Hermanns, R.L., Hewitt, K., Strom, A.L., and Weidinger, J.T., 2007. Giant landslides, topography, and erosion. *Earth Planet Sci. Lett.*, vol. 261(3–4), pp. 578-589. <https://doi.org/10.1016/j.epsl.2007.07.025>
- Kumar, A., Sanoujam, M., 2007. Landslide studies along the national highway (NH 39) in Manipur. *Natural Hazards*, vol. 40, pp. 603-614.
- Kusre, B.C., and Singh, K.S., 2012. Study of spatial and temporal distribution of rainfall in Nagaland. *Intl. Jour. Geomatics Geosc.*, vol. 2(3), pp. 712-722.
- Laimer, H.J., 2017. Anthropogenically induced landslides – A challenge for railway infrastructure in mountainous regions, *Eng. Geol.*, vol. 222, pp. 92-101, <https://doi.org/10.1016/j.enggeo.2017.03.015>
- Lambe, T.W., Whitman, R.V., 1979. *Soil Mechanics*. SI version. John Wiley & Sons, New York, 553p.
- Lashari, L., Kusumawardani, R., Upomo, T.C., Supriyadi, S., and Mugiayulhaq, A., 2019. Application of 2D spatial imaging method for identification of fault lines and subsurface landslide at “Taman Unnes”, Semarang, Indonesia. *MATEC Web of Conferences*, vol. 258: 03005.
- Lee, M.L., Ng, K.Y., Huang, Y.F., and Li, W.C., 2014. Rainfall-induced landslides in Hulu Kelang area, Malaysia. *Nat. Hazards*, vol. 70, pp. 353-375. <https://doi.org/10.1007/s11069-013-0814-8>
- Lim, T.T., Rahardjo, H., Chang, M.F., and Fredlund, D.G., 1996. Effect of rainfall on matric suctions in a residual soil slope. *Canadian Geotechnical Journal*, vol. 33 (4), pp. 618-628. <https://doi.org/10.1139/t96-087>

- Li, D., and Wang, W., 2019. Quantitative analysis of the influence of saturation on rock strength reduction considering the distribution of water. *Geomechanics and Geophysics for Geo-Energy and Geo-Resources*, vol. 5, pp. 197-207. <https://doi.org/10.1007/s40948-019-00106-3>
- Li, W., Liu, C., Hong, Y., Sahaia, M., Sun, W., Yao, D., and Chen, W., 2016. Rainstorm-induced shallow landslides process and evaluation- A case study from three hot spots, China. *Geomat., Nat. Hazards Risk*, vol. 7(6), pp. 1908-1918. <https://doi.org/10.1080/19475705.2016.1179685>
- Longkumer, L., Luirei, K., Moiya, J.N., and Thong, G.T., 2019. Neotectonic activity in the Schuppen Belt of Mokokchung, Nagaland: Evidences from morphotectonic features. *Journal of Asian Earth Sciences*, vol. 170, pp. 138-154. <https://doi.org/10.1016/j.jseaes.2018.11.010>
- Lotha, K.A., 1994. A note on the geotechnical investigation on landslide at Cheipfutsiepe, Lower AG colony, Kohima Town, Nagaland. Unpubl. Rep. Geoenviron. Cell, DGM, Nagaland.
- Ludman, A., and Coch, N.K., 1982. *Physical Geology*. McGraw-Hill Book Co., London.
- Luino, F., 2005. Sequence of instability processes triggered by heavy rainfall in the northern Italy. *Geomorphology*, vol. 66, pp. 13-39. <https://doi.org/10.1016/j.geomorph.2004.09.010>
- Malizia, J.P., and Shakoor, A., 2018. Effect of water content and density on strength and deformation behavior of clay soils. *Engineering Geology*, vol. 244, pp.125-131. <https://doi.org/10.1016/j.enggeo.2018.07.028>
- Markland, J.T., 1972. A useful technique for estimating the stability of rock slopes when the rigid wedge sliding type of failure is expected. *Imperial College Rock Mech. Res. Rep. No. 19*.
- Mathur, L.P., Evans, P., 1964. Oil in India. *Int. Geol. Cong. (22nd session)*, New Delhi.
- Matsushi, Y., Hattanji, T., and Matsukura, Y., 2006. Mechanisms of shallow landslides on soilmantled hillslopes with permeable and impermeable bedrocks in the Boso Peninsula, Japan. *Geomorphology*, vol. 76, pp. 92-108. <https://doi.org/10.1016/j.geomorph.2005.10.003>
- Meneses, B.M., Pereira, S., and Reis, E., 2019. Effects of different land use and land cover data on the landslide susceptibility zonation of road networks. *Nat. Hazards and Earth System Sciences*, vol. 19(3), pp. 471-487. <https://doi.org/10.5194/nhess-19-471-2019>

- Meusburger, K., and Alewell, C., 2008. Impacts of anthropogenic and environmental factors on the occurrence of shallow landslides in an alpine catchment (Urseren Valley, Switzerland). *Nat. Hazards Earth Syst. Sci.*, vol. 8, pp. 509-520.
- Moiya, J.N., Luirei, K., Longkumer, L., Kothiyari, G.C., and Thong, G.T., 2019. Late Quaternary deformation in parts of the Belt of Schuppen of Dimapur and Peren districts, Nagaland, NE India. *Geological Journal*, vol. 55(1), pp. 1-20. <https://doi.org/10.1002/gj.3413>
- Mukhopadhyay, M., Biswas, U., Mandal, N., and Misra, S., 2019. On the Development of Shear Surface Roughness. *J. Geophys. Res. Solid Earth*, vol. 124(2), pp. 1273-1293. <https://doi.org/10.1029/2018JB016677>
- Murthy, V.N.S., 2001. *Principles of Soil Mechanics and Foundation Engineering* (5th ed.), UBS Publishers & Distributors, New Delhi, 842p.
- Msilimba, G.G., 2002. Landslides: Geohazard assessment of the Vunguvungu/Banga Catchment Area in Rumphi District. M.Sc. Environmental Science. Unpubl. thesis, University of Malawi, Zomba.
- Nandy, D.R., 1976. The Assam syntaxis of the Himalaya: A re-evaluation. *Sem. Rec. Geol. Study, Him. Misc. Publ., Geol. Surv. India*, vol. 24, pp. 363-368.
- Nandy, D.R., 2000. *Geodynamics of Northeastern India and the adjoining region*. ACB Publications, Dehradun.
- Nishii, R., Matsuoka, N., Daimaru, H., and Yasuda, M., 2013. Precursors and triggers of an alpine rockslide in Japan: the 2004 partial collapse during a snow-melting period. *Landslides* vol.10, pp.75-82. <https://doi.org/10.1007/s10346-012-0353-5>
- Nowamooz, H., and Masrouri, F., 2008. Hydromechanical behaviour of an expansive bentonite-silt mixture in cyclic suction-controlled drying and wetting tests. *Engineering Geology*, vol. 101, pp. 154-164. <https://doi.org/10.1016/j.enggeo.2008.04.011>
- Palacky, G.J., 1987. Resistivity characteristics of geological targets. In: Nabighian, M.N. (ed), *Electromagnetic Methods in Applied Geophysics - Theory*, vol. 1 Soc. Expl. Geophys, pp. 53-129, *Investigations in Geophysics Series*, No. 3.
- Palmström, A., 1982. The volumetric joint count - a useful and simple measure of the degree of rock jointing. *Proc. 4th Intl. Conf. Assoc. Engg. Geol.*, New Delhi, vol. 5, pp. 221-228.
- Park, H.J., Lee, J.H., Kim, K.M., and Um, J.G., 2016. Assessment of rock slope stability using GIS-based probabilistic kinematic analysis. *Eng. Geol.*, vol. 203, pp. 56-69.

- Pellet, F.L., Keshavarz, M., and Boulon, M., 2013. Influence of humidity conditions on shear strength of clay rock discontinuities. *Engineering Geology*, vol. 157, pp. 33-38. <https://dx.doi.org/10.1016/j.enggeo.2013.02.002>
- Penna, I., Abellán, A., Humair, F., Jaboyedoff, M., Daicz, S., and Fauqué, L., 2016. The role of tectonic deformation on rock avalanche occurrence in the Pampeanas Ranges, Argentina. *Geomorphology*, vol. 289, pp. 18-26. <http://dx.doi.org/10.1016/j.geomorph.2016.07.006>
- Petit, J.P., 1987. Criteria for the sense of movement on fault surfaces in brittle rocks. *J. Struct. Geol.*, vol. 9, pp. 597-608. [https://doi.org/10.1016/0191-8141\(87\)90145-3](https://doi.org/10.1016/0191-8141(87)90145-3)
- Petley, D., 2012. Global patterns of loss of life from landslides. *Geology*, vol. 40(10), pp. 927-930. <https://doi.org/10.1130/g33217.1>
- Punmia, B.C., 1994. *Soil Mechanics and Foundations* (13th ed.). Laxmi Publications (P) Ltd., New Delhi, 970p.
- Piteau, D.R., and Peckover, F.L., 1989. Engineering of rock slopes. In: Goodman, R.E. (Ed.), *Introduction to Rock Mechanics* (2nd ed.). John Wiley & Sons, 576p.
- Rahman, M.S., Ahmed, B., and Di, L., 2017. Landslide initiation and runout susceptibility modelling in the context of hill cutting and rapid urbanization: a combined approach of weights of evidence and spatial multi-criteria. *J. Mt. Sci.*, vol. 14(10), pp. 1919-1937.
- Ramsay, J.G., 1967. *Folding and fracturing of rocks*. Blackburn Press, Caldwell, N.J., USA, 568p.
- Rauch, H.P., Florineth, F., Lammeranner, W., and Wibmer, S., 2002. *Soil Bioengineering Slope Protection Investigations in Nepal*. Final Report for the Austrian Commission of Development Research.
- Reichenbach, P., Busca, C., Mondini, A.C., and Rossi, M., 2014. The influence of land use change on landslide susceptibility zonation: The Briga catchment test site (Messina, Italy). *Environmental Management*, vol. 54(6), pp. 1372-1384. <https://doi.org/10.1007/s00267-014-0357-0>
- Roback, K., Clark, M.K., West, A.J., Zekkos, D., Li, G., Gallen, S.F., Chamlagain, D., and Godt, J.W., 2018. The size, distribution, and mobility of landslides caused by the 2015 Mw7.8 Gorkha earthquake, Nepal. *Geomorphology*, vol. 301, pp. 121-138. <https://doi.org/10.1016/j.geomorph.2017.01.030>
- Roccati, A., Faccini, F., Luino, F., Ciampalini, A., and Turconi, L., 2019. Heavy rainfall triggering shallow landslides: A susceptibility assessment by a GIS-approach in a Ligurian Apennine Catchment (Italy). *Water*, vol. 11: 605 pp. <https://doi.org/10.3390/w11030605>

- Roccati, A., Faccini, F., Luino, F., Turconi, L., and Guzzetti, F., 2018. Rainfall events with shallow landslides in the Entella catchment, Liguria, northern Italy. *Nat. Hazards Earth Syst. Sci.*, vol.18, pp. 2367-2386. <https://doi.org/10.5194/nhess-18-2367-2018>
- Rocscience Inc., 1998. Dips Version 7.0 - Graphical and statistical analysis of orientation data. www.rocscience.com, Toronto, Ontario, Canada.
- Rocscience Inc., 2005. RocData Version 5.0 - Rock, soil, and discontinuity strength analysis. www.rocscience.com, Toronto, Ontario, Canada.
- Romana, M., 1985. New adjustment ratings for applications of Bieniawski classification of slopes. *Intl. Symp. Rock Mech., Zacatecas*, pp. 49-53.
- Roy, R.K., and Kacker, R.N., 1986. Cenozoic deformation pattern and mechanism in the Belt of Schuppen and their role in hydrocarbon accumulation: Further exploratory concepts for Assam-Arakan Basin. In: Ghose NC, Varadarajan S (eds) *Ophiolites and Indian Plate Margin*. Sumna Publishers, Patna, pp. 197-221.
- Sahu, V.K., Gahalaut, V.K., Rajput, S., Chadha, R.K., Laishram, S.S., and Kumar, A., 2006. Crustal deformation in the Indo-Burmese region: Implications from the Myanmar and SE Asia GPS measurements. *Current Science*, vol. 90(12), pp. 1688-1692. <https://www.jstor.org/stable/24091921>
- Sarma, H., 1985. Systematic geological mapping around Pukha-Lungwa-Chenwentyu-Champang areas of Mon district, Unpub. Prog. Rep., GSI, FS 1984-85.
- Sengupta, A., Gupta, S., and Anbarasu, K., 2010. Rainfall thresholds for the initiation of landslide at Lanta Khola in north Sikkim, India. *Nat. Hazards* vol.52, pp.31-42.
- Senthilkumar, V., Chandrasekaran, S.S., and Maji, V.B., 2018. Rainfall-induced landslides: case study of the Marappalam landslide, Nilgiris district, Tamilnadu, India. *Int J Geomech.* vol. 18(9).
- Sharda, Y.P., and Bhambay, G.C., 1980. Kohima town, Nagaland: A decade of environmental geoscientific studies. GSI Sp. Publ. Series, No. 9.
- Siddiqui, S.H., and Parizek, R.R., 1971. Hydrogeologic factors influencing well yields in folded and faulted carbonate rocks in central Pennsylvania. *Water Resour. Res.*, vol. 7, pp. 1295-1312. <https://doi.org/10.1029/WR007i005p01295>
- Siddique, T., Pradhan, S.P., Vishal, V., Mondal, M.E.A., and Singh, T.N., 2017. Stability assessment of Himalayan road cut slopes along National Highway 58, India. *Environmental Earth Sciences*, vol. 76: 759. <https://doi.org/10.1007/s12665-017-7091-x>

- Singh, M.P., Soibam, I., Thong, G.T., and Aier, I., 2008. Impact of human settlement and land use on slope stability: Phikomei (Mao) Slide, an example from NH 39, Imphal-Mao road section, Manipur. *Bulletin of the Indian Geologists' Association*, vol. 41, pp. 25-39.
- Singh, P.K., Singh, K.K., and Singh, T.N., 2016. Slope failure in stratified rocks a case from NE Himalaya, India. *Landslides*, vol. 14, pp. 1319-1331. <https://doi.org/10.1007/s10346-016-0785-4>
- Singh, P.K., Wasnik, A.B., Kainthola, A., Sazid, M., and Singh, T.N., 2013. The stability of road cut cliff face along SH-121: A case study. *Nat. Hazards*, vol. 68(2), pp. 497-507. <https://doi.org/10.1007/s11069-013-0627-9>
- Singh, T.N., Kainthola, A., and Venkatesh, A., 2012. Correlation between point load index and uniaxial compressive strength for different rock types. *Rock Mech. Rock Eng.*, vol. 45, pp. 259-264. <https://doi.org/10.1007/s00603-011-0192-z>
- Smith, K., 1996. *Environmental Hazards: Assessing Risk and Reducing Disaster*. Routledge, London.
- Sondhi, V.P., 1941. A note on landslips on the Dimapur-Manipur road, Assam. GSI Unpubl. Rep., Strategic Br.
- Sothu, H.N., 2009. Geological investigations of instability along National Highway 150, between Kohima and Chakabama, Kohima District, Nagaland. Unpublished Ph.D. thesis, Nagaland University, Kohima.
- Sothu, H.N., Aier, I., and Thong, G.T., 2009. Evaluation of two unstable sites along NH 150, SE of Kohima Town, Nagaland. *Indian Landslides*, vol. 2, pp. 27-30.
- Sothu, H.N., Aier, I., and Thong, G.T., 2011. Analysis of Chakhabama subsidence and its surroundings along NH 150, Nagaland, NE India. *Disaster and Development*, vol. 5, pp. 131-137.
- Stanchi, S., D'Amico, M., Zanini, E., and Freppaz, M., 2015. Liquid and plastic limits of mountain soils as a function of the soil and horizon type. *CATENA*, vol. 135, pp. 114-121. <https://doi.org/10.1016/j.catena.2015.07.021>
- Strupler, M., Danciu, L., Hilbe, M., Kremer, K., Anselmetti, F.S., Strasser, and M., Wiemer, S.A., 2018. Subaqueous hazard map for earthquake-triggered landslides in Lake Zurich, Switzerland. *Nat. Hazards*, vol.90, pp.51-78.
- Sultan, A.S., and Santos, F.A.M., 2008. 1D and 3D resistivity inversions for geotechnical investigation. *J. Geophys Eng.*, vol. 5, pp. 1-11.

- Sun, D.M., Li, X.M., Feng, P., and Zang, Y.G., 2016. Stability analysis of unsaturated soil slope during rainfall infiltration using coupled liquid-gas-solid three-phase model. *Water Sci. Eng.*, vol. 9(3), pp. 183-194. <https://doi.org/10.1016/j.wse.2016.06.008>
- Supongtemjen, 2013. Geological investigation of land instability between Kohima and Zhadima. Unpublished Ph.D. thesis, Nagaland University, Kohima.
- Supongtemjen, and Thong, G.T., 2014. Risk analyses along part of NH 2, north of Kohima town, Nagaland. *Indian Landslides*, vol.7, pp. 35-44.
- Supongtemjen, Walling, T., Tep, S., and Thong, G.T., 2015. Stability analyses of two fresh cut slopes along NH 2, Meriema, Nagaland. *Proceedings of the National Seminar on Landslides: Management and Mitigation Strategies. Journal of Engineering Geology*, vol. XL, pp. 158-170.
- Susilo, A., Sunaryo, Fitriah, F., and Sarjiyana, 2018. Fault analysis in Pohgajih village, Blitar, Indonesia using resistivity method for hazard risk reduction. *Int J GEOMATE* vol.14, pp.111-118.
- Takahashi, T., 1991. Debris Flow: Monograph series of IAHR (International Association for Hydraulic Research), A.A. Balkema Publishers, Rotterdam, Netherlands, 165p.
- Telford, W.M., Geldart, L.P., and Sherrif, R.E., 1990. *Applied Geophysics*, 2nd edn. Cambridge University Press.
- Terzaghi, K., 1950. Mechanism of landslides. In: Paigse, S. (Ed.), *Application of Geology to Engineering Practice. Geol. Soc. Amer. Mem.*, pp. 83-123.
- Thong, G.T., Aier, I., and Walling, T., 2004. Preliminary geological report of Mao slide. BRO Report.
- Trandafir, A.C., Ertugrul, O.L., and Giraud, R.E., and McDonald, G.N., 2015. Geomechanics of a snowmelt-induced slope failure in glacial till. *Environ. Earth Sci.*, vol. 73(7), pp. 3709-3716. <https://doi.org/10.1007/s12665-014-3658-y>
- Tsai, C.H., Huang, C.L., Hsu, S.K., Doo, W.B., Lin, S.S., Wang, S.Y., Lin, J.Y., and Liang, C.W., 2018. Active normal faults and submarine landslides in the Keelung Shelf off NE Taiwan. *Terr. Atmos. Ocean. Sci.*, vol. 29, pp. 31-38. <https://doi.org/10.3319/TAO.2017.07.02.01>
- Turner, A. K., and Schuster, R. L., 1996. *Landslides, Investigation and Mitigation*. Transportation Research Board, Special Report 247, National Research Council, National Academy Press, Washington, D.C., 673p.

- Umrao, R.K., Singh, R., Sharma, L.K., and Singh, T.N., 2016. Geotechnical investigation of a rain triggered Sonapur landslide, Meghalaya. IndoRock, 6th Indian Rock Conference, Mumbai, India, 17-18 June 2016, pp. 302-313.
- Uribe-Etxebarria, G., Morales, T., Uriarte, J. A., and Ibarra, V., 2005. Rock cut stability assessment in mountainous regions. *Environ. Geol.*, vol. 48, pp. 1002-1013. <https://doi.org/10.1007/s00254-005-1323-1>
- Vanacker, V., Vanderschaeghe, M., Govers, G., Willems, E., Poesen, J., Deckers, J., and De Bievre, B., 2003. Linking hydrological, infinite slope stability and land-use change models through GIS for assessing the impact of deforestation on slope stability in high Andean watersheds. *Geomorphology*, vol. 52(3-4), pp. 299-315. [https://doi.org/10.1016/S0169-555X\(02\)00263-5](https://doi.org/10.1016/S0169-555X(02)00263-5)
- Van Asch, T.W.J., Buma, J., and Van Beek, L.P.H., 1999. A view on some hydrological triggering systems in landslides. *Geomorphology*, vol. 30(1-2), pp. 25-32. [https://doi.org/10.1016/S0169-555X\(99\)00042-2](https://doi.org/10.1016/S0169-555X(99)00042-2)
- Varnes, D.J., 1978. Slope Movement and Types and Process. In: Schuster, R.L. and Krizek, R.J. (Eds.), *Landslides: Analysis and Control*. Transportation Res. Board Spl. Rep., 176, National Academy of Sciences, Washington, DC, pp 11-80.
- Veder, C., and Hilbert, F., 1980. *Landslides and their stabilization*. ISBN, USA.
- Verma, K.P., and Yedekar, D., 1983. Systematic geological mapping in Unger-Dikhu-Mangmetong-Chungtiya-Longjang area, district Mokokchung, Nagaland. Miscellaneous Publication No. 30, Part IV, vol. 1 (Part-2), Geological Survey of India.
- Verma, R.K., 1985. Gravity field, seismicity, and tectonics of the Indian Peninsula and the Himalaya. Allied Publishers, New Delhi, pp. 155-189.
- Vishal, V., Pradhan, S.P., and Singh, T.N., 2010. Instability assessment of mine slope - A finite element approach. *Int. J. Earth Sci. Eng*, vol. 3(6), pp. 11-23.
- Walling, T., 2005. Geological investigation of land instability in Kohima Town, Nagaland. Unpublished Ph.D. thesis, Nagaland University, Kohima.
- Walling, T., Lotha, K.A., Thong, G.T., and Aier, I., 2005. Chiepfütsiepf slide, Kohima, Nagaland. Causes and mitigation measures. *Proc. NRDMS (DST) Sem. Landslide. Haz. Miti., NE Ind.*, pp. 48-54.
- Walling, T., Supongtemjen, Chang, C.N., and Thong, G.T., 2016. Geotechnical analyses of debris slide near Secretariat junction, Kohima, Nagaland. In: Srivastava, S.K. (Ed), *Recent Trends in Earth Science Research with Special Reference to NE India*, Today and Tomorrow Publishers, New Delhi, pp. 277-289.

- Watakabe, T., and Matsushi, Y., 2019. Lithological controls on hydrological processes that trigger shallow landslides: Observations from granite and hornfels hillslopes in Hiroshima, Japan. *CATENA*, vol. 180, pp. 55-68. <https://doi.org/10.1016/j.catena.2019.04.010>
- Willenberg, H., Loew, S., Eberhardt, E., Evans, K.F., Spillmann, T., Heincke, B., Maurer, H., and Green, A., 2008. Internal structure and deformation of an unstable crystalline rock mass above Randa (Switzerland): Part I - Internal structure from integrated geological and geophysical investigations. *Eng. Geol.*, vol. 101(1-2), pp. 1-14. <https://doi.org/10.1016/j.enggeo.2008.01.015>
- Winter, M. G., Shearer, B., Palmer, D., Peeling, D., Harmer, C., and Sharpe, J., 2016. The Economic Impact of Landslides and Floods on the Road Network, *Procedia Eng.*, vol. 143, pp. 1425-1434. <https://doi.org/10.1016/j.proeng.2016.06.168>
- Yang, K.H., Uzuoka, R., Thuo, J.N., Lin, G.L., and Nakai, Y., 2017. Coupled hydro-mechanical analysis of two unstable unsaturated slopes subject to rainfall infiltration. *Eng. Geol.*, vol. 216, pp. 13-30. <https://doi.org/10.1016/j.enggeo.2016.11.006>
- Yano, K., 2017. Soil erosion in Kohima district, Nagaland: A geographical analysis. Ph.D. thesis, Nagaland University.
- Zaruba, Q., and Mencl, V., 1969. Landslides and their control. *Developments in geotechnical engineering*, Czechoslovakia Academy of Sciences, Prague, vol. 2.
- Zischinsky, U., 1969. On the Deformation of High Slopes. *Proceedings, 1st Congress of the International Society of Rock Mechanics*, vol.2, pp. 179-185.
- Zêzere, J.L., Garcia, R.A.C., Oliveira, S.C., and Reis, E., 2006. Probabilistic landslide risk analysis considering direct costs in the area north of Lisbon (Portugal). *Geomorphology*, vol. 94(3-4), pp. 467-495. <https://doi.org/10.1016/j.geomorph.2006.10.040>

BIO-DATA OF THE CANDIDATE

I. Publication

C. Nokendangba Chang, Meripeni Ezung, Mehilo Apon, Supongtemjen, Temsulemba Walling and Glenn T. Thong (2021). Assessment of Landslides Along NH 29 in the Kevüza Area, Kohima, Nagaland. *Indian Geotechnical Journal*, vol. 51, pp. 841-860.

II. Paper presented

- National seminar on *Geology, Geochemistry, Tectonics, Energy and Mineral Resources of North East India* organised by the Department of Geology, Nagaland University, Kohima Campus, Meriema, from 9th-11th November, 2016
- *3rd National Geo-Research Scholars Meet-2019* organised by Wadia Institute of Himalayan Geology, Dehradun, on 6th -8th June, 2019

III. Seminars and Workshops attended

- Regional workshop for Young Earth Scientists on *Tectonics, Sedimentation and Geohazards with special reference to North East India*, conducted by the Department of Geology, Nagaland University, Kohima Campus, Meriema from 16th-21st November 2015
- Geologic Field Course on *Practical Applications of Neotectonics and Quarternary Geology in Geologic Hazards Assessment*, Aizawl from 12th-21st October, 2016
- Global Initiative of Academic Networks (GIAN) – *Landslide and Debris Flow Systems: Prediction, Control and Reclamation*, conducted by Nagaland University from 7th-11th March, 2017 at Department of Geography, NU Lumami
- International *LARAM* (Landslide Risk Assessment and Mitigation) India Course 2020, held in IIT Roorkee from 17th to 22nd February 2020

IV. Project Fellow

- Geotechnical investigations of major subsidence affecting Lower Officer's Hill and NH 39, Kohima. *Department of Science and Technology (DST), New Delhi*.